Politecnico di Torino

Politecnico di Torino

Master's Degree in Automotive Engineering
Academic Year 2021/2022
Graduation Session October 2022

Bake-hardening of Aluminum Alloys for Automotive Applications

Influence of Temperature, Time and Pre-Strain Parameters

Advisors:
Dr. Davide Paolino
Dr. Daniel E. Green

Candidate:
Giorgio Rolle

Declaration of originality

I hereby certify that I am the sole author of this thesis and that no part of this thesis has been published or submitted for publication.

I certify that, to the best of my knowledge, my thesis does not infringe upon anyone's copyright nor violate any proprietary rights and that any ideas, techniques, quotations, or any other material from the work of other people included in my thesis, published or otherwise, are fully acknowledged in accordance with the standard referencing practices. Furthermore, to the extent that I have included copyrighted material that surpasses the bounds of fair dealing within the meaning of the Canada Copyright Act, I certify that I have obtained a written permission from the copyright owner(s) to include such material(s) in my thesis and have included copies of such copyright clearances to my appendix.

I declare that this is a true copy of my thesis, including any final revisions, as approved by my thesis committee and the Graduate Studies office, and that this thesis has not been submitted for a higher degree to any other University or Institution.

Abstract

An experimental evaluation of the effect of bake hardening on aluminum alloys for automotive lightweight applications is developed through tensile tests and dent tests. All the alloys belong to the 6xxx series and include high formability alloys, improved hemming types and improved bake response alloys. An experimental matrix which contains different time-temperature baking conditions is built, and two pre-strain conditions are considered: no pre-strain and 2% pre-strain. After a data analysis phase performed by means of MATLAB software, the results of the different alloys are compared in terms of mechanical resistance and bake response to identify the materials that are potentially more suitable for certain applications. Furthermore, the outcomes are discussed in correlation to the alloys' chemical content as well. The improved hemming alloy from North America turned out to be the best in terms of mechanical resistance (both tensile strength and resistance to indentation), while the improved bake response alloy from North America gave the best strength gain after the baking phase. Last, the high formability alloy, as expected, stood out as the alloy with the best ductility. Baking at lower temperatures (120°C and 130°C) was not particularly effective for durations of 10 and 20 minutes, as similar final tensile strength was obtained by just aging specimens at ambient temperature. Furthermore, an increase of baking time by 10 minutes caused the final strength to be higher than what was obtained by raising the baking time by 10°C. A numerical modeling approach was also attempted by means of experimental data fitting by adapting a model for strain aging originally developed for steels. This was done to show what should be the step that immediately follows the data gathering phase, which is building a predictive model for the 6xxx alloys based on the aforementioned data that can be implemented into CAE softwares. Unfortunately, the obtained results turned out to be not satisfying, as the modeled bake-hardening values were constant when varying baking temperature and time. However, the adopted approach can be further developed in future studies.

Acknowledgements

First, I would like to thank my Academic Advisor of Politecnico di Torino, Dr. Davide Paolino for his support, communicating multiple times with me and making himself always available despite the distance and a time difference of 6 hours.

I would like to extend my sincerest thanks to Dr. Maria Pia Cavatorta and Dr. Giovanni Belingardi, the academic coordinators of Politecnico for the Dual Degree program, who made me very passionate about this program in the previous years, contributing to my decision of applying to it, and helped me moving my first steps once I was selected for this experience.

I would like to express my deepest gratitude to Stellantis for the opportunity that they gave me; it was a lifechanging experience, not only on an academic point of view. I am deeply indebted to all my industrial advisors: Jugraj Singh, from Stellantis US, for his incredible support and courtesy throughout the whole year, and his visit during my brief stay in Detroit; Michele Tedesco and Daniele De Caro for their availability and constant presence to help me with both logistic and theoretical matters; Marie Mills, as the Stellantis coordinator of the DIMD program, for her constant presence and guidance.

I am immensely grateful to the Novelis company, in particular to Tony Hambley and Allison Podnar for welcoming me at their branch in Novi, MI, for the dent tests, and for their constant support in the materials supply.

I am extremely thankful for the support of my academic advisor from University of Windsor, Dr. Daniel Green, for the huge dedication he put into following me and my project who communicated multiple times with me and made himself always available despite the distance and a time difference of 6 hours.

I would also like to make a special mention of Mohammad Dastgiri, Yang Song and all Dr. Green's research group, who strongly supported me and always promptly helped me when technical issues arose, and Kevin Harkai, the technician who always provided test specimens in time.

Special thanks to Dr. Jennifer Johrendt for her continuous support as the academic coordinator of the DIMD program in Canada.

Now, I would like to express my gratitude to the people who I shared my life in Windsor with. Words cannot describe the appreciation I feel for Michael Mele, Stefanie Mele and their family, who constantly gave their all to make my stay in Windsor the

most enjoyable and comfortable possible, first of all by giving me a safe place to stay; for Riccardo Ninfa and Edoardo Branda, former classmates and friends at Politecnico and now colleagues in the DIMD program; Kieran Johnson and Nick Vinten, my Canadian counterparts of the program who I will be glad to guide around Torino; Giampiero Mastracci and Ivana Perfetto, who made me feel at home at their restaurant and were a second family to me here in Canada.

Most importantly, none of this could have happened without my parents and my family, whose unconditional support, economic and moral, has been massive throughout my whole life, constantly encouraging and always being there for me. I am forever grateful to them and to my beautiful Sabrina for her love and patience and for making me feel motivated and close to her, keeping me company even in these months so far away from each other. This accomplishment would not have been possible without them. Thank you.

Giorgio Rolle

Content

List of Tables

List of Figures

List of Abbreviations

AH	age-hardening
BH	bake-hardening
BR	improved bake response alloy
CAE	computer aided engineering
EDM	electrical discharge machining
EU	Europe
GP	Guinier-Preston
HF	higher formability alloy
HS	higher strength alloy
ICE	internal combustion engine
IH	improved hemming alloy
NA	North America
OEM	original equipment manufacturer
P-S	pre-strain
SH	strain-hardening
YS	yield strength

List of Symbols

Δ	inter-precipitate distance
ΔL	elongation
$\Delta\sigma$	overstress due to bake-hardening
δ_{BH}	saturation level of solute atoms into dislocations
δ_{prec}	saturation level of precipitates into dislocations
$\bar{\epsilon}$	equivalent strain
ε_0	true strain at onset of plastic deformation
ρ_{f_x}	dislocations density after x pct pre-strain
$\bar{\sigma}$	equivalent stress
σ_0	true yield stress at onset of plastic deformation
σ_s	saturation stress
A	interaction energy between dislocations and solute atoms
A_0	initial cross section area
a	dislocations slip distance
C_0^{at}	solute segregated at the end of the first bake-hardening step
D	diffusion coefficient for the solute
e	engineering strain
I	nucleation site density
K	strength parameter
k	Boltzmann constant
$k_1 \dots k_6$	parameters of the simplified Harper model
L_0	initial gauge length
N	number of solute atoms per unit volume in dislocations
N_0	total number of dislocation slots
n	strain-hardening exponent
n_0	number of solute atoms in the matrix
P	load
R	radius of precipitates
$R_{el,t}$	lower yield strength after heat treatment
R_{max}	maximum radius of precipitates
$R_{p2,r}$	tensile strength at 2% pre-strain

S	engineering stress
T	absolute temperature
t	time

1 Introduction

1.1 Background

The automotive industry is continuously striving for innovative solutions in terms of performance, efficiency, cost, agile manufacturing and overall competitiveness in the market. Currently, global pollution has forced governments to take action more firmly. As a result, more strict emission regulations have been emitted, with high fines for the companies that don't comply (in Europe, it is 95€ per each vehicle sold per each gram of CO_2 in excess with respect to the average fleet consumption threshold). Other than that, the transition to electrification of vehicles is now inevitable and closer than ever: it is recent news that the European Union has decided to completely ban the sales of internal combustion engine vehicles from 2035, as part of a campaign that aims to reach net-zero greenhouse gas emissions by 2050. However, the concern is global, not just for pollution reasons, but also for high gas prices that make large-size ICEs very expensive to afford throughout their usage. Hence, huge efforts are requested to automotive companies for the design of more efficient vehicles. This new scenario puts pressure to the companies to re-invent their products, but it also constitutes an opportunity for the development of new high level engineering solutions. In particular, research is now focused on high-efficiency internal combustion engines, hybrid/electric architectures and lightweight solutions for body design. A lower vehicle mass enhances performances and fuel consumption in internal combustion engine powered cars, while it compensates for the heavy and bulky batteries of electric vehicles, allowing for lower energy consumption and battery downsizing. Consequently, the availability of lightweight materials is a need of primary importance: as mentioned, light weighting primarily gives advantages in terms of fuel/energy economy and vehicle performance, allowing car brands to design competitive products for the market [1]. At the same time, these lightweight structures must be formable enough for the production process of the vehicle parts, and then be capable of complying with strength and crashworthiness requirements. Suitable materials for these applications, to make some examples, are carbon fiber, magnesium alloys and aluminum alloys. This Thesis will focus on the latter ones.

The metal bake-hardening phenomenon, which is taken advantage of during the body painting process, allows to fulfil the previous requirements, as it will be explained

in detail in this dissertation. Basically, after being treated at temperatures higher than ambient for a certain amount of time (which is the case of the painting process), the material exhibits a higher yield strength than before and it results to be more resistant to indentations. Therefore, studying the bake-hardening phenomenon of aluminum alloys means giving some instruments and data that can be useful to optimize the production process and obtain the required mechanical properties for automotive purposes, while taking advantage of the good properties of aluminum in terms of light weighting.

1.2 Motivation

The motivation for this work is primarily of industrial interest. As explained before, electrification has put even more in evidence the importance of lightweight solutions for vehicle design, and the usage of aluminum alloys instead of steel in some body parts can be convenient. Due to this expected increase in the adoption of alloys different from traditional steel, it is essential to gather as much data as possible about the mechanical characteristic of these materials. In particular, there is the need of reliable data that can describe the behaviour of some aluminum alloys employed by a global OEM in the painting treatment, when varying the parameters of the process. Being able to deeply characterize their mechanical response means having the possibility of setting the most suitable painting temperature and duration and performing eventual prior treatments such that optimal material properties can be obtained after the whole process. Furthermore, it is a matter of energy consumption and process optimization: it would be possible, based on the data, to consider the temperature-time condition that minimizes the painting process energy consumption while still obtaining the required esthetic and mechanical properties.

1.3 Objective of the research

The objective of this project is to experimentally determine the mechanical response of selected aluminum alloys when subjected to a range of bake hardening parameters that affect the production process.

It is required to define and apply a testing procedure for the mechanical validation of the alloys of interest, allowing a final comparison between the same alloys. In this sense, the aim is to get in the end a reliable and reproducible data matrix that can

be employed as a reference for future preliminary stages of design. Moreover, it can constitute the basis for future robust computer aided engineering (CAE).

1.4 Methodology

The organization of this project consisted in a set of different phases. After a first state-of-the-art analysis, the selection of the alloys was arranged with the industrial advisors, as well as the materials supply management. Then, the validation plan was defined and finally put into practice by means of tensile tests and dent tests. The test results were gathered and analyzed through Excel and MATLAB and presented in this Thesis.

1.5 Outline of the Thesis

After this introductory chapter, a state-of-the-art analysis and literature review is provided in Chapter 2. Then, Chapter 3 covers the methodology behind the project. The test results are presented in Chapter 4, and they are discussed and analyzed in Chapter 5. In Chapter 6, a short explanation of the attempt of modelling the experimental results through a simplified version of the Harper model is provided. Finally, Chapter 7 provides a conclusive summary, as well as limitations of this work and recommendations of further studies that can be made, and a description of the present contribution to research.

2 Literature review

2.1 State-of-the-art

Some important considerations associated with the use of aluminum alloys in the automotive industry are provided in this chapter. Starting from a state-of-the-art analysis of aluminum utilization for automotive purposes, a description of the physics of aging kinetics and thermal treatments is covered, as well as a quick review of numerical simulation approaches. In addition, the effects of pre-aging and pre-straining on resulting mechanical properties are discussed along with an overview of experimental procedures.

Over the past few decades, automakers have gradually replaced steel to fabricate panels with lighter materials. Aluminum sheets are one of the most effective and promising material options for the manufacture of automotive panels. Starting from low production volume vehicles, like the Audi R8 (for which a body shell weight of just 210 kg was achieved), aluminum has gradually been adopted for high volume platforms such as the Ford F-150 pickup truck.

Aluminum sheets used to manufacture lightweight automotive body panels predominantly include three alloy series:

- 5xxx (Al-Mg) alloys for unexposed thick structural parts or unexposed parts requiring high formability
- 6xxx (Al-Mg-Si) alloys for exposed panels, high strength structural parts or parts requiring improved formability
- 7xxx (Al-Zn-Mg) alloys for ultra-high strength applications.

The F-150 pick-up truck is an interesting example of the conversion from an all-steel body to a more extended aluminum adoption. Ford decided to switch to aluminum for the 2015 model (*Figure 1*): high-strength aluminum now represented 77% of the body frame compared to 23% in the previous model. Thanks to the adoption of a "Military-Grade" aluminum alloy (6000 series) [2], the F-150 lost 700 lbs of weight, allowing engine downsizing and a significant improvement in fuel consumption; furthermore, its towing capability was also enhanced. In the areas where higher strength and dent resistance were required, thicker body panels were used without increasing weight with respect to the equivalent part made of steel. This decision turned out to be successful, as the F-150 is still the top-selling vehicle in North America. It is true that

aluminum is more expensive than steel in terms of raw materials costs (approximately three times more, MIT sources); however, the usage of aluminum allowed for larger modularity of the body structure and a design optimized for maintenance and reduced repair costs. Therefore, considering the overall life cycle of the vehicle, the costs turned out to be competitive.

Figure 1. Body-in-white of the Ford F-150 pick-up truck made of aluminum

In the next-generation vehicle designs, aluminum will be featured more and more prominently in multi-material car bodies. It has been estimated that the percentage by mass of aluminum in North American car bodies will reach 16% by 2028 (from 10.4% in 2015) [1]. This trend is shown in the graph in *Figure 2* which shows the aluminum content in N.A light vehicles over time.

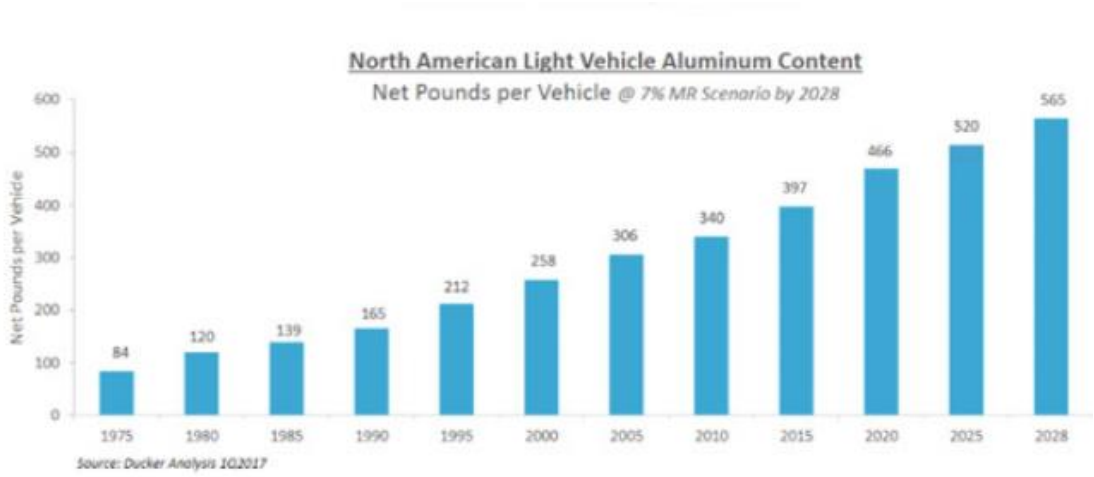

Figure 2. Evolution of the aluminum content in North American light vehicles over time [1].

General Motors's Cadillac CT6 is a good example of a multi-material vehicle: in the design phase, there was an extensive and systematic search for the most suitable material for each part and consequently an overall optimized body-in-white was achieved. As a result of this, 62% of the body was made of aluminum.

Decreasing fuel consumption is no longer simply an option but is now a matter of legislation, as governments are pushing towards stricter regulations on emissions of car fleets, putting CO_2 emission targets that, if not fulfilled, can lead to important fees (95€ for each gram of CO_2 in excess per each vehicle sold [3]). In this sense, light weighting becomes essential and extensive usage of aluminum instead of steel is one opportunity to move in this direction.

Electrification is nowadays the path that has been globally adopted to fulfill such regulatory scenarios. The introduction of battery packs, which are significantly heavier than fuel tanks, requires additional reductions in the global vehicle weight. Furthermore, new body layouts due to the high variability of the configuration battery-electric motors require enhanced modularity and packaging space. And again, an aluminum body can be a solution, such as the Audi R8 e-tron, whose body structure is shown in *Figure 3*.

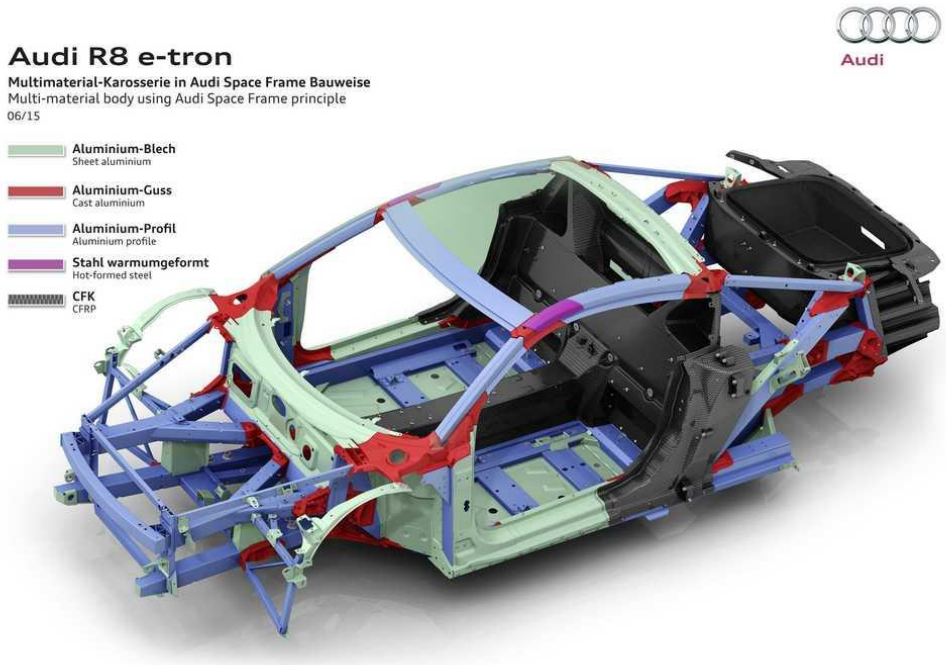

Figure 3. Body frame of the Audi R8 e-tron.

Aluminum alloys for automotive applications, as discussed, allow for good weight reduction. At the same time, they are still required to maintain good properties in terms of energy absorption and strength. Speaking of strength requirements, the phenomenon of bake hardening plays an important role, especially for body panels that are subjected to painting. In synthesis, bake hardening is the strength improvement that some materials, like steels or some aluminum alloys, achieve when heated for a certain amount of time, as during a vehicle paint-baking cycle. Many studies, theoretical and empirical, have been performed because of the industrial importance of this process. Most of the literature focuses on steels; however, it is still useful at least for approaching the case of the present discussion.

Bake-hardenable materials are characterized by good formability in their as-received condition, and this allows them to be easily deep drawn (the pre-strain phase). They then increase their strength after going through the oven during the painting cycle. The bake hardening mechanism is the same as strain aging, where aging at relatively low temperatures after cold working causes pinning of dislocations and the reappearance of a discontinuous yielding, with upper and lower yield stress: the material strength increases but some ductility is lost. However, during painting the part has already been formed to its final shape, therefore the loss of ductility is not an issue, and the higher strength improves the mechanical properties of the part itself, dent resistance included.

Bake hardenability is evaluated according to a standard procedure [4]: a specimen of a given material is deformed in uniaxial tension at room temperature up to 2% strain (this simulates the forming phase); then, an aging phase is carried out in which the pre-strained specimen is heated to 170°C for 20 minutes, which corresponds with the painting phase; finally, the specimen is tested in uniaxial tension at room temperature. The numerical value expressing the bake hardening of the specimen is computed by subtracting the yield stress after the pre-strain from the lower yield strength after baking.

2.2 Phenomenological models and correlation with physical phenomena

The solubility of interstitial atoms at room temperature in bake-hardenable materials is limited. At higher temperature, the solute atoms (carbon in the case of steels, magnesium and silicon in the case of aluminum), migrate towards the

dislocations, pinning them. As a consequence, the material experiences a strengthening. It should be mentioned that most of the literature that was considered refers to the bake-hardening of steel; however, they still provide useful information about the physical phenomena to take into consideration.

Studies were performed to underline the interaction between dislocations and grain boundaries for the carbon atoms segregation during strain aging for industrial bake-hardenable steels [5]. The strain aging process was found to be linked to the concurrent dissolution of interstitial atoms atmospheres that segregated along the grain boundaries and the formation of these atmospheres on the dislocations. For this reason, a key role is played by the availability for segregation of interstitial atoms in solution, which is granted by control of stabilizing elements [6]. For example, for the steels studied in [5], increasing the presence of free interstitial atoms with increasing temperature was theoretically explained with thermally caused disassociation of carbon complexes with alloying elements such as manganese atoms. In the same study, changes in Young's modulus were analyzed and were found to depend on aging time and temperature. Therefore, this dependence on aging time and temperature appears to be a major factor for the whole process.

Simulating the bake-hardening process through numerical approaches is not simple. Accurate physical models have been developed to predict the response of a bake-hardened material during thermal treatments. The key aspect is always the interaction between solute atoms and dislocations. During strain aging of steels, carbon diffusion leads to the formation of Cottrell atmospheres around the dislocation, which tends to block them. Then, if further strain is applied, local plastic instability areas, called Lüders bands, can be found.

Strain aging kinetics of steels can be described by the so-called Harper model [7], which considers the evolution in time of the saturation level of carbon atoms into the dislocations.

$$\delta_{BH} = \frac{N(t)}{N_0} = \frac{1 - \exp\left[3 \cdot (\rho_{f_x} - n_0 a)(\frac{\pi}{2})^{1/3} \left(\frac{ADt}{kT}\right)^{2/3}\right]}{1 - \frac{N_0}{n_0} \cdot \exp\left[3 \cdot (\rho_{f_x} - n_0 a)(\frac{\pi}{2})^{1/3} \left(\frac{ADt}{kT}\right)^{2/3}\right]} \qquad (1)$$

where $N(t)$ is the number of atoms per unit volume that are in the dislocations at time t, N_0 is the total number of dislocation spots (m^{-3}), A is the interaction energy between dislocations and solute atoms, k is the Boltzmann constant, T is the absolute temperature, a is the dislocation slip distance divided by the number of carbon atoms per atom plane, ρ_{f_x} is the dislocation density after a given pre-strain, n_0 is the number of solute atoms in the matrix and D is a diffusion coefficient for the solute.

If aging occurs at higher temperatures or for longer periods of time (as in the case of the vehicle paint-baking process), another hardening stage takes place, which depends on the availability of solute carbon atoms: both the yield strength and the yield point elongation increase further. It can be assumed that this is due to a densification of Cottrell atmospheres by means of some precipitates, whose radius depends on the concentration of carbon segregated at the end of the previous process [8]. Thus, a saturation level for precipitates in the dislocations can also be defined:

$$\delta_{prec} = \frac{R^2}{R_{max}^2} \quad (2)$$

where R is the radius of precipitates, normalized with respect to its maximum level. Finally, the total bake hardening effect is defined as a function of these two saturation coefficients:

$$BH = \delta_{BH} \cdot \Delta\sigma_{max}^{BH} + \delta_{prec} \cdot \Delta\sigma_{max}^{prec} \quad (3)$$

where $\Delta\sigma_{max}^{BH}$ and $\Delta\sigma_{max}^{prec}$ are constants that depend on the type of material.

Figure 4 shows that this model predicts the experimental data quite well. The more carbon is available in solution the more the bake hardening response is enhanced. Also higher temperatures do not affect the bake hardening saturation level, but they do speed up the aging kinetics. This observation is important, as it shows that the same level of strength can theoretically be achieved in automotive panels even if the temperature of the paint-baking oven is decreased.

Pre-strain also plays an important role since it increases the dislocation density: this means that in the second stage, more solute atoms are required to fill the dislocations spots, hence fewer solute atoms are available to form precipitates and

therefore the hardening level decreases. On the other hand, the first stage is not affected by pre-strain.

Ballarin et al. [7] proposed a numerical approach for the Piobert-Lüders phenomenon to be coupled with the previous model. This phenomenon consists in the formation of bands on the material, especially during tensile tests, and their propagation along the material causes a flat stress-strain curve, at a stress level called the lower yield stress; the amount of strain in this plateau is called the yield point elongation, or Lüders strain. Finite element analyses can be performed to simulate this phenomenon, and they can, in turn, be coupled with the previous strain aging model to simulate the bake hardening phenomenon. Literature also shows that small grain sizes are responsible for an increase in both lower yield stress and yield point elongation, with a behaviour that can be described by the Hall-Petch equation [8]. Higher strain rates also have the same effect.

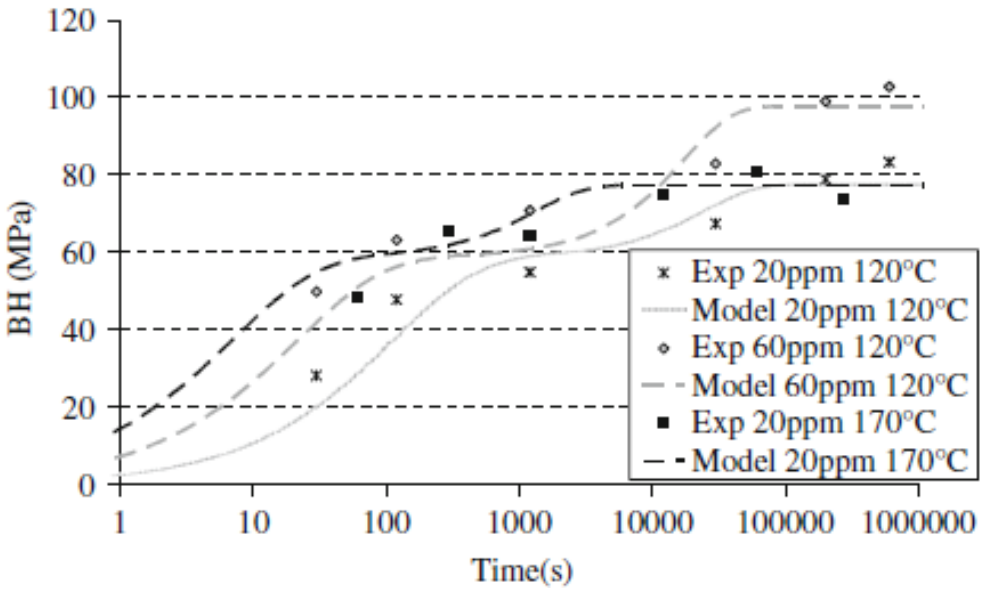

Figure 4. Influence of temperature and carbon content on bake hardening effect of steel [7].

It must be remarked that the previous model was only validated for uniaxial tension. However, the deformation mode in a dent test is closer to balanced biaxial stretching. For this loading condition, a polycrystalline homogenization model was proposed [9], in which the activation of slip systems is strongly dependent on the strain path.

Thuillier et al. [10] proposed a comparison between numerical simulations and experimental data of dent tests of an E220BH steel. Moreover, an example of the

procedure to be followed for baking is given. First, the oven is heated up to the required temperature for at least 100 minutes; the specimens are then placed in the oven and kept there for 15 minutes, then they are removed and cooled down to room temperature. It should be remarked that the temperature profile of the specimens while they are in the oven is not constant, as shown in *Figure 5*: there is a considerable temperature drop when the oven is opened and the specimens are first inserted into it, so the average temperature will be lower than that which was reached in the oven in its steady state condition prior to being opened. Therefore, temperature control is a crucial aspect of any experimental work.

Regarding the influence of pre-strain, Thuillier et al. found that bake-hardening effect decreases with increasing pre-strain, although theory and phenomenological models suggest an opposite trend [11]. This correlation is not always clear for aluminum alloys and would be an interesting aspect to investigate in future research.

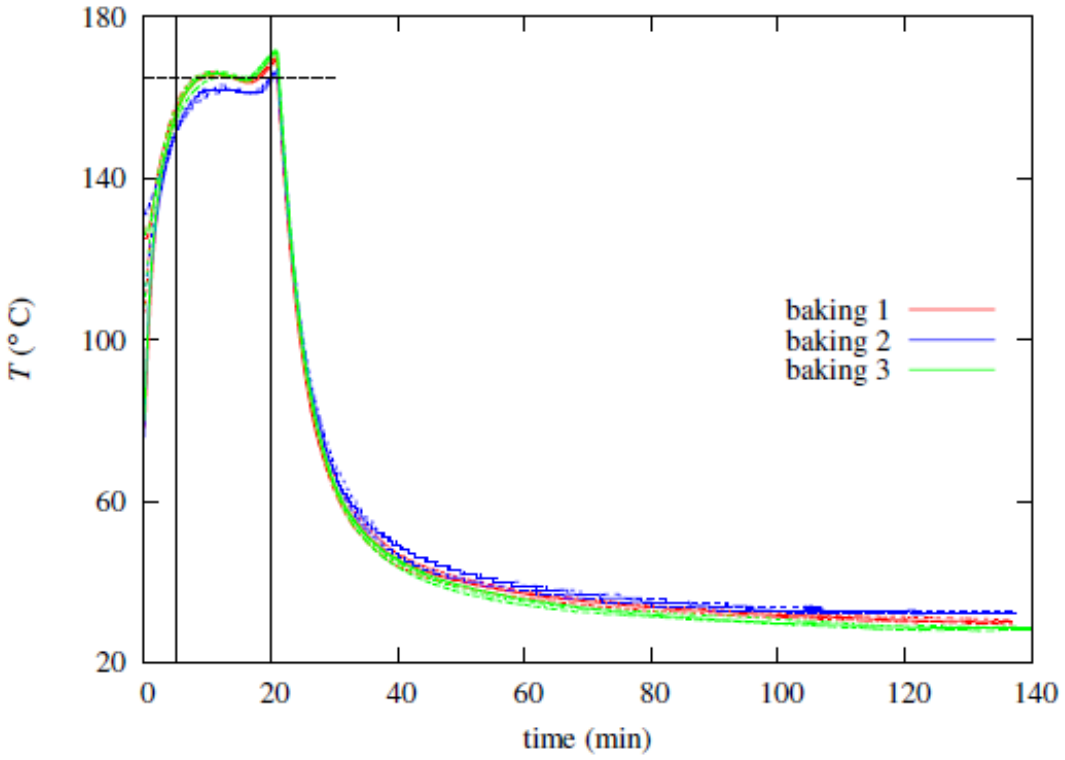

Figure 5. Temperature profile of steel samples bake-hardened for 15 minutes in a furnace at an average temperature of 165°C [10]

Experimental results of dent tests revealed that the applied load increases with the bake hardening effect, therefore for a given load the residual displacement is slightly lower. *Figure 7* shows this tendency. The shape of the loading-unloading curve is highly nonlinear and energy dissipative, as expected from such a test.

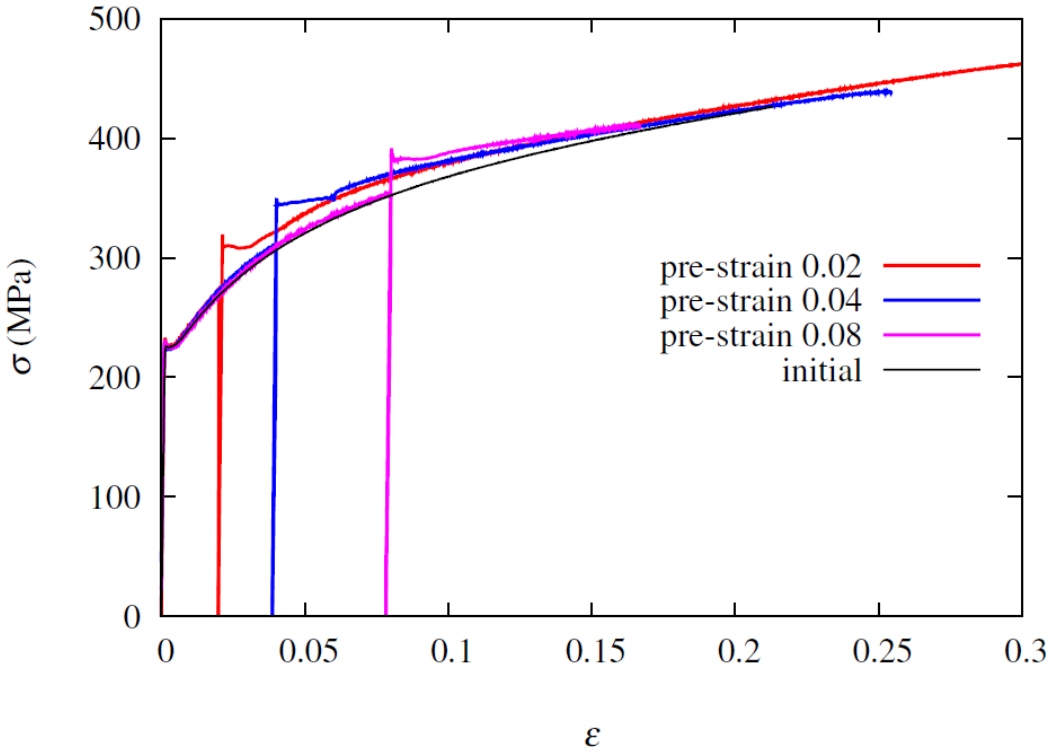

Figure 6. Effect of pre-strain application on an E220BH steel [10].

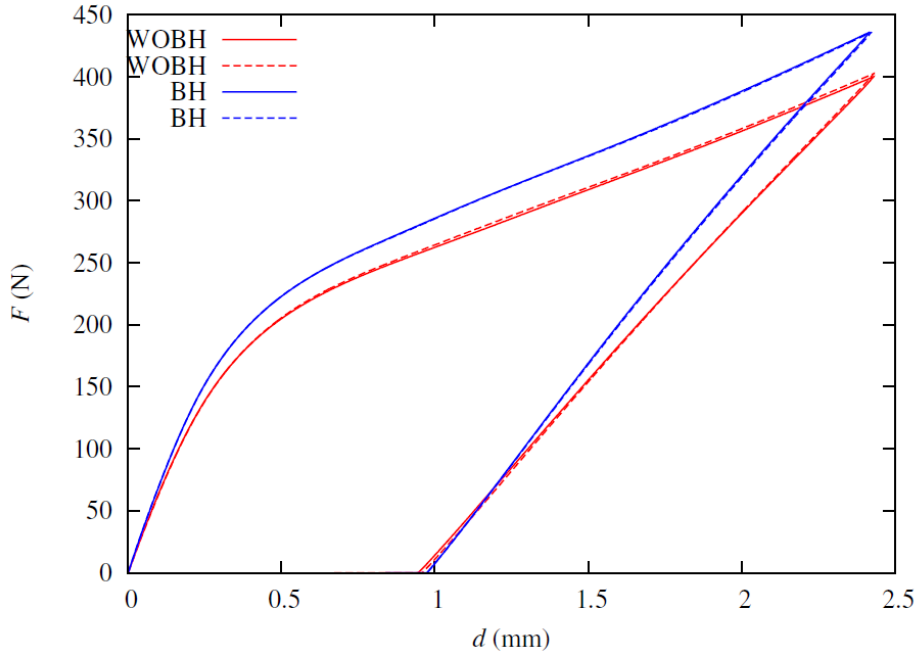

Figure 7. Loading-unloading curves obtained from dent tests of E220BH steel [10].

Finally, Thuillier et al. proposed a numerical model of bake hardening to apply in simulations, considering constant baking temperature and time. An equivalent stress function is introduced:

$$\bar{\sigma} = \sigma_Y - f\Delta\sigma \quad (4)$$

where σ_Y is described by the following equation:

$$\sigma_Y = K(\bar{\epsilon} + \epsilon_0)^n \quad (5)$$
$$\epsilon_0 = (\sigma_0/K)^{1/n} \quad (6)$$

where K(a strength parameter), n (the strain hardening exponent) and σ_0 are material dependent. Parameter f is equal to 1 when the material is bake hardened. The term $\Delta\sigma$, in fact, represents an overstress due to bake hardening:

$$\Delta\sigma = C_1\left(\left(2exp - \gamma_1(\bar{\epsilon} - \bar{\epsilon}^*)\right) - \exp(-\gamma_1\bar{\epsilon})\right) \quad (7)$$

where C_1 and γ_1 are material dependent parameters.

For aluminum alloys, the Voce law is more suitable to describe material hardening. In a power-law relationship the stress tends to infinity as the strain increases, which is experimentally incorrect since the true stress reaches a saturation level [12]. The Voce law is expressed as follows:

$$\sigma = \sigma_s - (\sigma_s - \sigma_0)exp[-k(\varepsilon - \varepsilon_0)] \quad (8)$$

where σ_0 is the true yield stress, ε_0 is the true plastic strain at the onset of plastic deformation and σ_s is the saturation stress at large strain values.

Thuillier et al. took advantage of this phenomenological description and defined a minimization problem of a cost function related to the set of material parameters introduced in the previous equations, based on a least squares approach. The equations were then implemented into a finite element Abaqus code, for plane stress conditions. Despite this simplified assumption (dent tests involve 3D stress states), and despite the

bake hardening level being determined only from uniaxial tension tests, the numerical results were consistent with the experimental data.

2.3 Effects of pre-aging and pre-straining

There are many ways to improve the bake hardening process. Juijerm et al. [13] proposed that the bake hardening effect can be enhanced by pre-aging processes. The alloy they used was an AA6110 aluminum alloy, and it was pre-aged immediately after quenching for about 15 minutes, at temperatures ranging from 135°C to 200°C. Results showed that strength and hardness improved with increasing pre-aging temperatures, as faster kinetics for solute elements are involved. This allows to counteract the negative effect of natural aging on bake hardening. However, such considerations are outside the scope of this project, since it aims to minimize the energy spent during the baking process while still obtaining a good increase in material strength. Adding another pre-aging phase to the manufacturing process would only increase the energy required.

Experiments conducted on a 6xxx series aluminum alloy [14] showed the beneficial effect of pre-aging on the bake hardening value (*Figure 8*). It was found that the optimal temperature which gives a peak in bake hardening enhancement is 160°C. At this temperature, the precipitation activation energy of the β'' phase, which is a metastable form of Mg_2Si responsible for the bake hardening response, is minimized. Furthermore, the pre-aging treatment causes an enlargement of the so-called Guinier-Preston (GP) zones, solute enriched areas that are ideal for nucleation of β'' phases and the consequent pinning of dislocations. However, without pre-aging, the baking phase causes a dissolution of the GP zones and a consequent decrease of the BH response.

Zhong et al. [15] found that pre-aging is responsible for a reduction in stretch formability. However, as a countereffect, alloy composition positively increases formability. For instance, increasing the Si content in a 6xxx series alloy leads to increased work hardening capability; and a similar effect can be obtained by adding 0.3% Cu by mass.

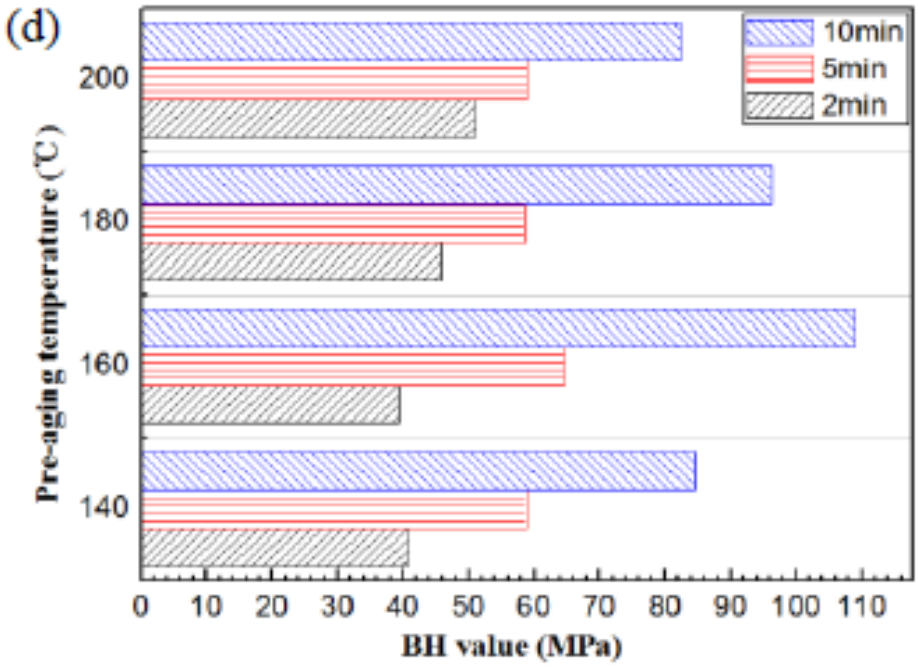

Figure 8. Pre-aging temperature influence on BH value [14].

With or without pre-aging, it is important to be aware of the effect of natural aging over time, as well as the influence of a pre-strain. Hirth et al. tried to correlate the aging behaviour with the volume fraction of Si in solution in a AA6016 alloy [16]. The natural aging process was found to be represented by a logarithmic law having the following form:

$$\sigma_t = \sigma_0 + k \cdot \log(t) \quad (9)$$

where σ_t is the yield strength after time t, σ_0 is the initial yield strength and k is a constant that accounts for aging kinetics. It was found that the Si content does not affect the aging kinetics, but a higher Si volume fraction available in solution for cluster hardening causes the initial strength σ_0 to increase. This is true up to a saturation level, at which Si exceeds the Mg availability to form metastable clusters. The copper content of the alloy seems to accelerate natural aging kinetics, since Cu is responsible for the precipitation of $CuAl_2$ phases [17]. In bake response, strength weakly increases with increasing Si levels. This suggests that the overall bake-hardening effect depends mainly on an improved solute strengthening by free Mg atoms.

Wuebbels et al. [18] studied the influence of room temperature aging on the BH value of automotive steels. This is a reasonable concern, as BH values obtained in standardized laboratory tests could be different from the results obtained in actual panel production processes because of the different strain paths that develop throughout body panels, or because of different aging times due to time delays between forming and painting and other logistical reasons. What they found is that without pre-strain, mechanical properties remained substantially the same after ambient aging. Thus, in this case bake hardening values are independent of natural aging time. When, instead, the samples were 2% pre-strained and then aged, strain aging occurred, and it increased with time. This can suggest that pre-straining is a source of new mobile dislocations, which leave new free sites for solute atoms segregation. On the contrary, the BH value was found to decrease with increasing aging time. Furthermore, the activation energy of the aging kinetics was found to be higher than the activation energy of the sole solute diffusion (carbon in the case of these steels): therefore, other factors probably contribute to aging, such as solute atoms clustering or rearrangements of dislocations; many factors remain unknown and should be the object of future research. However, it is interesting to notice that the total bake hardening increment, which is the sum of hardening due to aging and hardening due to baking, remained approximately constant, regardless of the aging path (*Figure 9*).

This is an interesting conclusion, as it shows that the overall hardening value with respect to the as-received material will be the same, regardless of the aging history (considering a fixed baking temperature; the 50°C and 100°C temperatures in the graph refer to the two ambient aging temperatures that were considered).

Even though the previous results refer to steels, they could be applied to some extent to aluminum alloys, as they match with the information provided by a global OEM for the 6xxx series alloys that have been tested in this project. According to the OEM, aging after pre-straining has negligible effects on hardening, and this is consistent with what has been found by Wuebbels et al. for steels. After pre-straining, instead, natural aging is said to have influence on mechanical properties, but it is overridden by the subsequent baking phase; therefore, a hypothesis like the constant overall hardening value described before should be applicable. Finally, once the specimens are baked, there are no further changes in properties at room temperature.

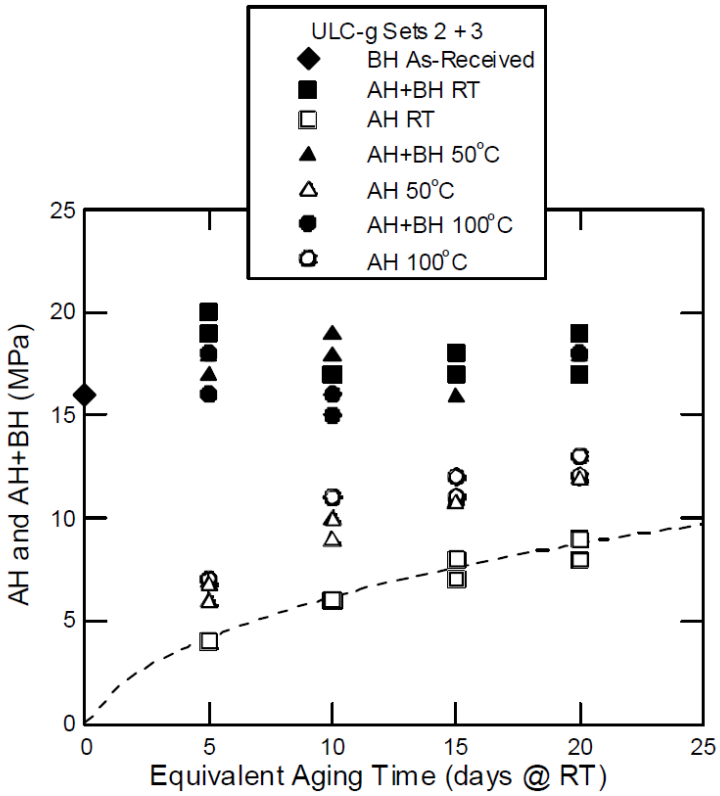

Figure 9. Influence of natural aging and baking on the total BH increment [18]

2.4 Standard procedures for bake hardening experiments

Careful experimental evaluation of the bake-hardening phenomenon is key to collecting reliable data that can be useful for the design & production of future vehicles and sub-assemblies made of these materials. In order to gather trustworthy data, experimental testing procedures must be as compliant as possible to existing standards. They must also be consistent throughout the entire testing phase and reproducible.

The European standard BS EN 10325:2006 defines the experimental procedure and the determination of strength increase due to baking [4]. Standard bake hardening assessment is made starting from a 2% plastic pre-strain and then baking the specimen at 170°C for 20 minutes. Pre-straining is performed at the same constant rate up to 2%, with a 0.05% tolerance. For baking, the prescribed temperature is 170°C ± 2°C, kept for 20 ± 0.5 minutes. The bake hardening index is computed as the difference between the tensile strength of the 2% pre-strained test piece $R_{p2,r}$ and the lower yield strength of the specimen after the heat treatment $R_{el,t}$ (calculated considering the cross section of the pre-strained specimen):

$$BH = R_{el,t} - R_{p2,r} \quad (10)$$

As discussed before, the strength of the specimen after pre-strain that must be considered for BH value computation increases with time after pre-strain because of natural aging. Thus, BH value computed in this way will decrease as aging time (i.e., the time span between pre-straining and baking) increases; it is the total bake hardening increment that will remain unchanged. This leads to the conclusion that, if the standard BH assessment is applied, the least possible amount of time should be allowed between pre-straining and baking. A good choice would be to perform the two processes within the same day. In this way, the effect of natural aging will be negligible, and equation (10) could be correctly applied. Otherwise, strengthening due to strain aging should be considered and removed from the bake hardening strengthening value.

It must be pointed out that tensile properties are useful to classify and catalog materials, or define their properties in a standardized way, but they are far from representative of actual formed parts: when formed, body panels are subjected to more complex strain paths. For this reason, an experimental part focusing on pan-shaping aluminum specimens and performing dent tests on these deformed parts is suitable to obtain a wider perspective on the influence of bake hardening phenomenon in actual formed automotive panels. Shi et al. [19] found that bake-hardenable steels perform better than non bake-hardenable ones, both in static and dynamic dent testing. Data gathered through these types of tests will be closer to industrial process conditions, so they will be complementary to the ones collected by tensile tests, thus providing a more complete and accurate experimental analysis.

2.5 Conclusions from the literature review

The aim of this literature review was to provide a general overview of the strengthening that is achieved by baking aluminum alloys and to consider the factors affecting this strengthening. Furthermore, it also presents the theoretical background that is necessary to undertake an experimental investigation. Indeed, it is important to have an understanding of the microstructural phenomena responsible for the bake hardening effect so that a series of experiments can be planned, carried out and correctly analyzed to determine the effects of aging, straining and heat treatments on the material's behaviour. The time span between the application of the pre-strain and the

baking was found to be critical, whereas the mechanical properties remain stable after baking, and therefore subsequent tests do not need to be carried out within a specific time frame.

3 Experimental procedures

Having in mind the background provided by the literature review presented in the previous chapter, and having defined the objective of this research, it is now possible to develop the methodology of the present work. The first step consists in the selecting sheet materials for the investigation and then establishing an experimental test matrix that specifies a practical range for each of the critical bake hardening process parameters (i.e. time and temperature). Then, meticulous testing procedures must be determined in order to obtain accurate and repeatable results. The mechanical properties and bake hardening response of the sheet materials are assessed through two characteristic tests: tensile tests and dent tests. In this way, not only is it possible to perform a standard validation, but the material is also tested in conditions that are close to real life applications, such as a door panel subjected to an indentation by impact from an outside object.

The following step is the results analysis: for each temperature-time condition, the force and displacement data exported by the tensile machine are imported into MATLAB, so that the yield strength can be obtained. The results must be graphically presented in a clear way, considering the effects of all the parameters affecting the process. Furthermore, the reliability of the tests that were performed is assessed in terms of variance and standard deviation.

3.1 Identification and selection of sheet materials

This investigation focuses on 6xxx series aluminum alloys whose main alloying elements are magnesium and silicon. These sheet materials are commonly used to stamp outer body panels as well as high strength structural parts or parts that still require improved formability [2]. The suppliers provided six different alloys of interest and these are shown in *Table 1*. From those six, five were tested, as the last one remained untested due to technical issues. All the alloys were tested in uniaxial tension, whereas only the alloys for external applications were subject to dent testing.

Table 1. List of alloys provided for the tests and their origin.

	North America		EMEA	
Grade	**Alloy/Temper**	**Supplier/Region**	**Alloy/Grade**	**Supplier/Region**
AA6000-IH90 Outer	IH90US	Novelis NA	IH90EU	Novelis EU
AA6000-HF90 Outer	HF90	Arconic		
AA6000-BR100	BR100US	Novelis NA	BR100EU	Novelis EU
AA6000-HS170			HS170	Novelis EU

In order to better understand the variations between these sheet materials it is useful to define their nomenclature. 6xxx series aluminum alloys are Al-Mg-Si age-hardenable alloys, and their general coding system has the following form:

AA6XXX – (grade designation code) – (pre-treatment) – (surface quality)

In the base alloy designation, the first digit "6" indicates that the principal alloying elements are silicon and magnesium; the second digit, if different from 0, denotes a modification with respect to the original alloy. The last two digits are used to identify various alloys within the group. The following two-letter code indicates special processing categories: BR designates an alloy with an improved "bake response", HF signifies a "higher formability" alloy, HS means a "higher strength" alloy and finally, IH indicates an alloy developed for "improved hemming" performance. Then, a code indicates the temper designation, and in our case, the T4 designation means that the alloy has been solution heat treated and naturally aged prior to its delivery to the carmaker. This is achieved by a continuously feeding the sheet through an induction oven which heats the metal to 500-520°C (near the melting point) for a few seconds. Then, the sheet is quenched to ambient temperature by means of vapor jets [20]. The phase diagram shown in *Figure 10* shows that high temperatures during solubilization allow for a higher concentration of the Mg_2Si phase in solid solution. Obviously, the temperature must be kept below the threshold of 595°C to avoid any melting. In the end, the alloy is subjected to natural aging during its stocking and shipment. A letter at the end of the alloy designation indicates the surface quality: U for unexposed and E

for exposed. Finally, a term is also assigned (P1 or P2) referring to coil pre-treatments for adhesive bonding; if no pre-treatment is needed, the code is NP.

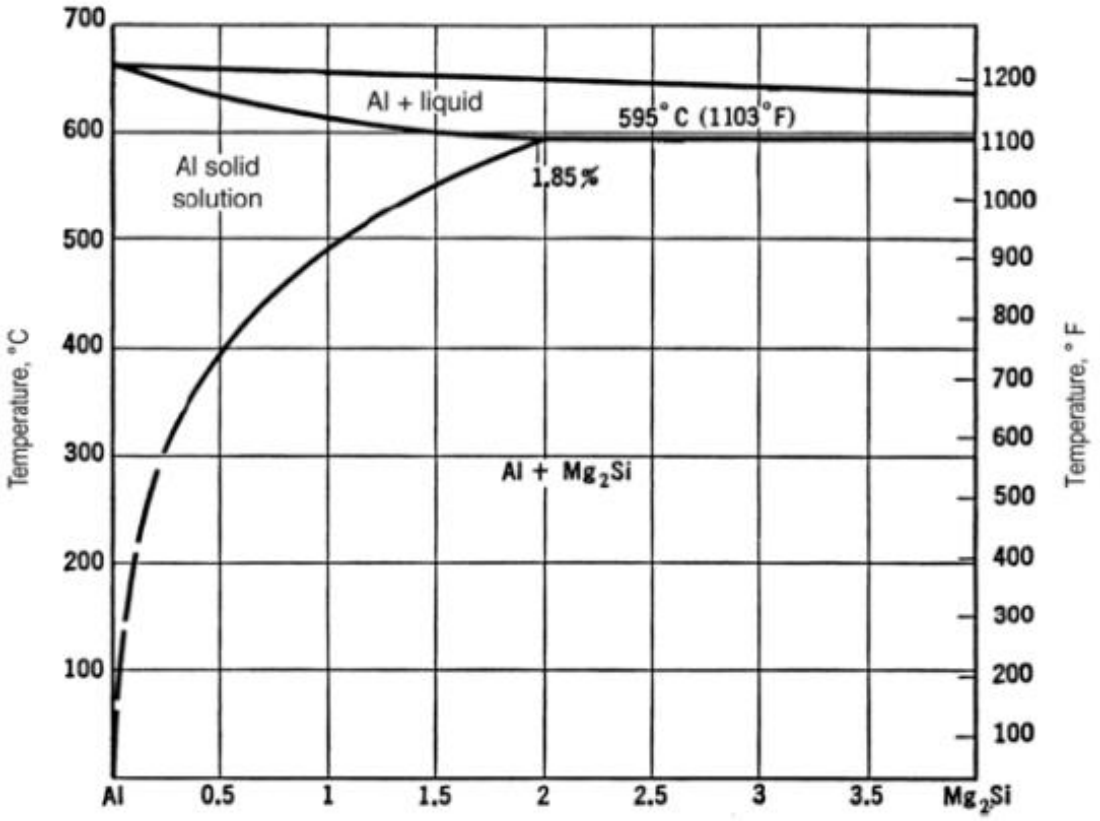

Figure 10. Al-Mg_2Si phase diagram (Kammer (1999), Warmuzek (2004)).

The chemical composition of the aluminum alloys is shown below in *Table 2*. The absence of the HF90 alloy and the ranges of composition of the IH90EU and BR100EU alloys are due to confidentiality reasons.

Table 2. Chemical composition of the selected 6xxx alloys, in percentage by mass.

	Si	**Fe**	**Cu**	**Mn**	**Mg**	**Cr**	**Zn**	**Ti**
IH90US	0.77	0.21	0.24	0.14	0.61	0.02	-	0.01
IH90EU	0.5 to 1.5	0.35 max	0.25 max	0.20 max	0.25 to 0.9	0.15 max	0.10 max	0.15 max
BR100US	0.79	0.24	0.12	0.084	0.64	0.026	0.008	0.027
BR100EU	0.6 to 1.5	0.35 max	0.25 max	0.35 max	0.2 to 0.8	0.10 max	0.20 max	0.15 max

A total of six alloys, belonging to four different categories, were selected in consultation with industrial advisors. The IH90 series is suitable for exposed Class-A

panels (i.e. outer hood, outer door). This type of alloy was shipped from both European and North American suppliers.

The HF90 series alloys are employed for complex outer parts requiring improved formability. This type of alloy was provided by Arconic US.

The BR100 series, which is developed to exhibit an improved bake response, is used for unexposed panels requiring better formability (ex. inner hood, large structural parts). Again, both European and North American suppliers provided this type of alloy.

The HS170 series, which is suitable for high strength structural parts, was sent by Novelis US and was the one that unfortunately was not possible to test.

The given expected mechanical properties were consistently obtained from specimens whose longitudinal axis was at 90° with respect to the rolling direction of the coil.

3.2 Experimental test matrix

The basis of the experimental part of the project is a test matrix like the one in *Table 3* for tensile tests. Different temperature-time conditions are taken into account, and there is a motivation for the choices that were made. In fact, the current OEM assembly paint process includes bake cycles of 20 minutes at a temperature range from 170°C to 180°C. This thermal cycle is based on recommendations from paint chemical suppliers and is needed for full cure of paint layers. However, new developments by the chemical suppliers of the OEM painting systems have the potential to lower the baking temperature to a range between 120°C and 130°C and/or will allow for a reduction in the oven dwell time from 20 minutes to 10 minutes. Temperature of 110°C and 150°C were added to the matrix to check the overall behaviour in bake response of the selected alloys.

Additionally, the effect of ambient temperature storage is also taken into consideration into the matrix. Finally, the effect of 2% pre-strain compared with the no-pre-strain condition is also considered. The method adopted to obtain a 2% pre-strain will be explained later in this chapter.

Table 4 shows the experimental test matrix for dent tests: the temperature ranges are the same, apart from the two lowest levels that are not considered (23°C and 110°C). Again, both 0% and 2% pre-strain levels are applied (note that in this case a 2% biaxial strain was considered, which means that the effective strain will be greater than 2%).

Table 3. Tensile test matrix – bake response

Time Temp.	**10 min**	**20 min**	**2% PS 10 min**	**2% PS 20 min**
23°C		AR		AR
110°C		X		X
120°C	X	X	X	X
130°C	X	X	X	X
150°C		X		X
170°C	X	X	X	X
180°C	X	X	X	X

Table 4. Test matrix for dent resistance tests on sheet materials for outer panels.

Bake Temperature	**10 min**	**20 min**
120°C	X	X
130°C	X	X
170°C	X	X
180°C	X	X

3.3 Experimental setup

3.3.1 Tensile test equipment

The “dog-bone” specimens were obtained using a wire-EDM (wire electrical discharging machining) process. The machine used is of the type AgieCharmilles CUT E 600. More in detail, the workpiece is machined thanks to a series of discrete sparks between the workpiece itself and a tool electrode, which is a wire located in a liquid dielectric medium (deionized water) [21]. In this case, the wire diameter was 0.25 mm. During the process, the dielectric medium is removed from the sparking spot; then, the electrical discharge melts and vaporizes the workpiece, and the metal scraps are moved away by the dielectric. The amount of energy associated with the sparks affects the surface finish. And the displacement of the wire is numerically controlled so that the final tensile specimen is machined to the specified geometry.

Tensile tests and pre-straining were performed using a 50 kN capacity MTS machine (*Figure 11*). The specimen is clamped by two arms and pulled to fracture or up to a pre-defined condition. Its load cell, which has a sensitivity of 2.099 mV/V, records the force over time. The displacement is measured by an MTS axial extensometer having a 50 mm gauge length (*Figure 12*). The testing apparatus is controlled by means of the MTS Suite software that allows to design the test procedure and select which set of data is exported. A digital caliper with 0.01-mm accuracy was used to measure the width and thickness of the specimen gauge before each test.

Figure 11. MTS Tensile testing apparatus.

Figure 12. MTS axial extensometer.

The baking process took place in a Quincy Lab bench convection oven (*Figure 13*). The model which is present in the Lab (the 21-350 ER) is embedded with a PID microprocessor for temperature control. It has a 198-liter capacity, and its temperature range lies between ambient temperature and 232°C (450°F) [22]. The structure of the oven is schematically shown in *Figure 14*. Being a convection oven, air circulation is fan-forced; it has Incoloy sheathed heating elements and an aluminized interior. Insulation is obtained by means of a 6-lb high-density mineral wool layer. Temperature stability is regulated by a thermostat, while the design of the air plenum and mixing chamber allows for an evenly heated horizontal circular flow. Heavy-duty chrome plated wire shelves can support up to 80 lbs and allow for up to 56 square feet of shelf surface. The oven is powered by 115 V, 50/60 Hz single-phase current.

Figure 13. Convection oven employed for tensile specimens.

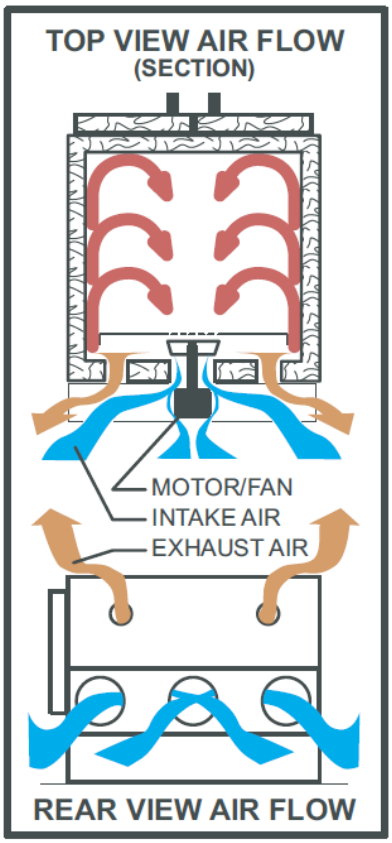

Figure 14. Schematical representation of the Quincy Lab convection oven [22].

Since the standards prescribe to start the baking time when the specimen temperature reaches 2°C below the steady-state value, the temperature value displayed by the oven (which refers just to the temperature inside the oven itself) is not sufficiently precise. For this reason, type-k thermocouples connected to a multimeter were employed: they were inserted through a small hole in the oven and directly attached to the specimen surface. Basically, any thermocouple takes advantage of the so-called Seebeck effect: a temperature gradient which is generated in an electrically conductive material generates a voltage. If two different conductive materials are "coupled" such that they both experience the same temperature gradient, a voltage difference can then be measured between them (*Figure 15*). In a thermocouple, the cold junction is kept at a reference temperature, while the hot junction is connected to the probe [23]. The voltage difference, which increases with temperature, can be measured at the cold junction and is usually between 1 and 70 μV/K. Therefore, what is actually measured is not the absolute temperature of the specimen, but the temperature difference between the specimen itself and the cold junction. In the past, the reference

temperature at the cold junction was usually maintained by means of an ice bath at 0°C. Nowadays, a more practical solution is adopted called *junction compensation*,. This approach basically consists in building an artificial cold junction by using thermally sensitive devices such as diodes or thermistors, which can measure the temperature at the input connections to the instrument (i.e., the multimeter).

The two conductive wires in the type-k thermocouple that was used in these tests are both nickel alloys: Chromel (90 % nickel and 10 % chromium) and Alumel (95% nickel, 2% manganese, 2% aluminium and 1% silicon). The sensitivity of type-k thermocouples is around 41 μV/K. It is important to make sure that the two wires are in contact at the hot junction level so that the circuit remains closed. This can be done by installing a cap at the tip or by welding the extremity, as was done in this work.

The adoption of thermocouples helped to obtain accurate real-time temperature measurements of the surface of the specimens, instead of considering a fixed time for the ramp-up phase and then starting to count the baking time. To initially check and plot the temperature-time profiles at the surface of the specimens, as well as temperature uniformity in the oven, other type-k thermocouples were inserted into the oven and plugged into a PC using the Labview software.

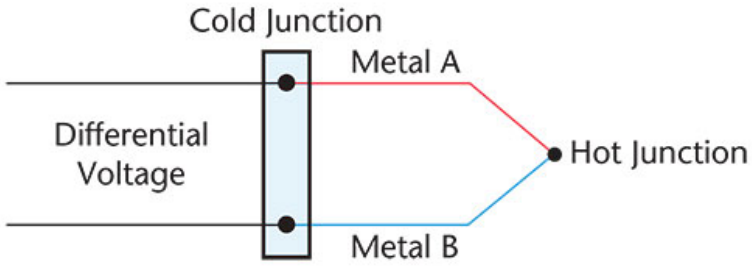

Figure 15. Basic schematic of a thermocouple.

3.3.2 Dent test equipment

The dent tests were conducted at the Novelis plant in Novi, Michigan. A hydraulic press was employed to stretch-form a blank measuring 355 mm × 355 mm into a circular, pie-pan-shape, having an external diameter of 300 mm, and a 2% biaxial strain across the flat central portion.

Figure 16. Novelis' hydraulic press for stretch-forming dent-test specimens.

A mechanical convection oven (a Thermo Scientific Heratherm OMH180-S) was used for baking the dent test specimens (*Figure 17*). Its volume is 170 liters, and the operational temperature ranges from 50°C to 330°C. The guaranteed temperature special uniformity is ±1.5°C at 150°C, with a sensitivity of ±0.2°C. The supply voltage is 208-240 V with 60 Hz frequency [24]. Like the previous oven, it is PID controlled; an electrically controlled fresh air damper provides control over air exchanges. The fan's high-speed setting was selected as it ensures faster heating and recovery, as well as better temperature stability and uniformity. The inner chamber is made from corrosion-resistant stainless steel (AISI 304).

Figure 17. Thermo Scientific Heratherm OMH180-S convection oven.

The dent test apparatus used at Novelis' facility is shown in *Figure 18*. This test consists of raising a pendulum having a mass (the indenter) attached to a swing arm up to a specified level and allowing it to swing down and impact the pie-pan specimen that is held in place by a fixture at the bottom of the support structure. The kinetic energy of the indenter, which is the impact energy associated to a potential energy due to at a certain initial angle, is partially transferred to the workpiece as deformation energy, thus generating an indentation. Different indenters are available, each one with a different mass, so that the impact energy can be selected by considering both the initial angle and the indenter mass.

Figure 18. Mechanical pendulum for dent tests.

The indentation in the pie-pan specimen was measured after the dent test: its diameter was evaluated using a circle template, while its depth was measured by a Mitutoyo Absolute digital indicator, whose accuracy was 0.01 mm.

Figure 19. Mitutoyo digital depth indicator

3.4 Experimental procedure

The aluminum sheets were supplied as rectangular blanks with the rolling direction clearly marked, as the mechanical properties were to be determined at 90° with respect to the rolling direction, in compliance with the OEM's procedures.

The first step was to obtain two types of specimens: uniaxial tensile specimens and dent test specimens. The tensile specimens were prepared according to the ISO 527-2 standard (*Figure 20*), with a gauge length of 50 mm, and the nominal thickness of each sheet material is provided in *Table 5*.

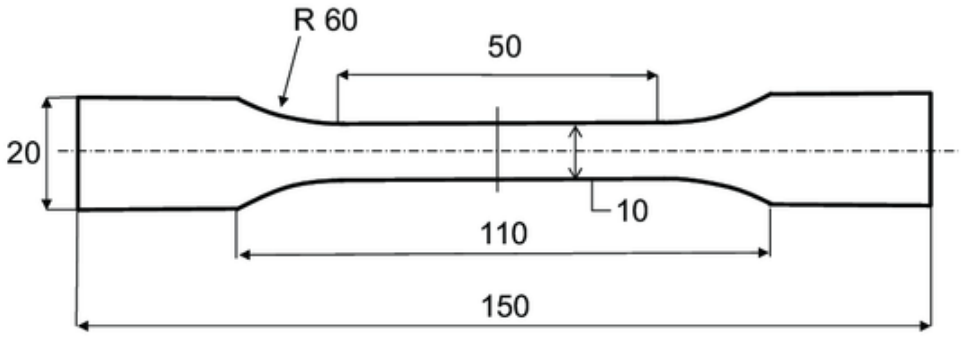

Figure 20. ISO 527-2 standard tensile specimen (dimensions in mm).

Table 5. Nominal thickness of each aluminum alloy sheet.

	Sheet Thickness
HF90	1 mm
IH90US	1mm
IH90EU	1 mm
BR100US	0.9 mm
BR100EU	0.8 mm
HS170	2.5 mm

The dent test specimens were square blanks each measuring 355 mm × 355 mm, according to the equipment requirements. The blanks that were received from each supplier were sheared to the required size using a manual shear.

3.4.1 Tensile testing procedures

The tensile specimens were obtained by wire-EDM, with the loading axis always oriented at 90° with respect to the coil rolling direction, since this is consistent with the OEM's practice.

First, the mechanical properties and flow behaviour of the "as received" sheet materials were determined by carrying out three repeat tensile tests up to fracture for each alloy. Each specimen was mounted in the machine grips by closing the clamps at its extremities. Attention was given to the load value displayed by the MTS Testsuite operating software (see the screenshot of the software in *Figure 21*); indeed the load on the specimen must be reduced to zero after clamping and prior to the start of the test. This was done by means of the scroll button on the portable controller (*Figure 22*). In addition, the test procedure were modified depending on the desired end condition: tests taken to fracture were terminated by the break detection, whereas tests carried out to pre-strain a specimen were terminated once a pre-defined strain threshold was reached. The crosshead displacement rate was set to 2.5 mm/min for all tensile tests, which corresponds to an average strain rate of 0.05 1/min in the gauge. Finally, the data acquisition rate was 10 Hz.

For each test, the engineering stress, S, and the engineering strain, e, were calculated from the experimental force-displacement data as follows:

$$S = \frac{P}{A_0} \qquad (11)$$

$$e = \frac{\Delta L}{L_0} \qquad (12)$$

where P is the load in N, A_0 is the initial cross section area, ΔL the difference between the deformed length and L_0, the initial gauge length.

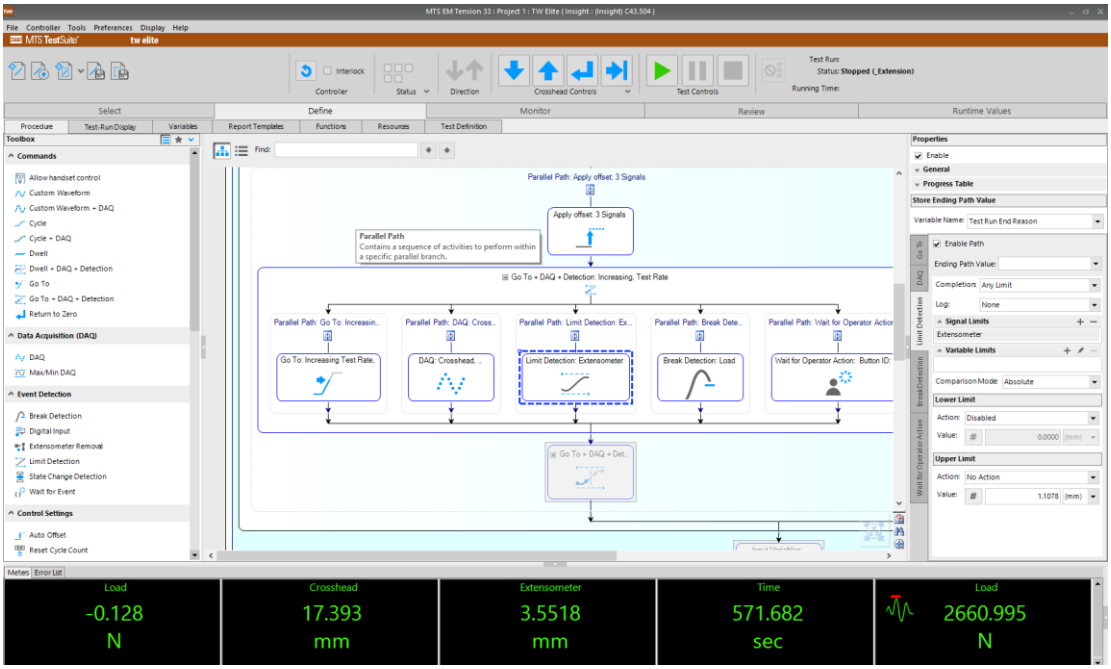

Figure 21. Screen view of the MTS TestSuite software for carrying out tensile tests

Figure 22. Tensile machine portable controller.

An example of an engineering stress-engineering strain curve is shown in *Figure 23*. The 0.2% offset yield stress was determined by, first, selecting some data

points in the initial elastic portion, and performing a linear regression of these data points using MATLAB in order to obtain Young's modulus, which is the slope of the linear elastic stress-strain curve (*Figure 24*). A suitable number of points is selected to interpolate so that Young's modulus is close to the usual value of 70 GPa for aluminum alloys. The yield stress was then determined as the intersection of the stress-strain curve with a line having the same slope as the elastic modulus and offset by 0.2% strain (*Figure 25*). These results were then be compared with the mechanical properties provided by the Stellantis material database to verify that they were consistent.

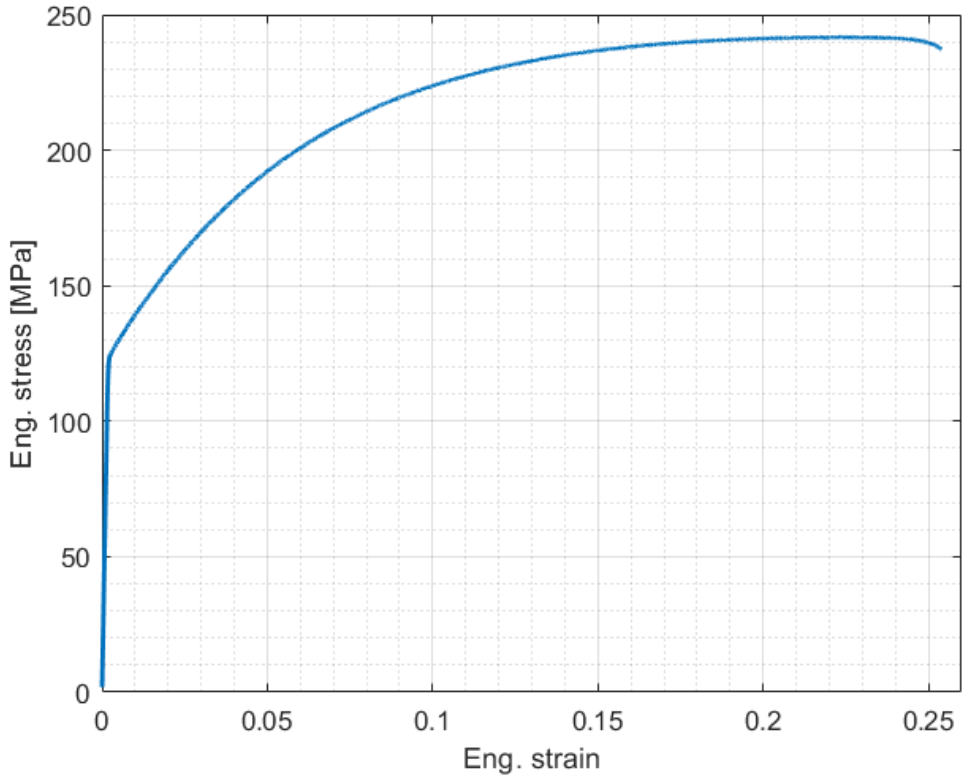

Figure 23. Engineering stress-strain curve of BR100 aluminum alloy.

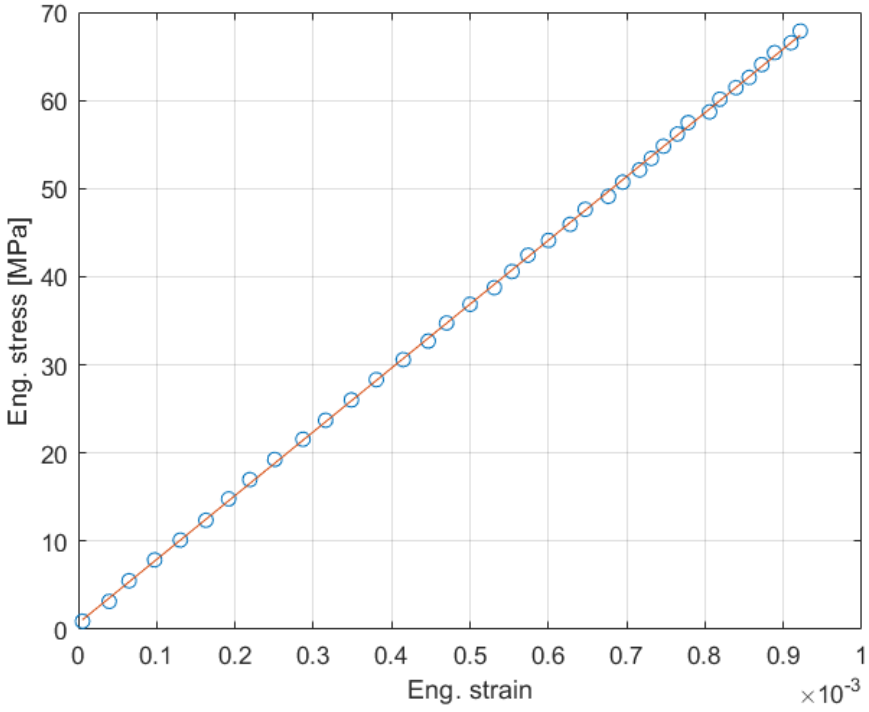

Figure 24. Linear regression of the elastic portion of the stress-strain curve.

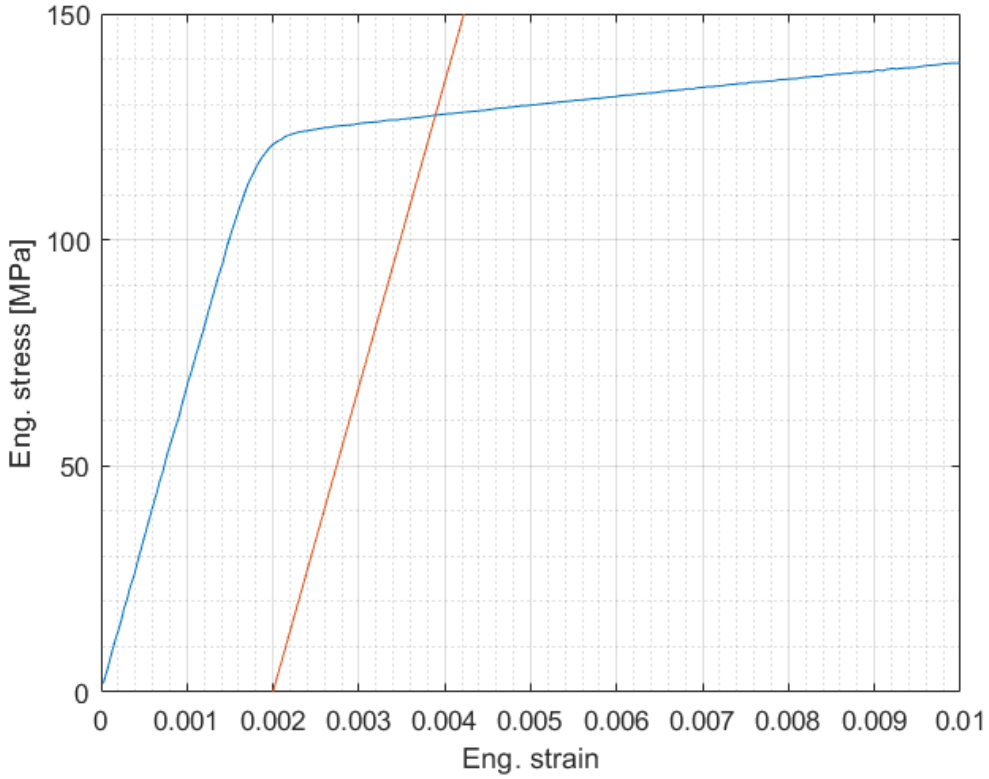

Figure 25. Determination of the 0.2% offset yield stress.

Approximately half of the tensile specimens required to be prestrained to 2% plastic strain. In order to interrupt the test at the right moment, a limit strain value slightly greater than 2% should be specified to the MTS Testsuite software, since the 2% prestrain is the plastic strain that remains after the specimen is unloaded. The limit strain value was determined as the average total strain obtained from the previous three tensile tests on "as received" specimens that corresponded with a 2% plastic strain after unloading: for each test, the stress-strain curve was intersected with a straight line having the same slope as the elastic modulus, but this time with a 2% strain offset. The intersection point gives the total strain value at which the machine is set to stop the test. And the average of these three values was the strain reference for the considered aluminum alloy. Finally, the total strain value was converted to an extensometer displacement considering a 50 mm gauge length:

$$extensometer\ displacement = \frac{strain\ (in\ \%)}{100} \cdot 50 \qquad (13)$$

The obtained value was then entered into the software as a termination condition (*Figure 26*). The Standard prescribes that the accuracy of 2% pre-strain value should be 0.05%, so the average strain value must be precise enough to fulfil this requirement.

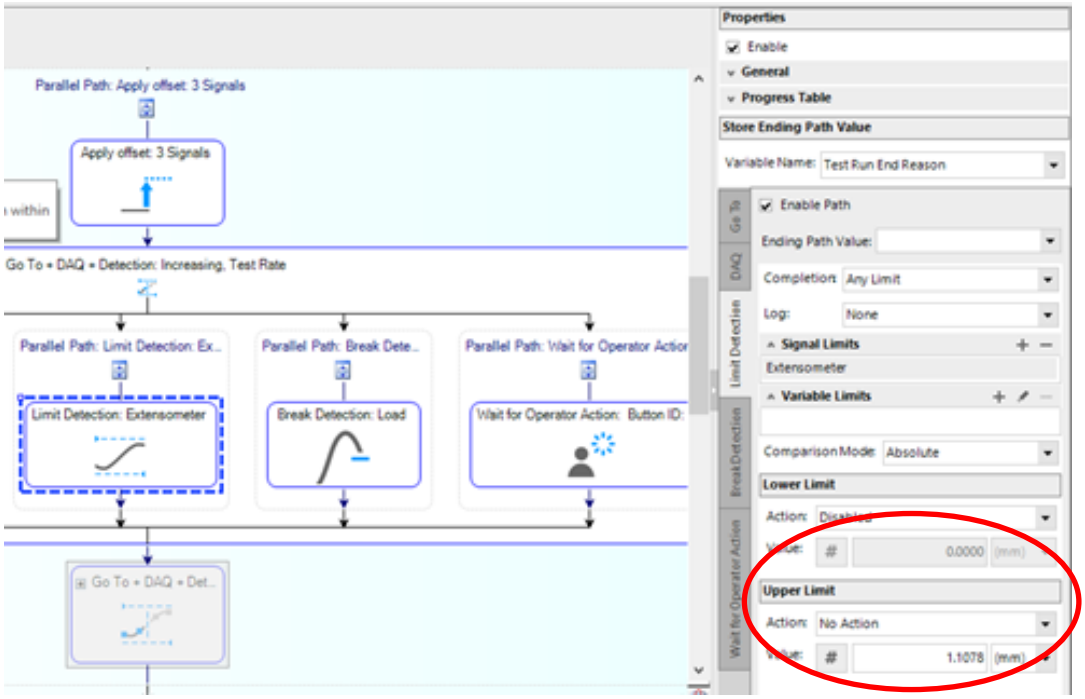

Figure 26. Termination condition for pre-straining a tensile specimen

The following MATLAB code was written in order to satisfy the previous computations.

```
clear all
close all
clc
T = readtable('Test3nuovo_HF90_mat.xlsx');
T = T{:,:}
x=T(1:15,1);
y=T(1:15,2);
n=1;
p = polyfit(x,y,n);
f = polyval(p,x);
figure
plot(x,y,'o')
hold on
plot(x,f)

%% Engineering curve
x_eng=T(1:4000,1);
y_eng=T(1:4000,2);
figure
plot(x_eng,y_eng)
grid on
hold on

%% Yield strength
m=p(1);
x_line=linspace(0,0.004,2000);
y_line=m*(x_line-0.002);
plot(x_line,y_line)
hold on

%% Strain to get 2%
x_pre=linspace(0.2,0.023,2000);
y_pre=m*(x_pre-0.02);
plot(x_pre,y_pre)
```

The linear regression was performed using the polyfit-polyval MATLAB functions. The polyfit function requires two sets of input data and the degree of the polynomial function, *n* (in this case *n*=1), and the output is a vector containing all the coefficients of the polynomial function. The coefficient associated with the first order

term will be Young's modulus. The two initial data sets must be selected within a suitable linear range; thus, the number of data points to make a proper linear fit will likely be different from one test to another.

3.4.2 Baking procedures

Baking is required for both pre-strained and as-received specimens. Standard bake-hardening assessment requires a 170°C ± 2°C baking temperature for 10 minutes. The baking period starts when the specimen temperature reaches the specified temperature level. In this project, several different baking temperatures and durations were applied, but in each case, the same temperature and time tolerances were maintained.

It was important to determine the temperature uniformity inside the oven. To verify this, three specimens were placed (on the same shelf) in the oven, with a thermocouple attached to each specimen. The thermocouples were connected to a computer that was able to record and display the temperature profiles over time using the *Labview* software. The measured temperature profiles of the three specimens demonstrated that the temperature gradients in the oven were kept under control, and that at any time during the baking process the specimen temperature remained within the temperature range of ± 2°C as required by the standard. This verification test was repeated for each temperature condition (110°C, 120°C, 130°C, 150°C, 170°C, 180°C). The uniformity of temperature within the oven allowed all three repeat specimens from a given condition in the test matrix to be baked at the same time, thus saving time. Some examples of the temperature profiles over time are provided starting from *Figure 27*. First, the empty oven was heated to the target temperature. Then the oven door was opened, and three specimens were placed inside, carefully spaced apart to avoid any kind of thermal interference and put in contact with the thermocouples. Inevitably, the temperature in the oven drops because of the door being opened, but it ramps up again after it is closed. Once the specimens reached the target temperature, the time counter was started. Although the ramp up time varies depending on the target baking temperature, the specimens' temperature remains between the upper and lower bounds defined by the standard. Therefore, the ability to measure each specimen's surface temperature allowed for a complete decoupling of the ramp up phase from the steady state temperature phase.

It was also important to make sure that, for pre-strained specimens, the pre-straining and the baking were performed within the same day to prevent natural aging effects. Therefore, the pre-straining was carried out in the morning and baking in the same afternoon. As shown in the literature review [18], the total hardening does not depend on natural aging. However, the computation of the standard bake-hardening effect is affected by it, and since all the results should be comparable, the specimens must be baked at the same aging stage. Specimens in the "as received" condition were not subject to any time constraints, since natural aging can be considered negligible in the absence of any pre-strain.

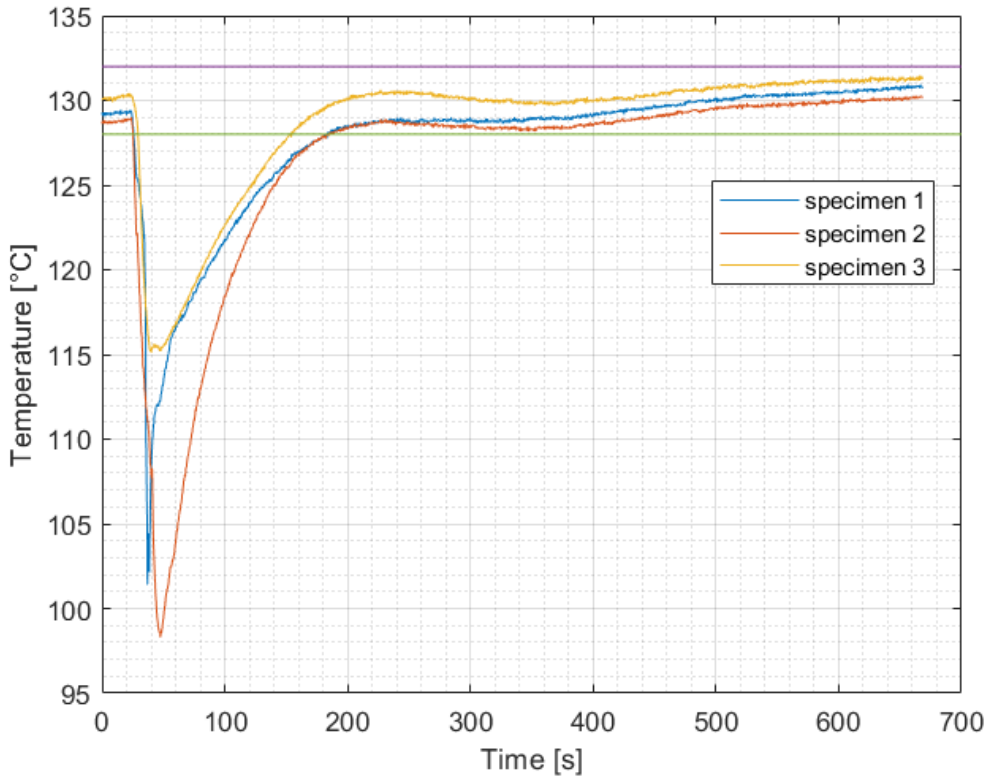

Figure 27. Temperature-history for the North American BR100 alloy, baked at 130°C for 10 minutes.

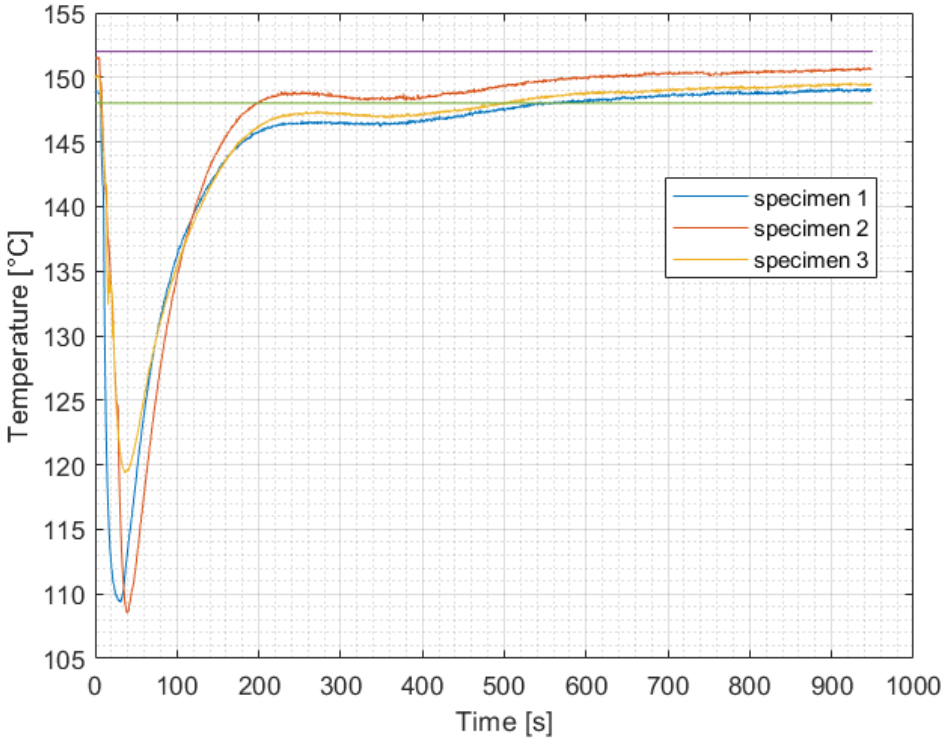

Figure 28. Temperature-history for the North American BR100 alloy, baked at 150°C for 10 minutes.

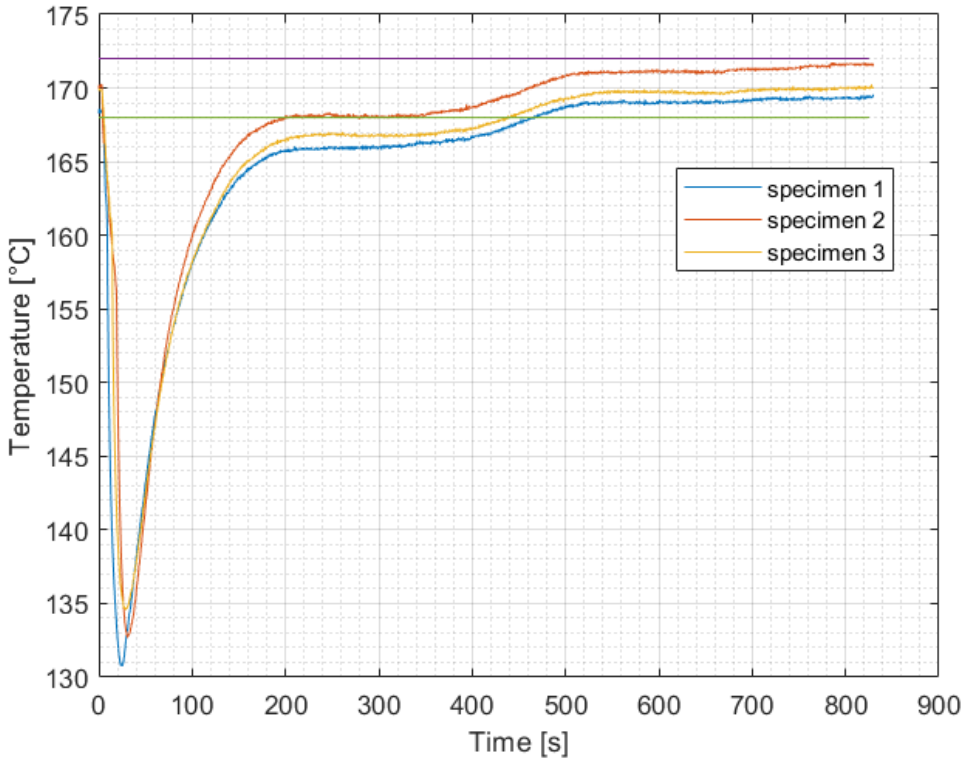

Figure 29. Temperature-history for the North American BR100 alloy, baked at 170°C for 10 minutes.

After being baked, the specimens were put into labelled envelopes and stored at ambient temperature until the final tensile testing. Natural aging at ambient temperature after baking is considered negligible, which means that no time restrictions needed to be applied between baking and final testing. Baked specimens were then testing in uniaxial tension up to fracture according to the same procedure as the initial testing of as-received specimens. The recorded force and displacement data were imported into MATLAB, and the yield stress was calculated as described previously.

The bake-hardening effect was then computed by subtracting the stress level reached at 2% pre-strain $R_{p2,r}$ (or the initial yield stress for specimens with zero pre-strain) from the yield stress obtained in the final tensile test $R_{el,t}$:

$$BH = R_{el,t} - R_{p2,r} \quad (14)$$

The full procedure is illustrated in the flow chart below:

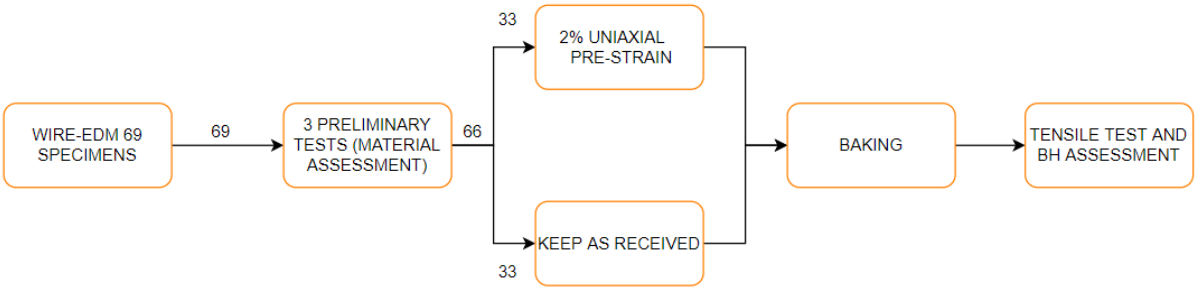

Figure 30. Sequence of experimental steps to determine the bake hardening effect.

3.4.3 Dent test procedures

The sequence of experimental steps to evaluate the dent resistance of each baked sheet material are described in *Figure 31* and were carried out at the Novelis plant in Novi, Michigan. The dent test specimens were 355 mm × 355 mm square blanks. 48 blanks were required for each alloy to determine the effect of bake hardening on the dent resistance. Again, each temperature-time condition required testing 3 repeat specimens. For each alloy, half of the sheet specimens were pre-strained, while the other half remained in the as-received condition. The blanks were pre-strained to 2% by stretch-forming them into the shape of a pie-pan (*Figure 32*). As remarked before, 2% strain in both in-plane principal directions means that the effective strain will be greater than 2%. Although the 2% strain is the conventional pre-strain value prescribed

for uniaxial tension, the dent test leads to an altogether different mode of deformation compared to a tensile test. Therefore, no constraint was imposed to make the effective prestrain value equivalent in both types of tests. Finally, since the oven at Novelis was sufficiently accurate, the 3 sheet specimens were stacked in a support rack and placed into the oven (*Figure 33*).

The specimens were then tested by mounting each one in a fixture with four clamps and subjecting it to an impact using the mechanical pendulum. To achieve the same impact energy for each trial, the mass of the indenter was kept the same (400 g), as well as the initial angle (50°) of the pendulum arm. These values were determined after a series of trial tests in which an appreciable difference in the resulting dent size could be observed for the whole range of material conditions. It was also important to control the position of the clamping fixture, so that both the pie-pan (pre-strained) specimens and the flat (as-received) specimens were oriented at the same angle and in the same position when the indenter contacts the specimen. Finally, the swing arm had to be manually stopped after the first stroke to make sure that each specimen was subject to only one impact.

Since the mechanical pendulum was not instrumented with a displacement transducer, no experimental data could be recorded in real time. The only option was to perform measurements after testing. Considering these “restrictions”, the indentation was measured in two ways: first, the depth of the indentation was measured with a digital depth indicator. Its precision was relatively low (0.01 mm); however, the results were sufficient to be able to distinguish between the various material conditions. Alternatively, if further precision was required, other methods (more time-consuming) could be adopted, such as surface 3D scanning. Then, the indentation diameter was also measured by means of a circle template, which allowed to obtain a measurement by comparison.

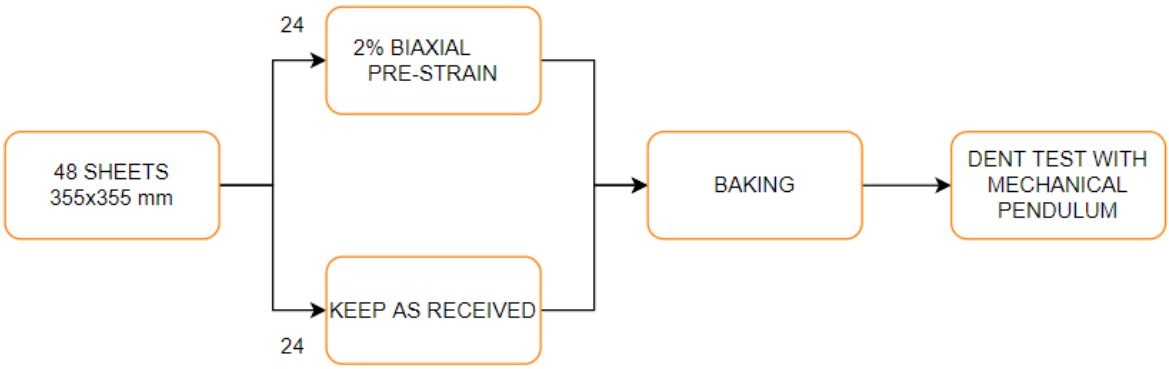

Figure 31. Sequence of experimental steps for sheet specimens subject to dent testing

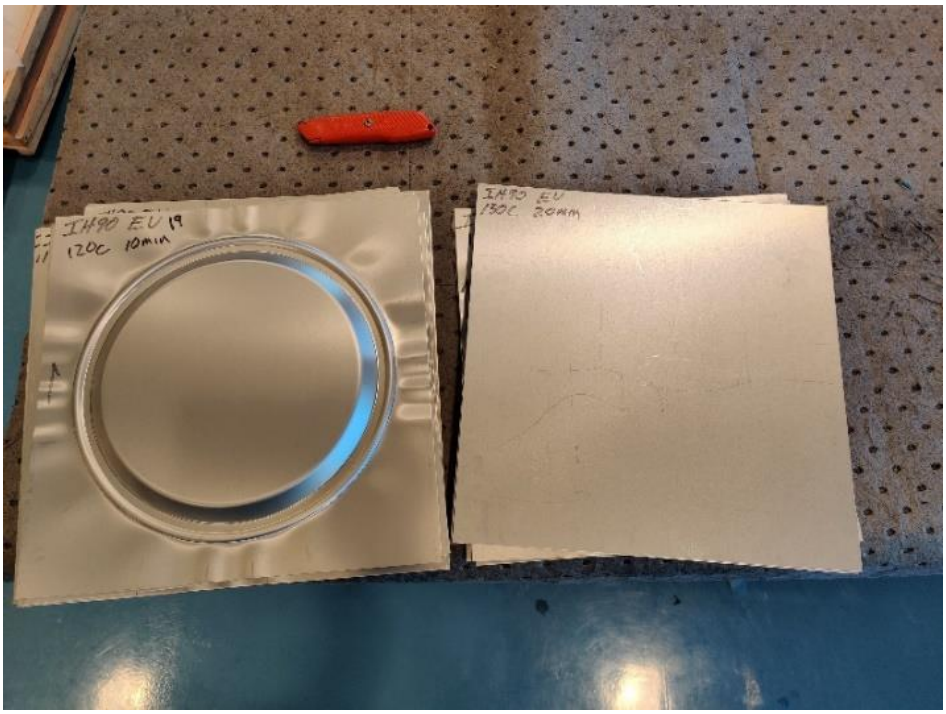

Figure 32. Pre-strained pie-pan-shaped specimens (left) and flat, as-received specimens (right) used for dent tests

Figure 33. Baking phase of dent test specimens.

3.5 Computation and representation of results

For any considered test condition (time-temperature, indentation depth and indentation diameter), three repeat tests were carried out. The average and standard deviation were then computed for each set of three test results. The standard deviation can be expressed as follows:

$$\sigma = \sqrt{\frac{\sum(x_i - \mu)^2}{N}} \qquad (15)$$

where x_i is each one of the three values, μ their mean and $N = 3$. The standard deviation is particularly useful, as it gives an idea of the level of dispersion of the data. If the test is accurate and repeatable, the data dispersion will be low and so will be the standard deviation.

Once all the results were computed, it was helpful to graphically represent them to show them in a clear, exhaustive way. Furthermore, it must be remarked that this investigation is a multi-dimensional problem: there are 3 independent variables: time, temperature, and pre-strain. The simplest approach is to show how the relevent mechanical property changes considering one independent variable at a time and analyzing its effect. Considering each variable separately allows for a clear and simple representation of the results: for example, with fixed pre-strain and baking time, the temperature effect on the bake-hardening level can be easily determined. And the results can also be easily compared between the different alloys. With all of this in mind, bar charts appear to be a good compromise between immediate data visualization and precise representation; and error bars can also be embedded in each bar. However, 3D graphs can also be very helpful, particularly when the effect of two or more parameters need to be visualized at the same time.

Another interesting aspect to be discussed is if the effect of concentrations of alloy elements (previously reported in *Table 2*) on the computed mechanical properties is recognizable. As already explained in Chapter 2, different alloying elements are responsible for the improved bake response. For example, silicon and magnesium concentrations influence the formation of clusters, while copper enhances the bake-hardening kinetics. This kind of analysis, if successful, can constitute a further validation of the experimental data with respect to theoretical considerations that were previously highlighted.

4 Results

All the experimental results of the project are reported in this chapter. First, the stress-strain curves are plotted to see how the curve shape changes with thermal treatment and pre-strain. Then, the results of the experimental work are shown. These are respectively the bake-hardening value for the tensile tests and the indentation depth and diameter for the dent tests. Bar charts were selected to plot the data for immediate and easy visualization, along with the error bars referring to the standard deviation in the case of tensile test results. To compare the various alloys, the percentage strength gain after the heat treatment is plotted.

4.1 Stress-strain curves

After the painting treatment, as mentioned, bake-hardenable materials exhibit an improvement in mechanical strength. This change can be visualized by plotting the engineering stress-strain curves before and after the bake-hardening treatment.

The engineering stress-strain curves of the “as received” specimen are useful to evaluate the effect of the baking process. An example is shown in *Figure 34* for the IH90US alloy, with one stress-strain curve for each temperature condition and for the 20-minute oven cycle. The curves shown in *Figure 35*, describe the entire cycle that simulates the forming and baking of automotive panels. The first portion on the left represents the pre-strain stage; therefore, the flow curve is the same as that for the “as received” specimen. Then each specimen was unloaded till the stress reached approximately zero, and the remaining plastic strain was 2%. After the paint cycle, however, the specimen exhibits a noticeably higher yield stress, and its stress-strain curve lies above the “as received” curve. It is also interesting to enlarge the initial portion of the stress-strain curves to observe the initial elastic and yielding behaviour and to visualize the differences between the 0% (*Figure 36*) and the 2% pre-strain (*Figure 37*) conditions.

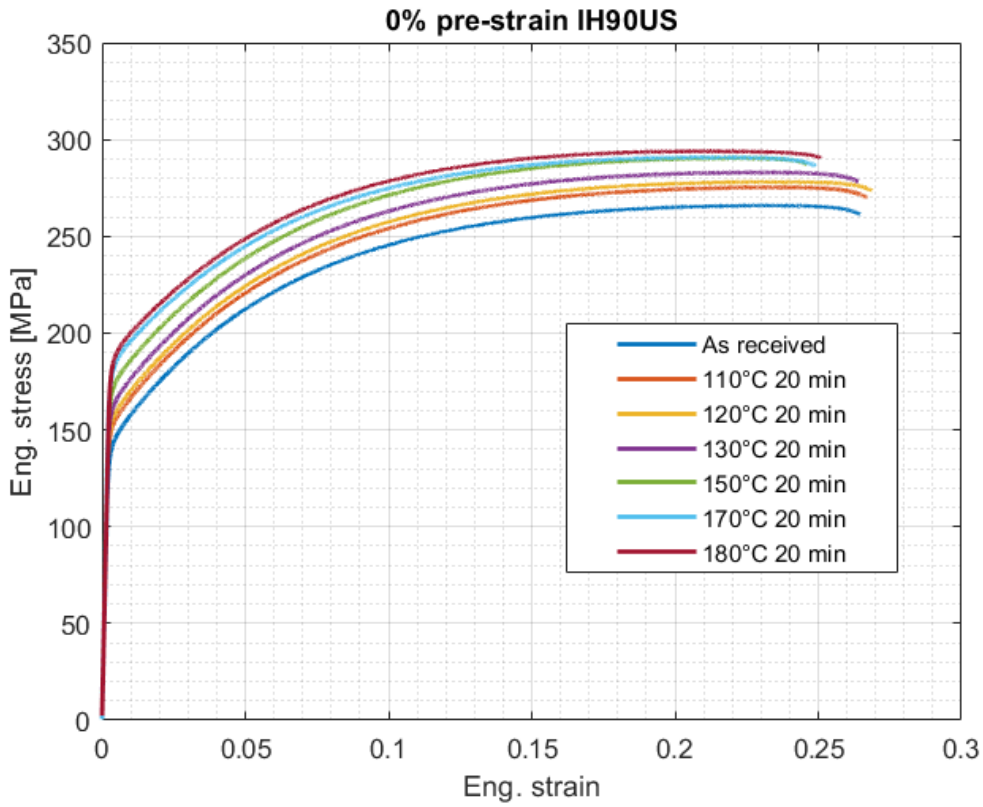

Figure 34. Engineering stress-strain curves of IH90US specimens with 0% pre-strain

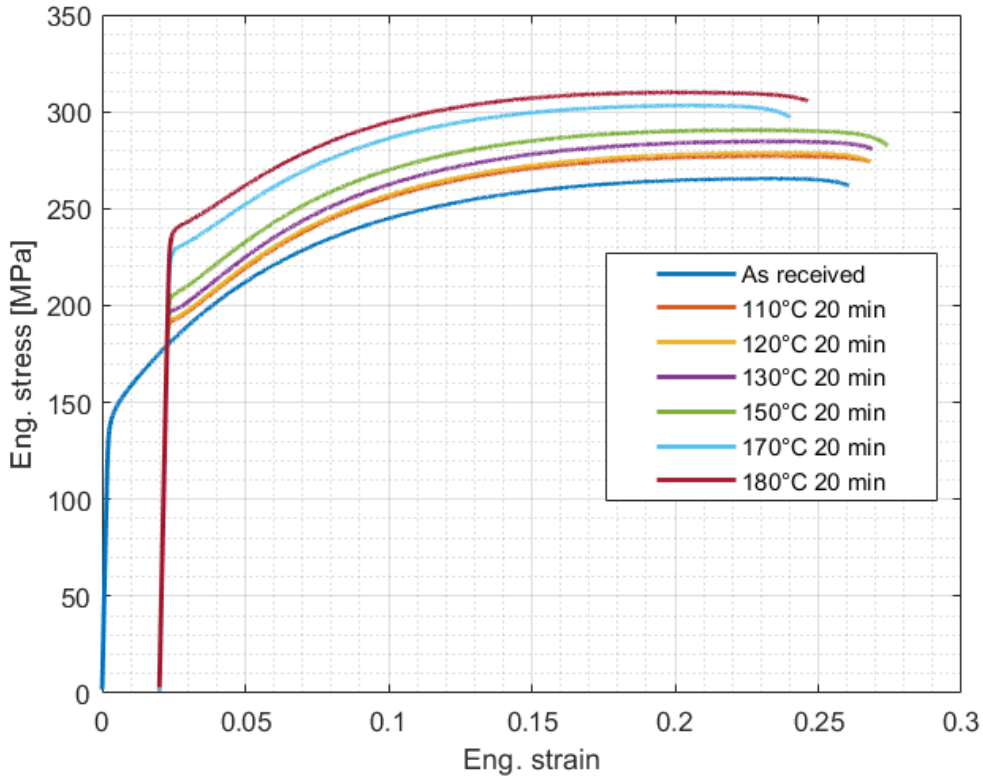

Figure 35. Engineering stress-strain curves of IH90US specimens after a 2% pre-strain

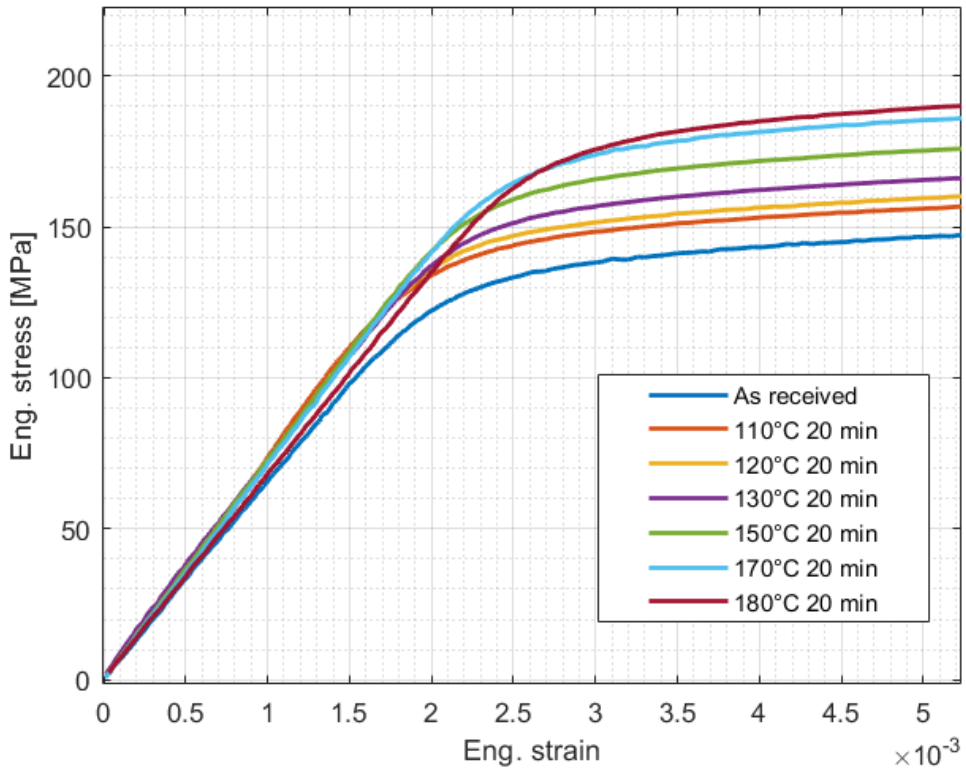

Figure 36. Initial portion of the IH90US engineering stress-strain curves with 0% pre-strain

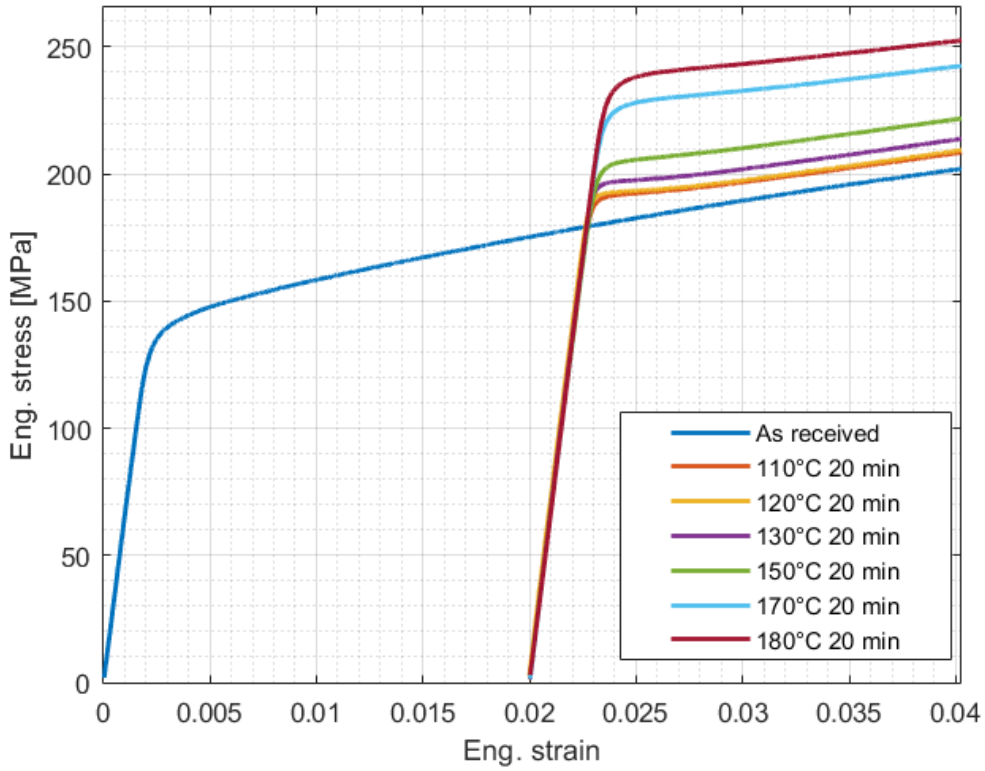

Figure 37. Initial portion of the IH90US engineering stress-strain curves after a 2% pre-strain

4.2 Tensile test results

The results obtained after processing the tensile test data are presented in the following tables. Each table shows the results for a particular alloy and a certain pre-strain level. For each temperature-time condition, the measurements taken from three different specimens are reported along with their average; the bake hardening value is also followed by its standard deviation.

At the beginning of the test phase, the yield stress of each as-received sheet material was determined through three repeat tensile tests. These results are reported in *Table 6*.

For each of the sheet materials, the 0% pre-strained specimens are fully characterized by their initial yield stress and final yield stress after bake hardening, and these results are presented in a first table. However, a strain hardening level is also required to fully characterize the specimens that were pre-strained to 2%. The sum of the strain hardening (increase in yield stress resulting from the pre-strain) and the bake-hardening (increase in yield stress resulting from the baking) is the total strength gain of the material. And for each alloy, these results are presented in a second table.

The bake-hardening levels after 0% and 2% pre-strains are also presented as a bar chart for each alloy, with error bars that represent the standard deviation for any given temperature-time condition.

Table 6. 0.2% offset yield stress of as-received sheet materials.

	0.2% Yield Stress [MPa]				
Alloys	**Spec. #1**	**Spec. #2**	**Spec. #3**	**Avg.**	**Std. Dev.**
HF90	116.5	116.4	118.6	117.2	1.0
IH90US	144.3	145.2	142.5	144.0	1.1
BR100EU	139.5	136.6	140.0	138.7	1.5
IH90EU	124.8	126.9	128.6	126.8	1.6
BR100US	126.8	127.6	128.7	127.7	0.8

4.2.1 HF90 alloy

Table 7. Tensile test results for the HF90 alloy with 0% pre-strain.

HF90 0%	0.2% YS [MPa]	BH0 [MPa]					Final Yield Stress [MPa]			
Baking condition	**Specimen >>>**	**#1**	**#2**	**#3**	**Avg.**	**Std. Dev.**	**#1**	**#2**	**#3**	**Avg.**
110°C, 20 min	117.2	3.7	5.3	5.0	4.7	0.7	120.9	122.5	122.2	121.8
120°C, 10 min	117.2	4.9	5.1	3.8	4.6	0.6	122.1	122.3	121.0	121.8
120°C, 20 min	117.2	6.3	6.6	6.1	6.3	0.2	123.4	123.7	123.3	123.5
130°C, 10 min	117.2	7.4	5.0	5.3	5.9	1.1	124.5	122.1	122.4	123.0
130°C, 20 min	117.2	10.7	9.6	9.9	10.1	0.4	127.9	126.8	127.1	127.2
150°C, 20 min	117.2	11.5	14.0	13.1	12.8	1.0	128.6	131.1	130.2	130.0
170°C, 10 min	117.2	12.4	14.0	13.1	13.1	0.6	129.6	131.1	130.2	130.3
170°C, 20 min	117.2	13.3	13.8	15.9	14.3	1.1	130.5	131.0	133.1	131.5
180°C, 10 min	117.2	21.9	21.8	19.6	21.1	1.0	139.0	139.0	136.8	138.3
180°C, 20 min	117.2	31.1	40.5	36.2	36.0	3.9	148.3	157.7	153.4	153.1

Table 8. Tensile test results for the HF90 alloy after a 2% pre-strain.

HF90 2%	0.2% YS [MPa]	SH2 [MPa]				BH2 [MPa]					Final YS [MPa]			
Baking condition	**Specimen >>>**	**#1**	**#2**	**#3**	**Avg.**	**#1**	**#2**	**#3**	**Avg.**	**Std. Dev.**	**#1**	**#2**	**#3**	**Avg.**
110°C, 20 min	117.2	36.4	38.2	36.7	37.1	7.5	5.8	6.0	6.4	0.8	161.1	161.2	159.8	160.7
120°C, 10 min	117.2	37.9	37.1	37.5	37.5	5.0	5.3	5.2	5.2	0.1	160.1	159.6	159.9	159.9
120°C, 20 min	117.2	34.4	31.7	35.4	33.8	5.6	8.4	5.3	6.4	1.4	157.2	157.3	157.8	157.4
130°C, 10 min	117.2	33.9	36.2	33.7	34.6	3.9	6.5	6.2	5.6	1.2	155.0	159.9	157.1	157.3
130°C, 20 min	117.2	34.5	35.2	35.6	35.1	6.9	5.4	6.8	6.4	0.7	158.6	157.8	159.6	158.7
150°C, 20 min	117.2	32.5	32.2	35.0	33.2	16.6	15.9	14.1	15.5	1.1	166.3	165.3	166.3	165.9
170°C, 10 min	117.2	37.1	37.0	36.1	36.7	15.3	17.3	16.0	16.2	0.8	169.6	171.4	169.3	170.1
170°C, 20 min	117.2	36.9	37.7	36.3	37.0	29.5	30.3	30.8	30.2	0.5	183.6	185.2	184.2	184.3
180°C, 10 min	117.2	32.0	33.0	33.9	33.0	31.6	40.3	36.0	36.0	3.6	180.8	190.5	187.1	186.1
180°C, 20 min	117.2	32.6	31.7	34.4	32.9	43.6	57.1	57.3	52.7	6.4	193.4	205.9	208.9	202.7

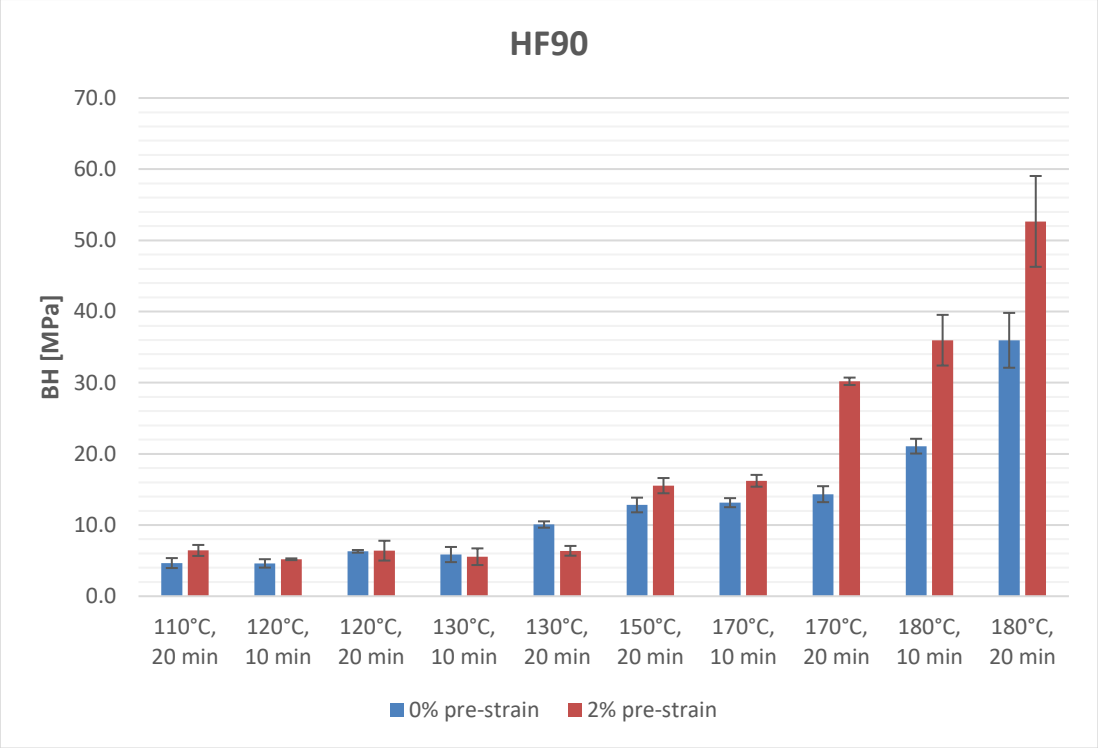

Figure 38. Bake-hardening levels for the HF90 alloy after 0% and 2% pre-strain with their relative standard deviation.

4.2.2 IH90US alloy

Table 9. Tensile test results for the IH90US alloy with 0% pre-strain.

IH90US 0%	0.2% YS [MPa]	BH0 [MPa]					Final Yield Stress [MPa]			
Baking condition	**Specimen >>>**	**#1**	**#2**	**#3**	**Avg.**	**Std. Dev.**	**#1**	**#2**	**#3**	**Avg.**
110°C, 20 min	144.0	11.4	9.8	11.2	10.8	0.7	155.4	153.8	155.1	154.8
120°C, 10 min	144.0	11.1	11.1	10.8	11.0	0.1	155.1	155.1	154.8	155.0
120°C, 20 min	144.0	12.9	13.2	12.3	12.8	0.4	156.9	157.2	156.2	156.8
130°C, 10 min	144.0	12.9	14.1	15.9	14.3	1.2	156.9	158.1	159.9	158.3
130°C, 20 min	144.0	15.9	19.3	17.5	17.6	1.4	159.8	163.3	161.4	161.5
150°C, 20 min	144.0	27.8	29.4	26.4	27.9	1.2	171.8	173.3	170.3	171.8
170°C, 10 min	144.0	26.8	30.0	30.3	29.1	1.6	170.8	174.0	174.3	173.0
170°C, 20 min	144.0	43.9	39.9	39.9	41.2	1.9	187.8	183.9	183.9	185.2
180°C, 10 min	144.0	31.6	30.0	34.5	32.0	1.9	175.5	174.0	178.5	176.0
180°C, 20 min	144.0	44.7	44.6	47.9	45.7	1.5	188.7	188.5	191.8	189.7

Table 10. Tensile test results for the IH90US alloy after a 2% pre-strain.

IH90US 2%	0.2% YS [MPa]	SH2 [MPa]				BH2 [MPa]					Final YS [MPa]			
Baking condition	**Specimen >>>**	**#1**	**#2**	**#3**	**Avg.**	**#1**	**#2**	**#3**	**Avg.**	**Std. Dev.**	**#1**	**#2**	**#3**	**Avg.**
110°C, 20 min	144.0	37.8	38.4	38.2	38.1	14.5	9.9	13.3	12.6	2.0	196.3	192.3	195.5	194.7
120°C, 10 min	144.0	35.6	38.6	35.9	36.7	13.2	12.5	8.6	11.4	2.0	192.8	195.1	188.5	192.1
120°C, 20 min	144.0	38.5	35.5	36.2	36.7	13.1	13.9	13.5	13.5	0.3	195.6	193.3	193.7	194.2
130°C, 10 min	144.0	36.4	35.1	38.1	36.5	13.1	12.6	10.3	12.0	1.2	193.5	191.7	192.4	192.5
130°C, 20 min	144.0	36.6	34.7	36.2	35.8	13.0	18.9	12.1	14.6	3.0	193.5	197.5	192.2	194.4
150°C, 20 min	144.0	39.0	36.4	38.7	38.0	20.3	25.4	22.5	22.7	2.1	203.2	205.7	205.2	204.7
170°C, 10 min	144.0	35.3	40.1	40.3	38.6	28.7	27.9	27.2	27.9	0.6	208.0	212.0	211.4	210.5
170°C, 20 min	144.0	38.6	37.3	36.0	37.3	58.2	47.3	59.2	54.9	5.4	240.8	228.6	239.2	236.2
180°C, 10 min	144.0	34.8	33.7	39.0	35.8	49.7	47.9	48.4	48.6	0.8	228.5	225.6	231.3	228.4
180°C, 20 min	144.0	36.1	38.4	36.6	37.0	55.5	57.0	52.1	54.8	2.1	235.6	239.3	232.6	235.8

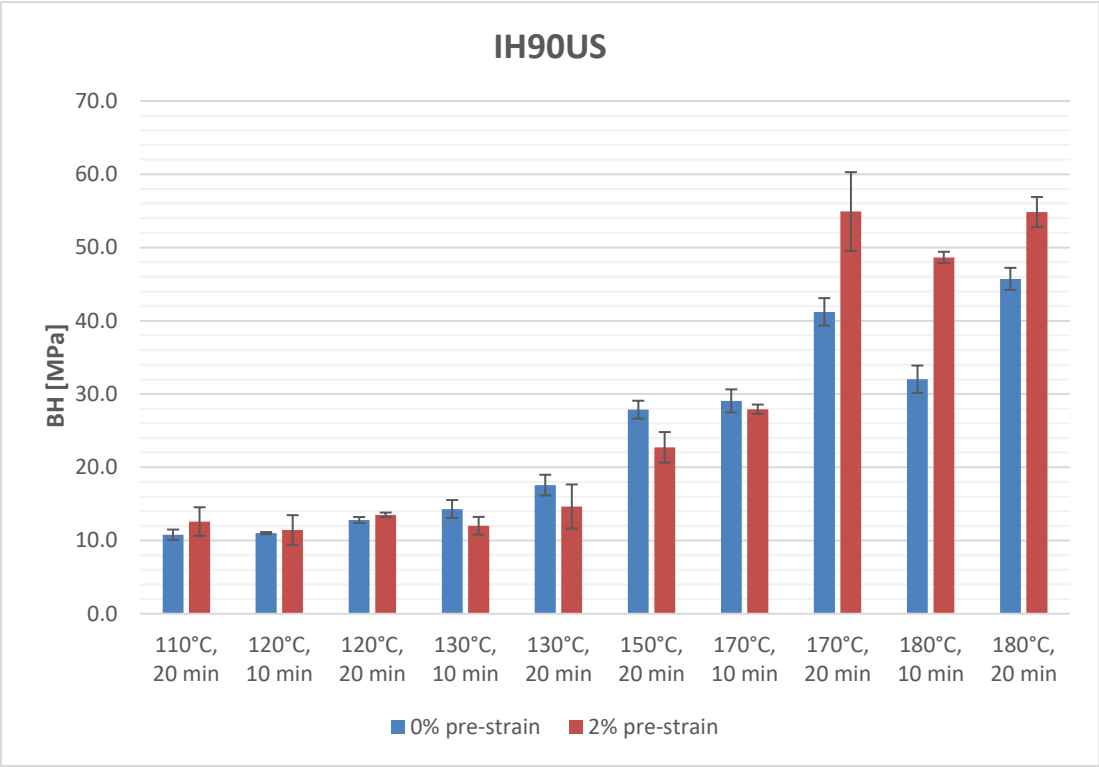

Figure 39. Bake-hardening levels for the IH90US alloy after 0% and 2% pre-strain with their relative standard deviation

4.2.3 BR100EU alloy

Table 11. Tensile test results for the BR100EU alloy with 0% pre-strain.

BR100EU 0%	0.2% YS [MPa]	BH0 [MPa]					Final Yield Stress [MPa]			
Baking condition	**Specimen >>>**	**#1**	**#2**	**#3**	**Avg.**	**Std. Dev.**	**#1**	**#2**	**#3**	**Avg.**
110°C, 20 min	138.7	4.71	7.49	6.33	6.2	1.1	143.4	146.2	145.0	144.9
120°C, 10 min	138.7	8.3	6.38	5.72	6.8	1.1	147.0	145.1	144.4	145.5
120°C, 20 min	138.7	9.83	8.96	7.27	8.7	1.1	148.5	147.7	146.0	147.4
130°C, 10 min	138.7	6.51	8.46	7.23	7.4	0.8	145.2	147.2	145.9	146.1
130°C, 20 min	138.7	9.35	11.69	11.67	10.9	1.1	148.1	150.4	150.4	149.6
150°C, 20 min	138.7	20.16	19.15	19.73	19.7	0.4	158.9	157.9	158.4	158.4
170°C, 10 min	138.7	21.31	20.29	20.82	20.8	0.4	160.0	159.0	159.5	159.5
170°C, 20 min	138.7	35.73	32.72	36.13	34.9	1.5	174.4	171.4	174.8	173.6
180°C, 10 min	138.7	26.75	25.75	24.81	25.8	0.8	165.5	164.5	163.5	164.5
180°C, 20 min	138.7	35.83	40.42	40.27	38.8	2.1	174.5	179.1	179.0	177.5

Table 12. Tensile test results for the BR100EU alloy after a 2% pre-strain.

BR100EU 2%	0.2% YS [MPa]	SH2 [MPa]				BH2 [MPa]					Final YS [MPa]			
Baking condition	**Specimen >>>**	**#1**	**#2**	**#3**	**Avg.**	**#1**	**#2**	**#3**	**Avg.**	**Std. Dev.**	**#1**	**#2**	**#3**	**Avg.**
110°C, 20 min	138.7	38.3	38.3	40.0	38.9	7.7	6.8	3.4	6.0	1.8	184.7	183.8	182.1	183.5
120°C, 10 min	138.7	37.0	40.1	36.8	38.0	7.9	7.4	10.6	8.6	1.4	183.6	186.2	186.1	185.3
120°C, 20 min	138.7	37.0	38.9	36.6	37.5	9.6	7.7	9.9	9.1	1.0	185.3	185.3	185.2	185.3
130°C, 10 min	138.7	33.6	36.1	36.2	35.3	14.0	11.6	11.3	12.3	1.2	186.3	186.4	186.2	186.3
130°C, 20 min	138.7	35.8	36.6	36.4	36.2	15.0	12.4	12.1	13.1	1.3	189.5	187.7	187.2	188.1
150°C, 20 min	138.7	39.4	36.5	38.4	38.1	15.3	20.7	18.7	18.2	2.2	193.4	195.9	195.8	195.0
170°C, 10 min	138.7	34.5	34.2	36.4	35.0	27.8	28.9	26.9	27.9	0.8	201.0	201.8	202.0	201.6
170°C, 20 min	138.7	35.8	38.6	34.1	36.2	31.4	31.2	37.1	33.2	2.7	205.9	208.5	209.9	208.1
180°C, 10 min	138.7	34.1	35.2	35.8	35.0	33.4	29.4	31.0	31.3	1.7	206.2	203.2	205.5	205.0
180°C, 20 min	138.7	35.8	35.9	37.4	36.4	51.9	54.3	50.8	52.3	1.5	226.4	228.9	226.9	227.4

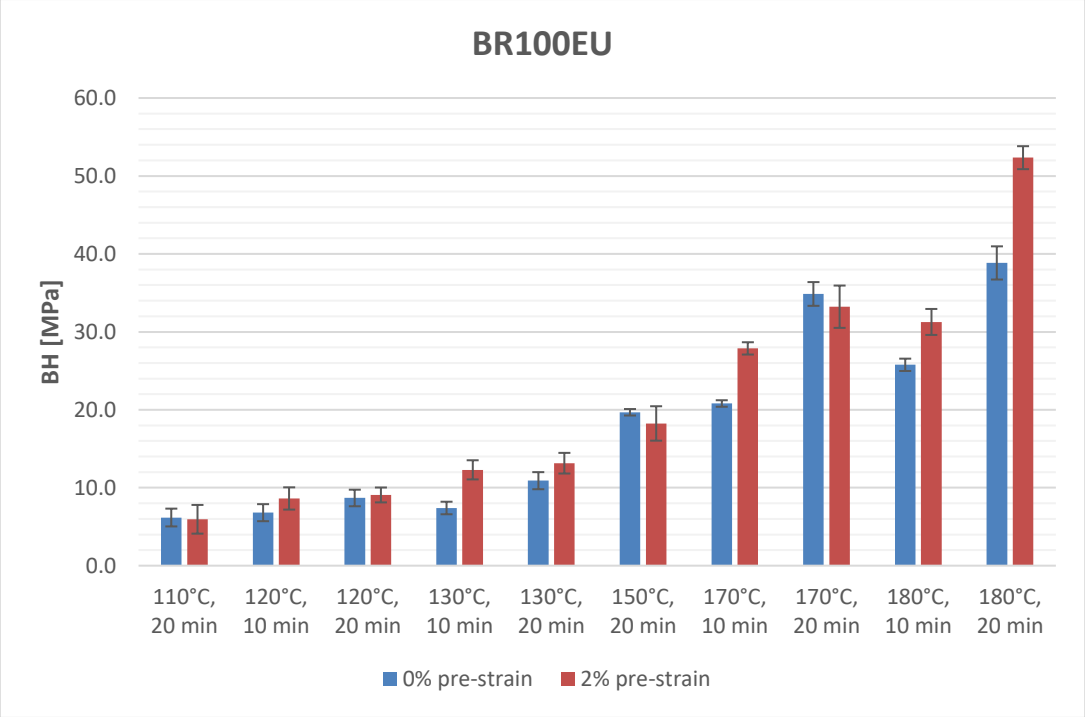

Figure 40. Bake-hardening levels for the BR100EU alloy after 0% and 2% pre-strain with their relative standard deviation.

4.2.4 IH90EU alloy

Table 13. Tensile test results for the IH90EU alloy with 0% pre-strain.

IH90EU 0%	0.2% YS [MPa]	BH0 [MPa]					Final Yield Stress [MPa]			
Baking condition	**Specimen >>>**	**#1**	**#2**	**#3**	**Avg.**	**Std. Dev.**	**#1**	**#2**	**#3**	**Avg.**
110°C, 20 min	126.8	3.1	2.9	3.6	3.2	0.3	129.9	129.7	130.4	130.0
120°C, 10 min	126.8	4.7	3.1	1.0	2.9	1.5	131.4	129.9	127.8	129.7
120°C, 20 min	126.8	6.7	6.7	6.9	6.8	0.1	133.5	133.5	133.7	133.5
130°C, 10 min	126.8	6.4	5.7	5.5	5.9	0.4	133.2	132.5	132.2	132.6
130°C, 20 min	126.8	9.5	7.5	10.2	9.1	1.1	136.3	134.3	136.9	135.8
150°C, 20 min	126.8	17.1	16.6	17.1	16.9	0.2	143.9	143.4	143.9	143.7
170°C, 10 min	126.8	16.8	19.1	17.6	17.8	0.9	143.6	145.9	144.3	144.6
170°C, 20 min	126.8	25.3	27.4	28.0	26.9	1.1	152.1	154.2	154.8	153.7
180°C, 10 min	126.8	18.0	21.9	18.6	19.5	1.7	144.8	148.7	145.3	146.3
180°C, 20 min	126.8	33.7	35.6	33.9	34.4	0.8	160.4	162.4	160.7	161.2

Table 14. Tensile test results for the IH90EU alloy after a 2% pre-strain.

IH90EU 2%	0.2% YS [MPa]	SH2 [MPa]				BH2 [MPa]					Final YS [MPa]			
Baking condition	**Specimen >>>**	**#1**	**#2**	**#3**	**Avg.**	**#1**	**#2**	**#3**	**Avg.**	**Std. Dev.**	**#1**	**#2**	**#3**	**Avg.**
110°C, 20 min	126.8	35.8	35.2	34.3	35.1	7.4	9.4	11.3	9.4	1.6	169.9	171.4	172.4	171.2
120°C, 10 min	126.8	34.7	35.2	35.5	35.1	8.1	9.7	10.1	9.3	0.9	169.6	171.7	172.4	171.2
120°C, 20 min	126.8	34.6	36.8	37.9	36.4	10.4	10.5	8.9	9.9	0.8	171.7	174.1	173.5	173.1
130°C, 10 min	126.8	35.6	35.1	35.4	35.4	11.0	10.6	10.3	10.6	0.3	173.3	172.5	172.5	172.8
130°C, 20 min	126.8	35.3	34.3	34.4	34.7	11.1	13.4	12.9	12.5	1.0	173.2	174.5	174.1	173.9
150°C, 20 min	126.8	33.5	33.1	36.2	34.2	17.9	18.6	18.7	18.4	0.4	178.1	178.5	181.7	179.4
170°C, 10 min	126.8	35.5	35.7	34.2	35.1	22.2	21.2	19.5	21.0	1.1	184.4	183.7	180.5	182.9
170°C, 20 min	126.8	37.1	33.7	33.0	34.6	28.4	29.3	31.4	29.7	1.3	192.2	189.8	191.2	191.1
180°C, 10 min	126.8	35.2	34.8	35.8	35.2	26.7	26.4	26.1	26.4	0.3	188.6	187.9	188.6	188.4
180°C, 20 min	126.8	35.5	36.1	34.6	35.4	40.3	43.8	40.3	41.4	1.6	202.6	206.7	201.7	203.6

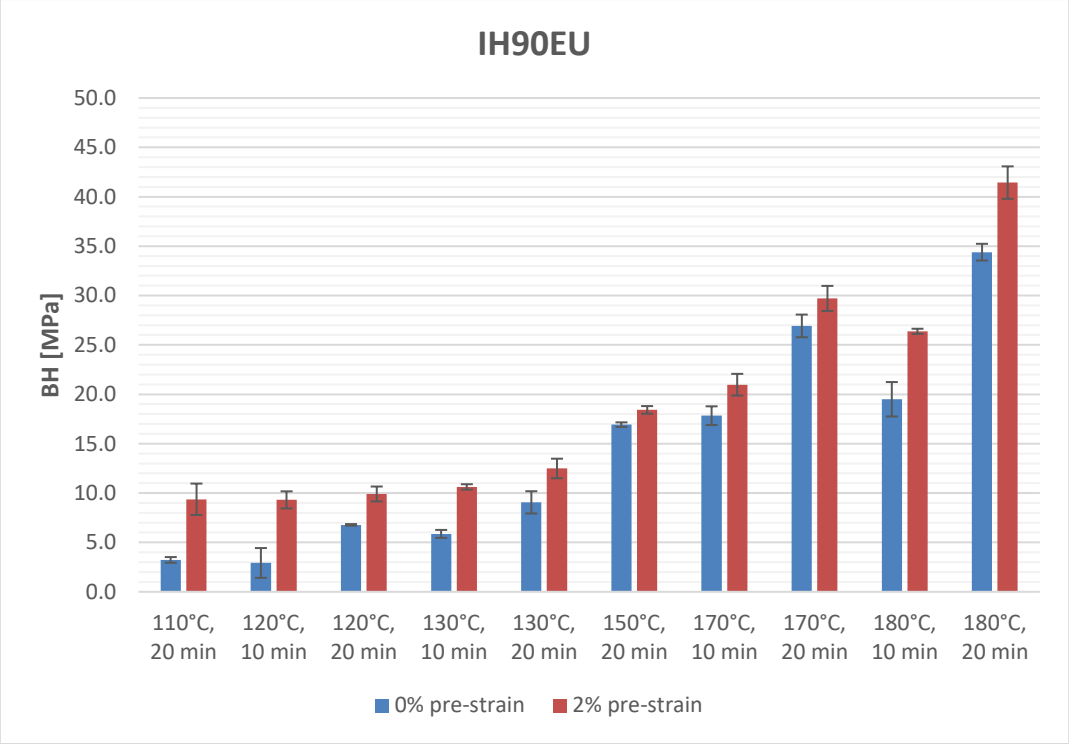

Figure 41. Bake-hardening levels for the IH90EU alloy after 0% and 2% pre-strain with their relative standard deviation

4.2.5 BR100US alloy

Table 15. Tensile test results for the BR100US alloy with 0% pre-strain.

BR100US 0%	0.2% YS [MPa]	BH0 [MPa]					Final Yield Stress [MPa]			
Baking condition	**Specimen >>>**	**#1**	**#2**	**#3**	**Avg.**	**Std. Dev.**	**#1**	**#2**	**#3**	**Avg.**
110°C, 20 min	127.7	9.8	9.1	13.5	10.8	1.9	137.5	136.8	141.2	138.5
120°C, 10 min	127.7	13.4	7.7	11.7	10.9	2.4	141.1	135.4	139.4	138.6
120°C, 20 min	127.7	15.9	10.3	15.2	13.8	2.5	143.6	138.0	142.9	141.5
130°C, 10 min	127.7	13.5	16.0	13.9	14.5	1.1	141.2	143.7	141.6	142.2
130°C, 20 min	127.7	19.3	19.5	18.7	19.2	0.4	147.0	147.2	146.4	146.9
150°C, 20 min	127.7	28.4	29.2	27.1	28.2	0.9	156.1	156.9	154.8	155.9
170°C, 10 min	127.7	34.2	32.5	33.5	33.4	0.7	161.9	160.2	161.2	161.1
170°C, 20 min	127.7	44.2	43.2	44.7	44.0	0.6	171.9	170.9	172.4	171.7
180°C, 10 min	127.7	34.7	34.4	40.5	36.5	2.8	162.4	162.1	168.2	164.2
180°C, 20 min	127.7	54.2	51.7	56.6	54.1	2.0	181.9	179.4	184.3	181.8

Table 16. Tensile test results for the BR100US alloy after a 2% pre-strain.

BR100US 2%	0.2% YS [MPa]	SH2 [MPa]				BH2 [MPa]					Final YS [MPa]			
Baking condition	**Specimen >>>**	**#1**	**#2**	**#3**	**Avg.**	**#1**	**#2**	**#3**	**Avg.**	**Std. Dev.**	**#1**	**#2**	**#3**	**Avg.**
110°C, 20 min	127.7	38.4	33.4	37.4	36.4	12.6	12.7	13.1	12.8	0.2	178.7	173.8	178.2	176.9
120°C, 10 min	127.7	36.1	33.4	35.4	35.0	14.8	14.6	14.5	14.6	0.1	178.6	175.6	177.6	177.3
120°C, 20 min	127.7	30.7	36.7	32.0	33.1	14.1	16.5	16.0	15.5	1.0	172.4	180.9	175.7	176.3
130°C, 10 min	127.7	35.5	34.4	34.9	35.0	13.8	14.5	14.0	14.1	0.3	177.1	176.6	176.6	176.8
130°C, 20 min	127.7	37.0	33.7	33.6	34.7	15.5	16.3	18.6	16.8	1.3	180.2	177.7	179.9	179.3
150°C, 20 min	127.7	34.6	34.0	33.1	33.9	28.9	28.0	27.1	28.0	0.8	191.2	189.7	187.9	189.6
170°C, 10 min	127.7	32.1	34.0	35.8	34.0	32.2	28.7	32.6	31.2	1.8	192.0	190.4	196.1	192.8
170°C, 20 min	127.7	33.7	32.6	34.9	33.7	44.1	41.7	42.7	42.8	1.0	205.5	201.9	205.3	204.2
180°C, 10 min	127.7	34.4	35.6	33.9	34.6	37.0	35.2	37.4	36.6	0.9	199.1	198.6	199.0	198.9
180°C, 20 min	127.7	33.5	32.8	34.0	33.4	53.2	54.2	55.9	54.4	1.1	214.4	214.8	217.5	215.6

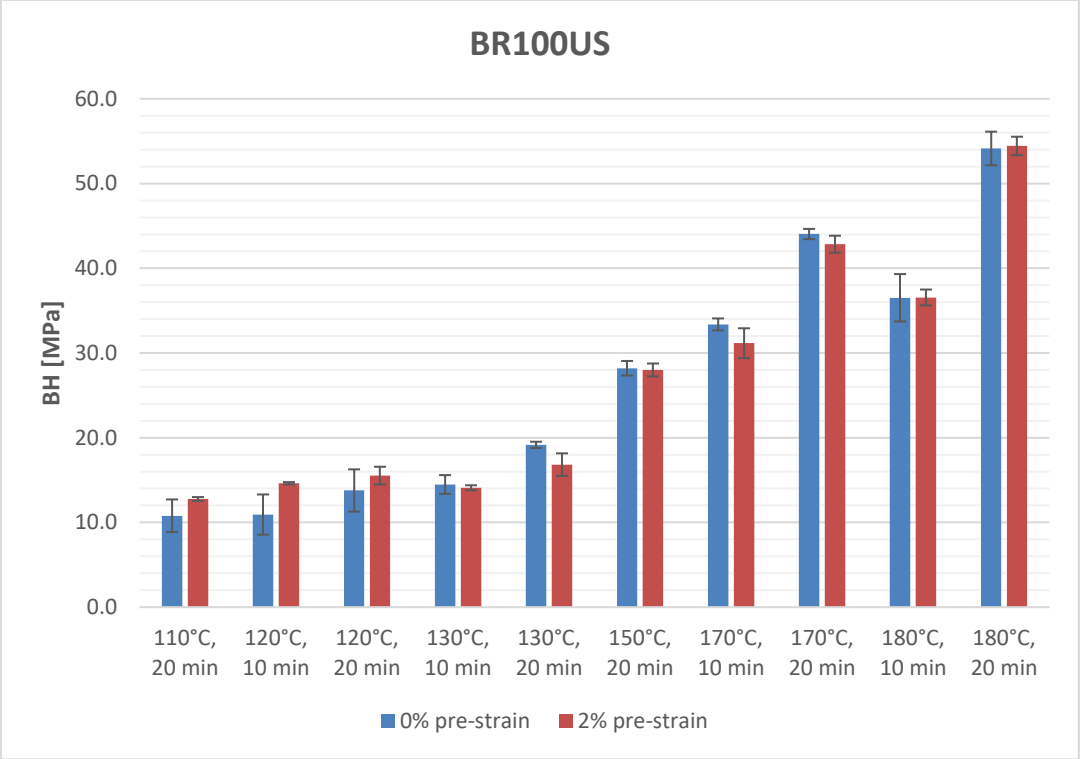

Figure 42. Bake-hardening levels for the BR100US alloy after 0% and 2% pre-strain with their relative standard deviation

4.2.6 Ambient temperature effect

The test matrix presented in *Table 3* contains two further test cases: ambient temperature for 0% and 2% pre-strain. These results are reported separately in this subsection because the gathered data about the bake-hardening phenomenon at ambient temperature cannot be directly compared to the data gathered at higher temperatures due to natural aging effects, as it will be better explained and justified in Chapter 5.

The data for test conditions at ambient temperature and 0% pre-strain are the same ones that were recorded to have an initial reference of the 0.2% yield strength (see *Table 6*).

Table 17. Tensile test data for each alloy after a 2% pre-strain and kept at ambient temperature (23°C±2°C).

Ambient Temp., 2% pre-strain	0.2% YS [MPa]	SH2 [MPa]				BH2 [MPa]					Final Yield Stress [MPa]			
Alloys	**Specimens >>>**	**#1**	**#2**	**#3**	**Avg.**	**#1**	**#2**	**#3**	**Avg.**	**Std. Dev.**	**#1**	**#2**	**#3**	**Avg.**
HF90	117.2	37.8	36.5	35.1	36.5	7.7	8.9	10.8	9.1	1.3	162.7	162.5	163.0	162.7
IH90US	144.0	43.2	43.0	42.0	42.7	6.4	9.5	9.8	8.6	1.6	193.5	196.5	195.8	195.3
BR100EU	138.7	34.9	37.3	39.2	37.1	11.0	11.5	7.4	9.9	1.8	184.6	187.5	185.3	185.8
IH90EU	126.8	39.1	38.1	37.3	38.1	10.2	9.3	9.4	9.6	0.4	176.0	174.2	173.5	174.6
BR100US	127.7	40.8	35.1	38.6	38.2	9.5	11.1	8.8	9.8	1.0	178.0	173.9	175.1	175.7

4.3 Dent test results

As previously explained, the results of the dent tests consist of two measurements: the indentation depth and the indentation diameter. The lower they are, the better the dent resistance of the sheet material. Again, summary tables are presented for 0% and 2% pre-strain conditions and show average values and standard deviations for each alloy tested. The tables show results for only three of the alloys (HF90, IH90US, IH90EU), since these sheet materials are used to form external panels.

4.3.1 HF90 alloy

Due to the limited quantity of HF90 blanks available for this investigation, only one measurement was carried out on as-received (0% pre-strain) sheet specimens for each temperature condition and for 20 minutes. These results are presented in *Table 18*.

Table 18. Indentation depth and diameter in as-received (0% pre-strain) HF90 specimens.

HF90 0%	Indentation depth [mm]	Indentation diameter [mm]
120°C, 20 min	0.37	31
130°C, 20 min	0.32	29
170°C, 20 min	0.3	26
180°C, 20 min	0.29	25

Table 19. Indentation depth in HF90 specimens pre-strained to 2%.

HF90 2%	Indentation depth [mm]				
Specimen >>>	**#1**	**#2**	**#3**	**Avg.**	**Std. Dev.**
120°C, 10 min	0.15	0.14	0.14	0.14	0.01
120°C, 20 min	0.13	0.15	0.13	0.14	0.01
130°C, 10 min	0.16	0.13	0.12	0.14	0.02
130°C, 20 min	0.13	0.13	0.14	0.13	0.01
170°C, 10 min	0.11	0.12	0.11	0.11	0.01
170°C, 20 min	0.09	0.1	0.1	0.10	0.01
180°C, 10 min	0.11	0.12	0.11	0.11	0.01
180°C, 20 min	0.09	0.09	0.09	0.09	0.00

Table 20. Indentation diameter in HF90 specimens pre-strained to 2%.

HF90 2%	Indentation diameter [mm]				
Specimen >>>	**#1**	**#2**	**#3**	**Avg.**	**Std. Dev.**
120°C, 10 min	15	15	16	15.33	0.58
120°C, 20 min	16	15	14	15.00	1.00
130°C, 10 min	14	15	15	14.67	0.58
130°C, 20 min	14	14	15	14.33	0.58
170°C, 10 min	14	14	14	14.00	0.00
170°C, 20 min	12	12	12	12.00	0.00
180°C, 10 min	14	13	13	13.33	0.58
180°C, 20 min	9	11	11	10.33	1.15

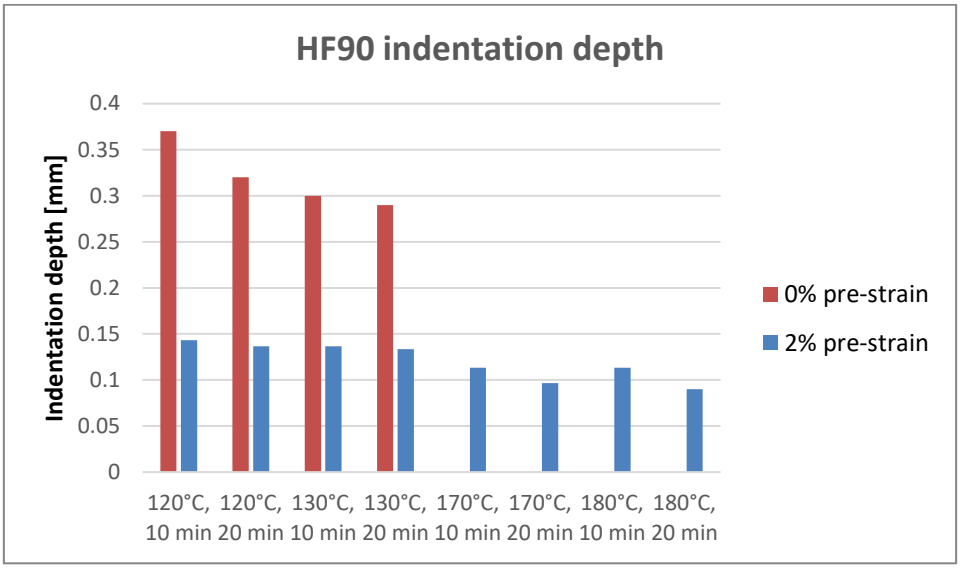

Figure 43. Indentation depth in HF90 sheet specimens pre-strained to 0% and 2%

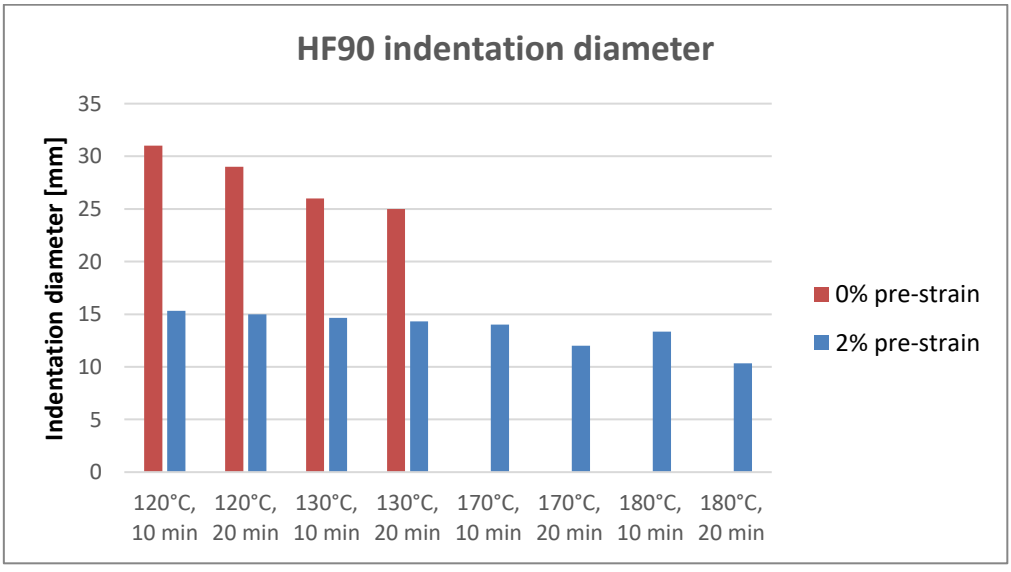

Figure 44. Indentation diameter in HF90 specimens pre-strained to 0% and 2%.

4.3.2 IH90US alloy

Table 21. Indentation depth in as-received (0% pre-strain) IH90US specimens.

IH90US 0%	Indentation depth [mm]				
Specimen >>>	#1	#2	#3	Avg.	Std. Dev.
120°C, 10 min	0.29	0.29	0.3	0.29	0.01
120°C, 20 min	0.28	0.28	0.28	0.28	0.00
130°C, 10 min	0.28	0.29	0.28	0.28	0.01
130°C, 20 min	0.27	0.27	0.25	0.26	0.01
170°C, 10 min	0.22	0.23	0.24	0.23	0.01
170°C, 20 min	0.21	0.23	0.21	0.22	0.01
180°C, 10 min	0.2	0.21	0.21	0.21	0.01
180°C, 20 min	0.18	0.18	0.18	0.18	0.00

Table 22. Indentation depth in IH90US specimens pre-strained to 2%.

IH90US 2%	Indentation depth [mm]				
Specimen >>>	#1	#2	#3	Avg.	Std. Dev.
120°C, 10 min	0.09	0.1	0.1	0.10	0.01
120°C, 20 min	0.1	0.08	0.09	0.09	0.01
130°C, 10 min	0.08	0.1	0.09	0.09	0.01
130°C, 20 min	0.09	0.09	0.09	0.09	0.00
170°C, 10 min	0.07	0.07	0.07	0.07	0.00
170°C, 20 min	0.06	0.07	0.06	0.06	0.01
180°C, 10 min	0.07	0.06	0.06	0.06	0.01
180°C, 20 min	0.05	0.07	0.05	0.06	0.01

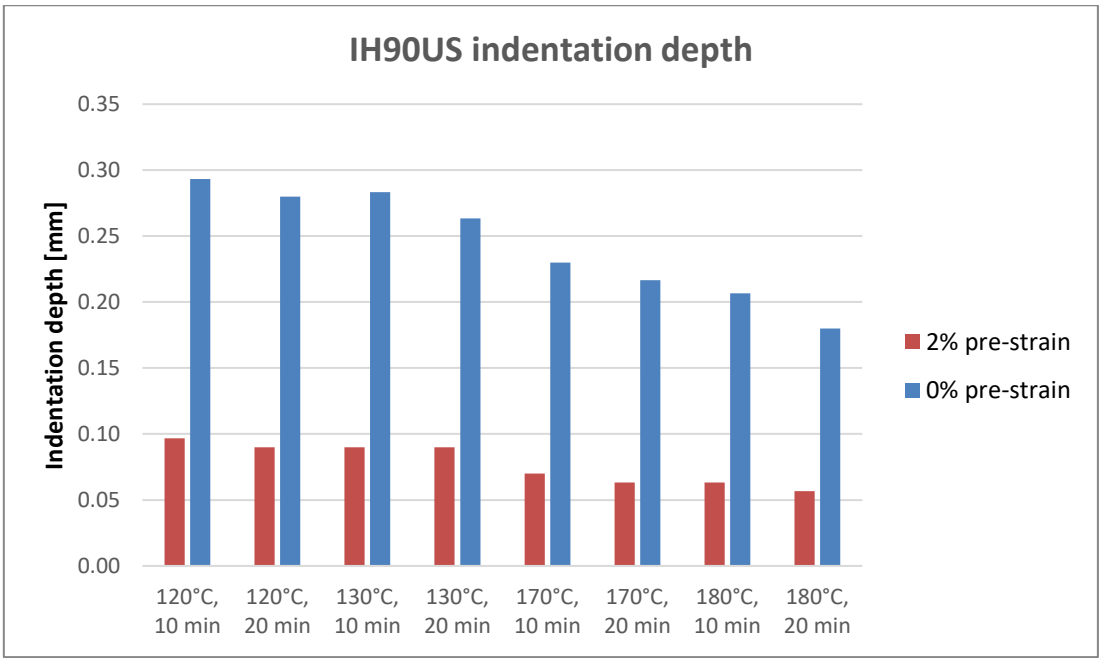

Figure 45. Indentation depth in IH90US specimens pre-strained to 0% and 2%.

Table 23. Indentation diameter in as-received (0% pre-strain) IH90US specimens.

IH90US 0%	Indentation diameter [mm]				
Specimen >>>	**#1**	**#2**	**#3**	**Avg.**	**Std. Dev.**
120°C, 10 min	32	29	30	30.3	1.5
120°C, 20 min	27	27	26	26.7	0.6
130°C, 10 min	28	28	26	27.3	1.2
130°C, 20 min	25	25	24	24.7	0.6
170°C, 10 min	22	23	24	23.0	1.0
170°C, 20 min	21	21	20	20.7	0.6
180°C, 10 min	23	20	21	21.3	1.5
180°C, 20 min	17	18	18	17.7	0.6

Table 24. Indentation diameter in IH90US specimens pre-strained to 2%.

IH90US 2%	Indentation diameter [mm]				
Specimen >>>	**#1**	**#2**	**#3**	**Avg.**	**Std. Dev.**
120°C, 10 min	11	11	12	11.3	0.6
120°C, 20 min	11	10	11	10.7	0.6
130°C, 10 min	10	12	11	11.0	1.0
130°C, 20 min	10	11	11	10.7	0.6
170°C, 10 min	8	7	8	7.7	0.6
170°C, 20 min	8	7	7	7.3	0.6
180°C, 10 min	8	7	8	7.7	0.6
180°C, 20 min	6	7	7	6.7	0.6

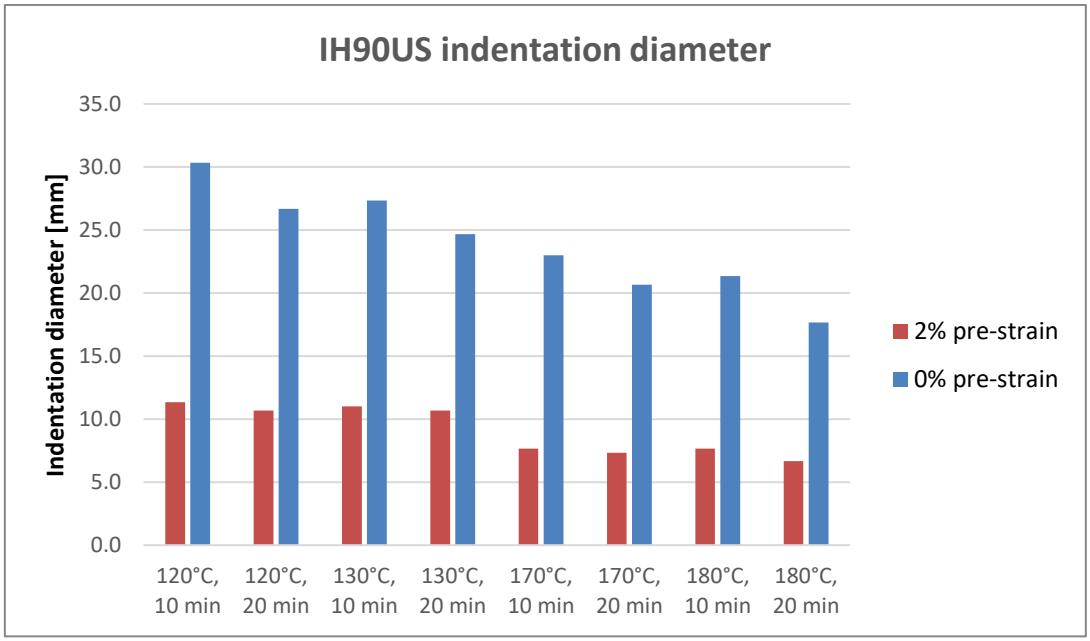

Figure 46. Indentation diameter in IH90US specimens pre-strained to 0% and 2%.

4.3.3 IH90EU alloy

Table 25. Indentation depth in as-received (0% pre-strain) IH90EU specimens.

IH90EU 0%	Indentation depth [mm]				
Specimen >>>	**#1**	**#2**	**#3**	**Avg.**	**Std. Dev.**
120°C, 10 min	0.32	0.33	0.33	0.33	0.01
120°C, 20 min	0.32	0.32	0.34	0.33	0.01
130°C, 10 min	0.32	0.32	0.33	0.32	0.01
130°C, 20 min	0.32	0.31	0.31	0.31	0.01
170°C, 10 min	0.3	0.3	0.29	0.30	0.01
170°C, 20 min	0.27	0.24	0.26	0.26	0.02
180°C, 10 min	0.3	0.28	0.3	0.29	0.01
180°C, 20 min	0.22	0.23	0.24	0.23	0.01

Table 26. Indentation depth in IH90EU specimens pre-strained to 2%.

IH90EU 2%	Indentation depth [mm]				
Specimen >>>	**#1**	**#2**	**#3**	**Avg.**	**Std. Dev.**
120°C, 10 min	0.11	0.1	0.1	0.10	0.01
120°C, 20 min	0.12	0.1	0.1	0.11	0.01
130°C, 10 min	0.12	0.12	0.12	0.12	0.00
130°C, 20 min	0.12	0.12	0.11	0.12	0.01
170°C, 10 min	0.1	0.11	0.1	0.10	0.01
170°C, 20 min	0.08	0.08	0.09	0.08	0.01
180°C, 10 min	0.1	0.1	0.09	0.10	0.01
180°C, 20 min	0.07	0.07	0.08	0.07	0.01

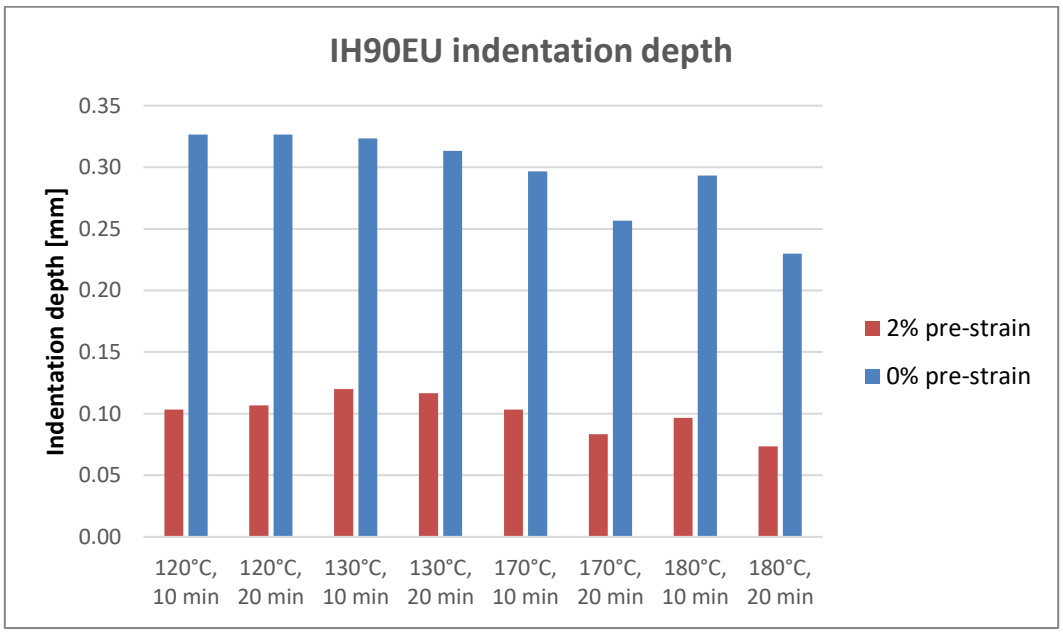

Figure 47. Indentation depth in IH90EU specimens pre-strained to 0% and 2%.

Table 27. Indentation diameter in as-received (0% pre-strain) IH90EU specimens.

IH90EU 0%	Indentation diameter [mm]				
Specimen >>>	**#1**	**#2**	**#3**	**Avg.**	**Std. Dev.**
120°C, 10 min	34	33	35	34.0	1.0
120°C, 20 min	33	33	34	33.3	0.6
130°C, 10 min	33	34	33	33.3	0.6
130°C, 20 min	29	32	32	31.0	1.7
170°C, 10 min	32	32	31	31.7	0.6
170°C, 20 min	28	27	28	27.7	0.6
180°C, 10 min	30	31	30	30.3	0.6
180°C, 20 min	26	27	27	26.7	0.6

Table 28. Indentation diameter in the IH90EU specimens pre-strained to 2%.

IH90EU 2%	Indentation diameter [mm]				
Specimen >>>	**#1**	**#2**	**#3**	**Avg.**	**Std. Dev.**
120°C, 10 min	12	12	13	12.3	0.6
120°C, 20 min	13	11	12	12.0	1.0
130°C, 10 min	14	13	14	13.7	0.6
130°C, 20 min	10	12	10	10.7	1.2
170°C, 10 min	12	11	10	11.0	1.0
170°C, 20 min	7	9	7	7.7	1.2
180°C, 10 min	9	8	9	8.7	0.6
180°C, 20 min	6	8	7	7.0	1.0

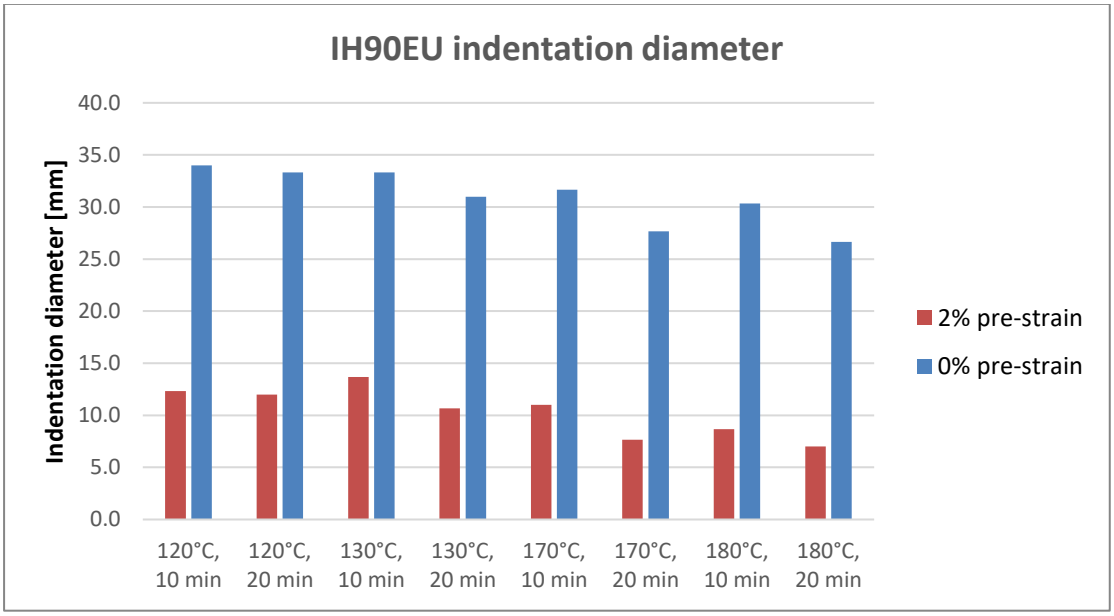

Figure 48. Indentation diameter in IH90EU specimens pre-strained to 0% and 2%.

4.4 Comparison between alloys

In this last section of the chapter, instead of analyzing the results separately, the mechanical properties of the various alloys are compared between each other. The key factor for comparison was chosen to be the strength gain percentage, which is defined as follows:

$$Strength\ gain = \frac{(Final\ Yield\ Strength - Initial\ Yield\ Strength)}{Initial\ Yield\ Strength} \cdot 100 \qquad (20)$$

The results are reported in *Table 29* and in the bar chart in *Figure 49* and *Figure 50*.

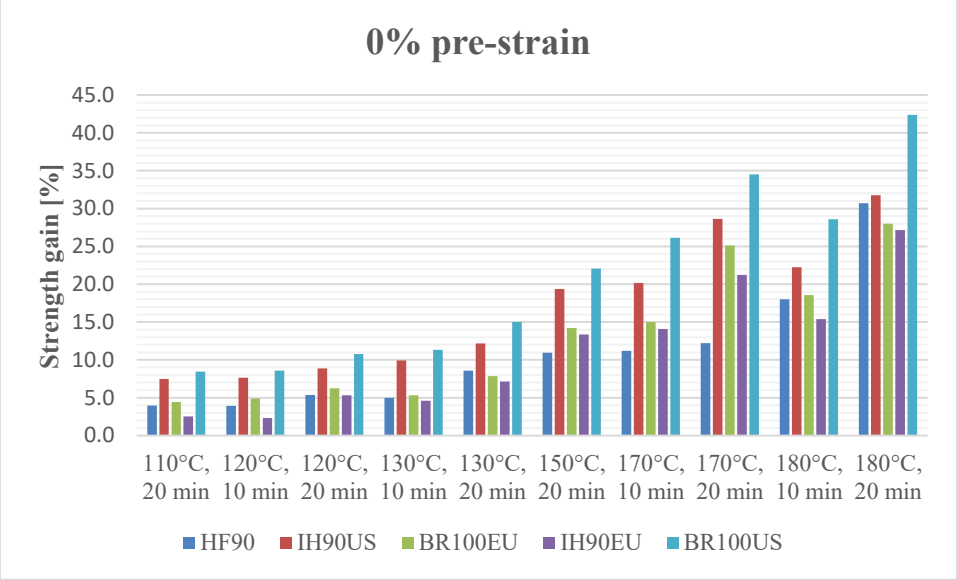

Figure 49. Strength gain achieved for each as-received alloy and baking condition.

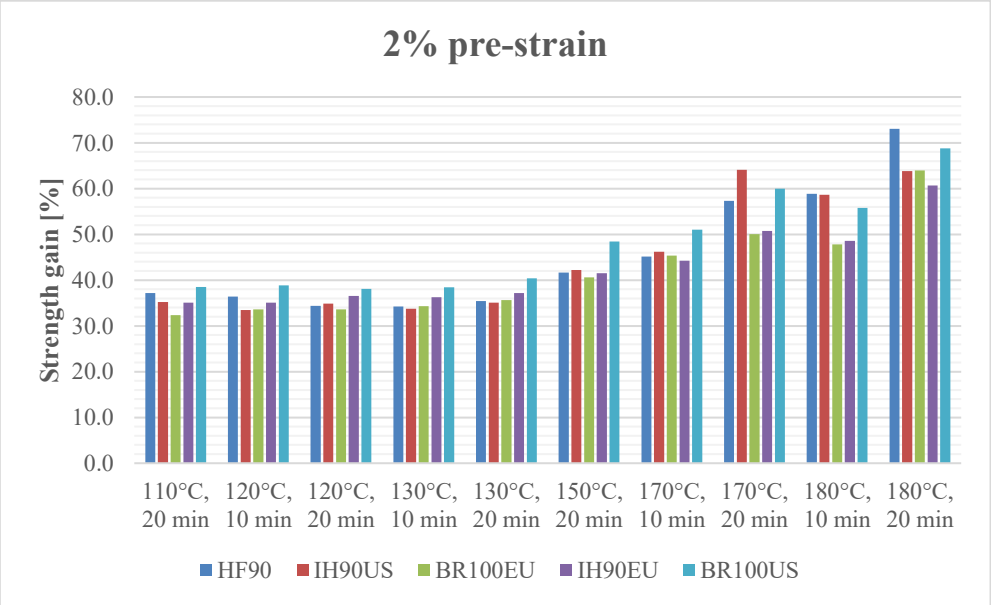

Figure 50. Strength gain achieved for each alloy and baking condition after a 2% pre-strain.

Table 29. Strength gains achieved for each alloy, baking and pre-strain condition.

	HF90		IH90US		BR100EU		IH90EU		BR100US	
Strength gain [%]	**0% p-s**	**2% p-s**	**0% p-s**	**2% p-s**	**0% p-s**	**2% p-s**	**0% p-s**	**2% p-s**	**0% p-s**	**2% p-s**
110°C, 20 min	4.0	37.2	7.5	35.2	4.5	32.3	2.5	35.1	8.4	38.5
120°C, 10 min	3.9	36.4	7.6	33.4	4.9	33.6	2.3	35.1	8.6	38.8
120°C, 20 min	5.4	34.3	8.9	34.9	6.3	33.6	5.3	36.5	10.8	38.1
130°C, 10 min	5.0	34.3	9.9	33.7	5.3	34.3	4.6	36.3	11.3	38.4
130°C, 20 min	8.6	35.4	12.2	35.0	7.9	35.6	7.1	37.2	15.0	40.4
150°C, 20 min	10.9	41.6	19.4	42.2	14.2	40.6	13.4	41.5	22.1	48.5
170°C, 10 min	11.2	45.2	20.2	46.2	15.0	45.4	14.1	44.2	26.1	51.0
170°C, 20 min	12.2	57.3	28.6	64.1	25.1	50.0	21.2	50.7	34.5	59.9
180°C, 10 min	18.0	58.8	22.2	58.7	18.6	47.8	15.4	48.6	28.6	55.7
180°C, 20 min	30.7	73.0	31.8	63.8	28.0	63.9	27.1	60.6	42.4	68.8

Furthermore, it can be useful to compare the final yield stress levels of the various alloys to understand which one has the best overall mechanical properties after forming and the paint bake cycle (*Figure 51* and *Figure 52*).

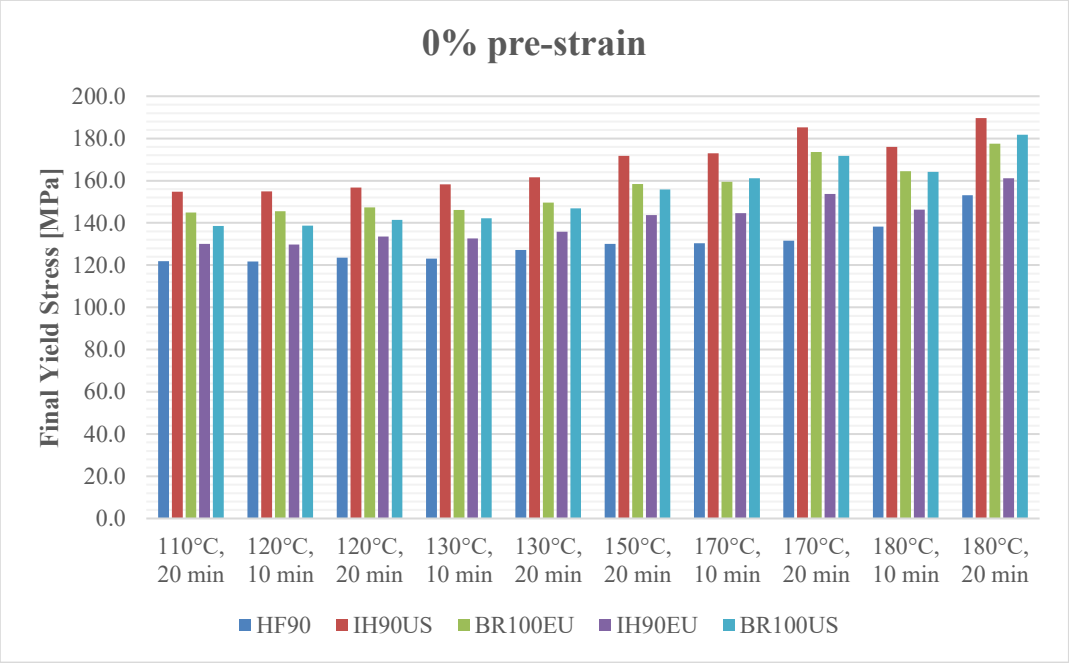

Figure 51. Final yield stress of as-received (0% pre-strain) alloys after each baking condition.

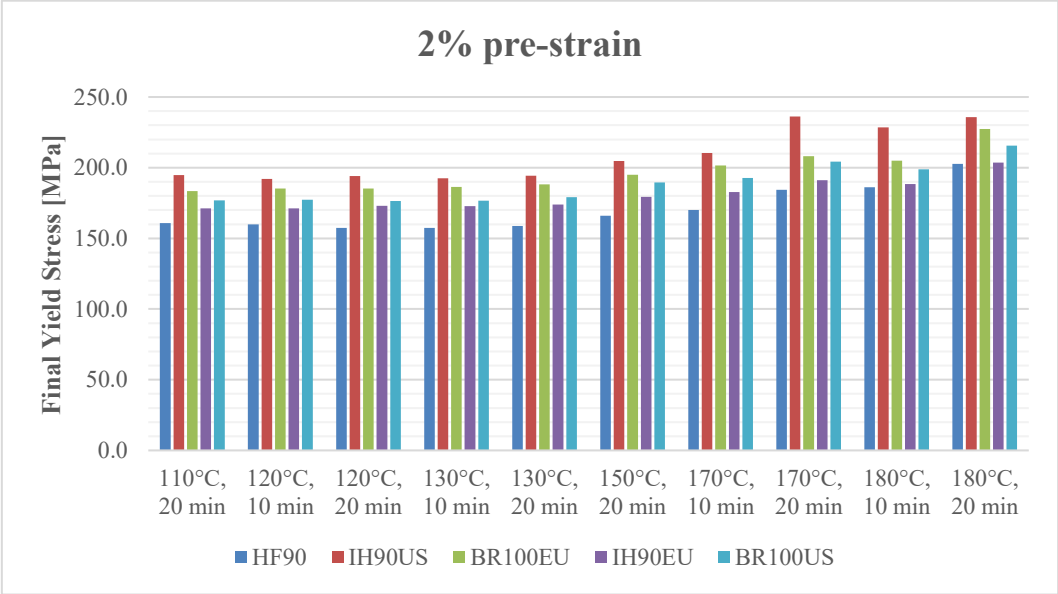

Figure 52. Final yield stress of each alloy after a 2% pre-strain and after each baking condition.

5 Discussion

In this chapter, the results previously reported are discussed and analyzed to understand if the outcomes comply with the initial hypotheses and, if not, explanations of those discrepancies are provided.

5.1 Stress-strain curves

Comparing *Figure 34* and *Figure 35*, it is immediately noticeable that a 2% pre-strain has a significant effect on the final yield stress improvement. This is because a pre-strain is a source of new mobile dislocations, which increases the dislocation pinning effect and, as a consequence, the plastic strength. It can be seen from these figures that the stress level reached at the onset of plastic deformation for the specimens pre-strained to 2% is clearly greater than for the 0% pre-strain case. On the other hand, the different in ultimate tensile stress is not as evident, because the pre-strained specimens are subjected to a lower rate of strain hardening after the onset of plastic deformation.

Figure 36 and *Figure 37* show an enlarged view in correspondence of the yield stress area. While the 0% pre-strain curves are monotonically increasing and exhibit continuous yielding, the 2% pre-strain curves present a shape that is similar to the behaviour of steels, when a lower yield stress appears after a pre-strain. However, not all the flow curves of the aluminum alloys under consideration presented a local minimum, even though the curves obtained after a 2% pre-strain resemble the shape of flow curves for steel which exhibit a change of concavity after the onset of plastic deformation.

It is also interesting to consider the elongation of the specimens at fracture (again, *Figure 34* and *Figure 35*). At 0% pre-strain, the “as received” specimens and those baked up to 130°C exhibit a final tensile elongation between 26% and 27%, whereas fracture is detected at around 25% elongation in specimens baked at 150°C, 170°C and 180°C. For specimens pre-strained to 2%, the specimen baked at 150°C aligns with those that were baked at lower temperature, while the specimens baked at 170°C and 180°C fracture at an even lower elongation (between 23% and 25%). Overall, the behaviour is quite clear and corresponds to the expectations: the specimens that exhibit greater yield stress due to a more “aggressive” pre-strain and baking cycle, lose ductility with respect to the other ones.

5.2 Tensile test results

The first step in the analysis of tensile test results was to check that the tensile test data comply with the guaranteed mechanical properties provided by the OEM.

The mechanical strength requirement was fulfilled in regard to the initial yield stress of every alloy considered. The same applies for the yield stress after baking.

Now, the results for each alloy can be further discussed. The HF90 alloy, as shown in *Figure 38*, is characterized by very low BH levels for baking temperatures from 110°C to 130°C: all the data in this range are very similar and are less than 10 MPa, and in some cases the BH response for 0% pre-strain is slightly higher than that for a 2% pre-strain. However, as said, the results are all very similar, which means that the difference in bake response in this temperature range is not significant. The first considerable improvement occurs at 150°C, where the BH value reached 15 MPa after a 2% pre-strain. No further improvement was detected after baking at 170°C for 10 minutes. But another significant increase in bake hardening effect occurred in the specimens pre-strained to 2% and baked at 170°C for 20 minutes; in this case, the bake hardening reached 30 MPa. However, this level of improvement was not detected for the 0% strain case. A further 5 MPa were gained by baking at 180°C for 10 minutes, but the greatest improvement took place after baking at 180°C for 20 minutes: in this case, the BH level increased to 36 MPa and 52.7 MPa for specimens pre-strained to 0% and 2%, respectively. It can also be noted that at 180°C the yield stress data showed more variation, as the standard deviation increased from about 1 MPa to 4 and 6 MPa.

The IH90US alloy showed similar increases in mechanical strength when baked at 180°C (see *Figure 39*), but it exhibits a better bake-hardening response at low temperatures, as the strengthening level is always at least about 10 MPa. In addition, the difference between baking at 170°C and at 180°C is not as significant as for the HF90 alloy. And similar to the HF90 alloy, as-received (0% pre-strain) specimens sometimes give a higher BH level with respect to those that were pre-strained to 2%, but this only occurs at lower temperatures (up to 170°C baking for 10 minutes). Lastly, the greatest variation in the test data was observed when baking at 170°C for 20 minutes after a 2% pre-strain (the standard deviation reached 5.4 MPa).

The BR100EU alloy showed a similar bake hardening response as the HF90 alloy at low temperatures (*Figure 40*): the increase in strength remained around 10 MPa or less. At higher temperatures (170°C and 180°C), the BH levels in BR100EU and

HF90 are similar for specimens pre-strained to 2%, however the differences in mechanical strengthening for the 0% and 2% pre-strain conditions are not so pronounced in the BR100EU.

The IH90EU alloy, if pre-strained to 2% and baked at temperatures between 110°C and 130°C, presents a bake response which is almost constant at around 10 MPa (*Figure 41*). It can also be seen that the strength of as-received specimens improves with increasing baking time and temperature. At high temperatures, lower bake-hardening levels were detected with respect to the other alloys. It appears that for this alloy the effect of baking time is more significant than the effect of temperature: baking for 20 minutes at a certain temperature almost always yields better mechanical strength than baking for 10 minutes at the next higher temperature. Even baking at 150°C for 20 minutes leads to a bake hardening response that is quite similar to that obtained by painting at 170°C for 10 minutes.

Finally, the BR100US alloy presents a good BH response at low temperatures, of approximately 15 MPa (*Figure 42*). Then, a noticeable improvement takes place at 150°C. And for temperatures above 150°C, it can be noted that 0% strain causes an equal or even higher strengthening level than that reached after a 2% pre-strain. Similar to its counterpart from Europe, the BR100US alloy is designed for improved bake response; the most evident effect, based on the experimental data, seems to be an enhanced strengthening level for specimens that were not pre-strained.

For what concerns natural aging phenomena, presented in Section 4.2.6, it was noted that specimens kept at ambient temperature after pre-strain exhibited unexpectedly high bake-hardening values. To better understand this phenomenon, *Figure 53* shows the BH levels reached at ambient temperature as well as those obtained after a 2% pre-strain followed by baking at 110°C for 20 minutes. In some cases, like in the HF90 and the BR100EU alloys, the bake hardenability at ambient temperature is clearly higher than at 110°C.

Considering again the stress-strain curves for the BR100US alloy obtained after a 2% pre-strain, the flow curve for the ambient temperature condition (i.e. the curve in bright red in *Figure 54*) happens to lie above that obtained after baking at 130°C. This means that some natural aging took place between the first tests for initial yield strength assessment and the 2% pre-straining for the ambient temperature condition. One way to immediately confirm that natural aging happened is to plot the stress-strain curve of the initial tests along with the pre-strain curve of the samples that would have then been

kept at ambient temperature (*Figure 55*). As a matter of fact, the pre-strain curve is already above the initial one, so natural aging actually took place before pre-straining. At around 2% strain, the difference in engineering stress between the two curves is about 5 MPa.

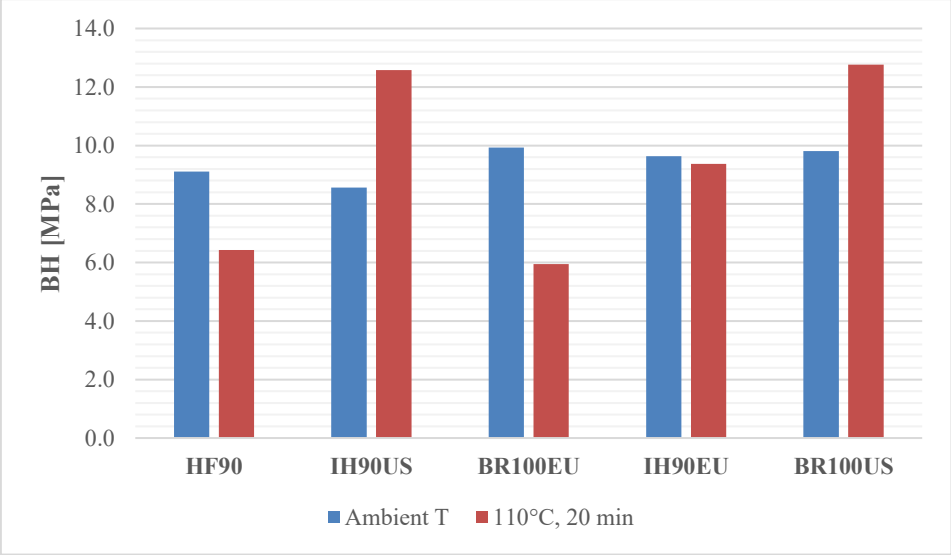

Figure 53. Comparison of BH level for specimens kept at ambient temperature or baked at 110°C for 20 minutes.

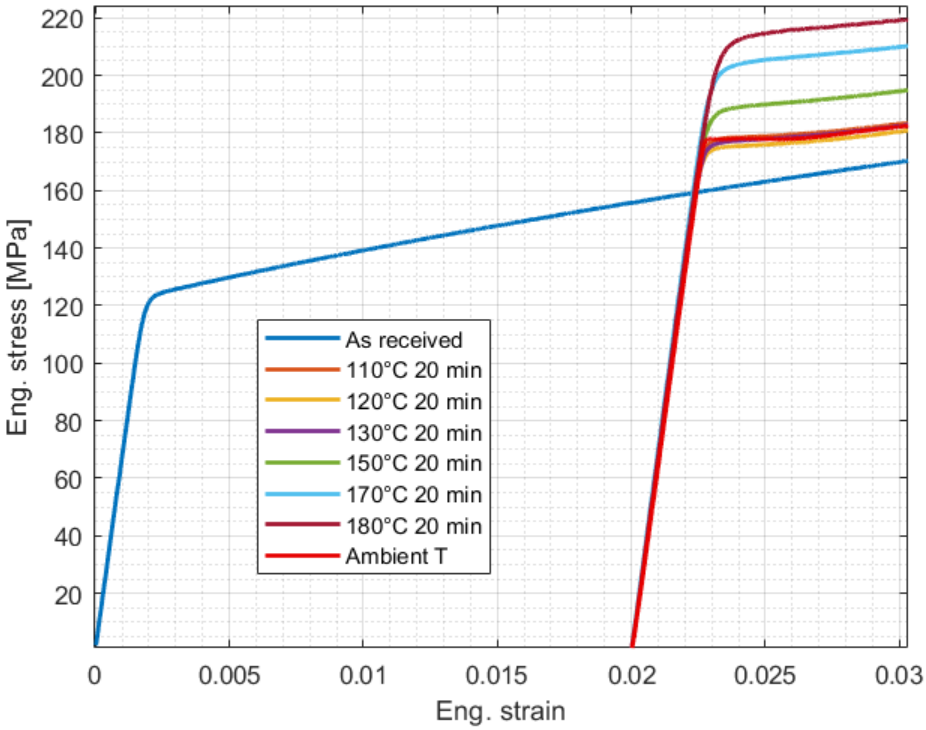

Figure 54. Comparison of BR100US engineering stress-strain curves at 2% pre-strain, including the ambient temperature condition.

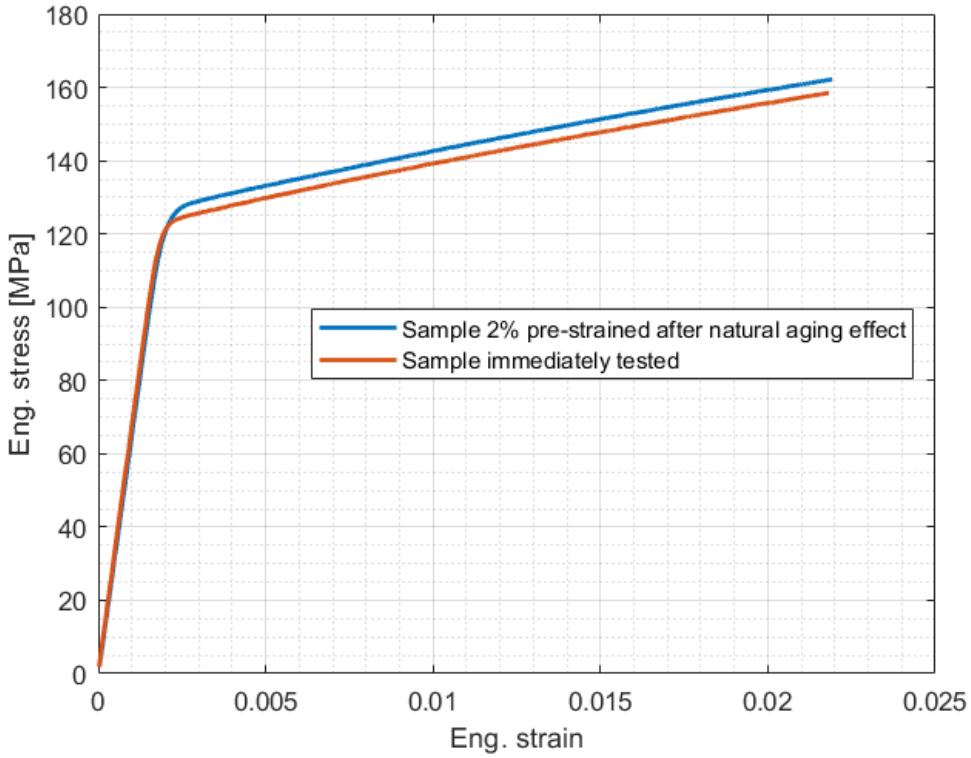

Figure 55. Initial flow curve of BR100US alloy and that obtained after keeping a specimen at ambient temperature and then pre-straining it to 2%.

The same graphs can be plotted for example for the IH90US alloy, in which the flow curve obtained at ambient temperature does not surpass that obtained after baking at 110°C for 20 minutes. In *Figure 56* and *Figure 58*, it can be noticed that for both alloys there is a steep slope decrease right after the onset of plastic deformation: hence, the 2% pre-strain, ambient temperature curves are similar to the stress-strain curves of steel that show a lower yield stress. Due to this conformation, the ambient temperature curves of the two alloys initially reach higher stress levels with respect to the ones representing low temperature baking (110-130°C), but after yielding they stabilize at lower stresses instead. However, as shown in *Figure 55* and *Figure 57*, it is clear that natural aging occurred for these alloys. An interestingly surprising result is that for both the IH90US and the BR100US alloys, the stress difference between the pre-strain curve and the initial test curve at 2% strain is about 5MPa, which is the same value that was found for all the other alloys: this is quite a small value, but nevertheless, some natural aging was detected. To better understand what this outcome means, it is useful to explain the timeframe of the testing phase.

The five aluminum alloys have been presented in this project with a particular order, which is the chronological order of shipment. The HF90 alloy, in fact, was shipped to the University Labs in April, while the BR100US arrived in June. Moreover, the testing phase of the specimens pre-strained to 2% and kept at ambient temperature was scheduled at the end of June, for all the alloys. This means that the HF90 alloy specimens experienced a two-month wait, whereas the BR100US specimens only experienced natural aging for a few days. Still, natural aging as the absolute value of stress difference between the pre-strained curve and the "as received" curve was found not to regularly increase over time, as it is almost constant for all the alloys. As natural aging is not linear over time, one could hypothesize that, having also in mind the results from Wüebbels et al. [18], the aging kinetics may not be particularly relevant without prior pre-strain. What could have happened is a minor strengthening in a relatively short time after the specimens were machined, and then a stabilization of the phenomenon occurred with no further strengthening: this could explain why even the last alloy received (BR100US) also exhibits a small stress increase. The assumption of a nearly uniform aging behaviour may find another proof in the fact that, looking back at *Figure 53*, the bake-hardening values of ambient temperature aged specimens are quite close (around 9 MPa), independently from the alloy. Assuming the natural aging response is similar for all these alloys, a material which on the contrary has a better bake response will suffer less in proportion from this initial aging effect. In our analysis, the IH90US alloy seems to fulfill these characteristics, as confirmed by *Figure 56*.

Another consideration that can be made is that there was no knowledge of the alloy life prior to shipment for testing. In particular, the time span between solution heat treatment and delivery to the university is not known, and it may have been different for each alloy.

In any case, the strengthening level due to natural aging is relatively small compared to the amount of hardening generated by baking at higher temperatures such as 170°C and 180°C; it would be much more relevant in the time span between the pre-straining and the baking. For this reason, as explained in the Methodology chapter, each specimen was baked immediately after carrying out the pre-strain. On the other hand, the same aging effect gives mechanical strength results that in some cases overlap the experimental outcomes after baking at low temperature. Thus, a reasonable conclusion is that baking at lower temperatures (under 150°C) for an amount of time not higher

than 20 minutes does not provide appreciable mechanical strengthening, as their effect may be the same as simply aging the material at ambient temperature.

To completely avoid any natural aging, a solution consists in putting the samples in freezers right after their machining. This possibility was not available, but as said great attention was put in maintaining a time span between the pre-straining and the baking as consistent as possible throughout the entire experimental phase.

It should be remembered that, according to the results of Wüebbels et al. [18], natural aging just affects the bake hardening value, but the total strengthening and the final tensile strength remain unchanged. A more detailed future study on the effect of natural aging on these aluminum alloys would be interesting in order to obatin a more complete background on the behaviour of 6xxx alloys after baking.

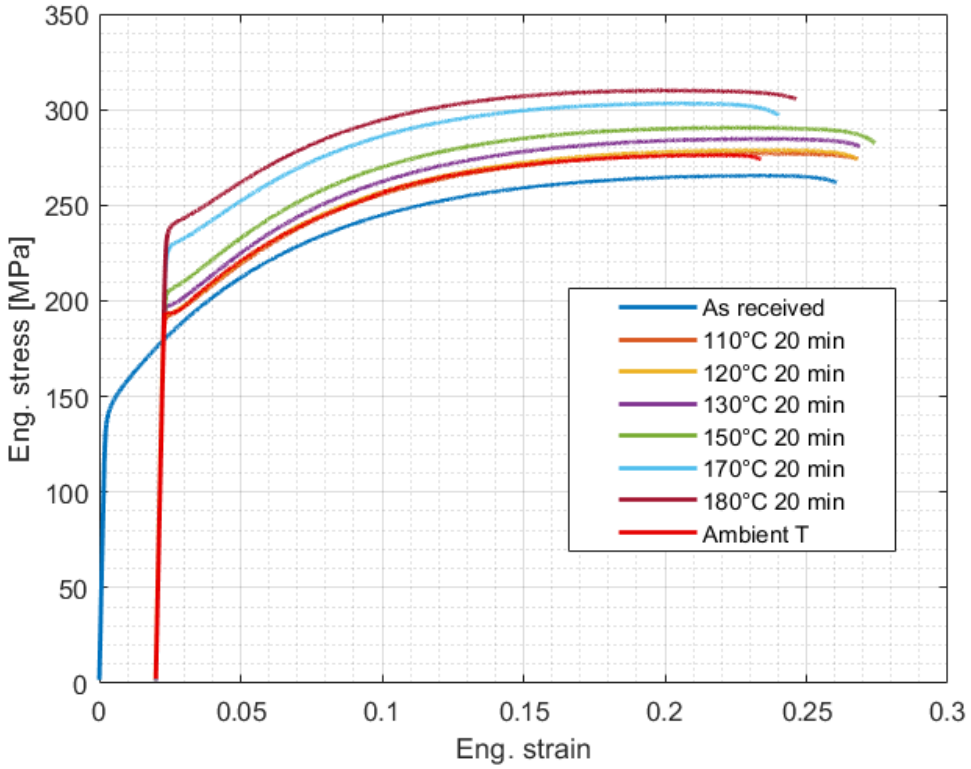

Figure 56. Comparison of IH90US engineering stress-strain curves at 2% pre-strain, including the ambient temperature condition.

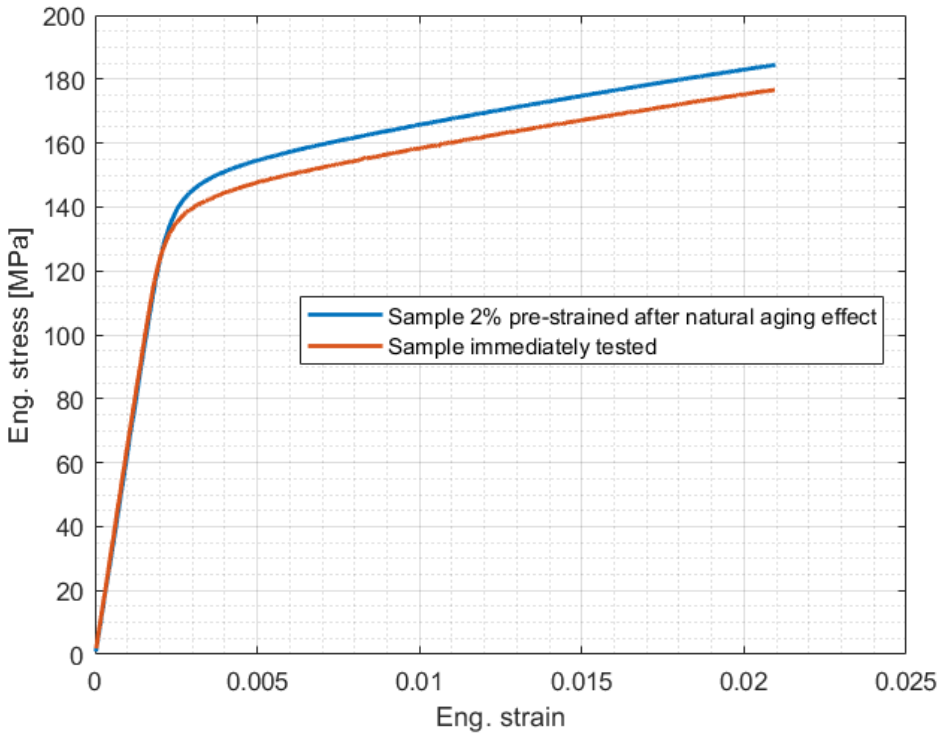

Figure 57. IH90US initial test curve and pre-strain curve for specimen kept at ambient temperature afterwards.

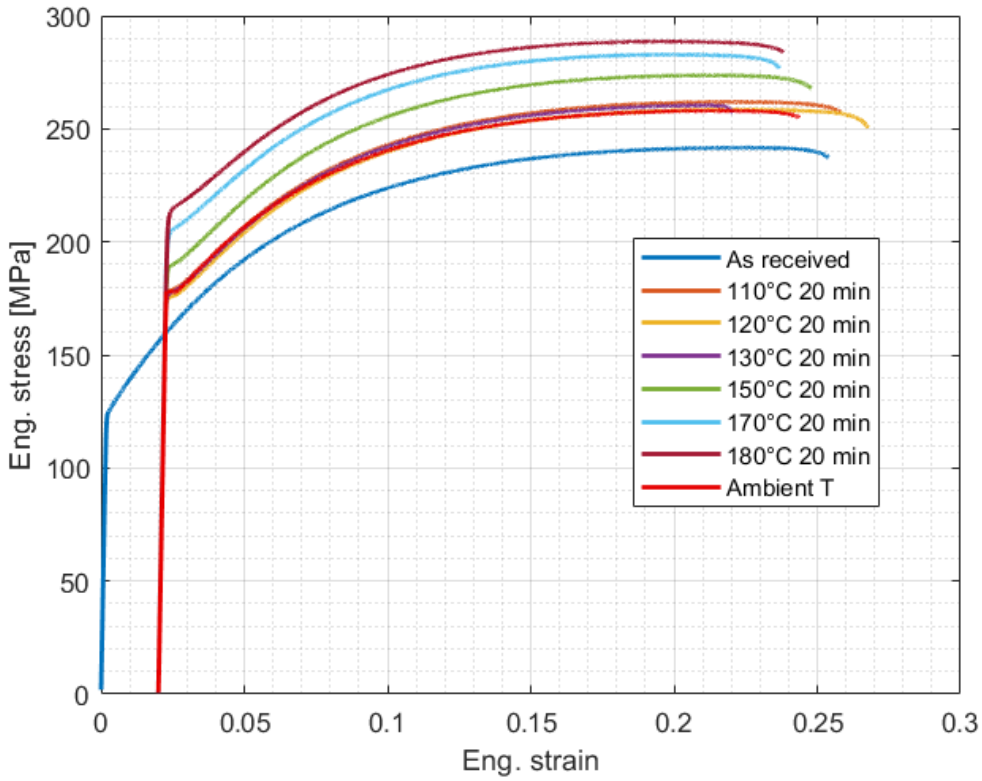

Figure 58. Comparison of BR100US engineering stress-strain curves at 2% pre-strain, including the ambient temperature condition.

5.3 Dent test results

Even though there were limited data that could be recorded for the HF90 alloy, a clear difference between unstrained and strained blanks is noticeable; after baking at 120°C and 130°C, the indentation depth is more than halved if the sheet is subjected to a 2% biaxial strain, while the indentation diameter is nearly halved (*Figure 43* and *Figure 44*). For as-received blanks, both the depth and the diameter gradually decrease from baking at 120°C for 10 minutes to baking at 130°C for 20 minutes. In contrast, the pre-strained specimens exhibit a less perceivable change for the same baking conditions. At higher temperatures (170°C and 180°C) it is very evident that the time effect prevails over the temperature effect: baking at 170°C for 20 minutes is more effective than baking at 180°C for 10 minutes.

The IH90US alloy proved to have a good response after pre-straining: it exhibited an indentation depth in pre-strained specimens that was only 32%-35% that for as-received sheets, and the indentation diameter of pre-strained specimens was between 37% and 43% that of as-received specimens. Similar to the HF90 alloy, the dent resistance response after baking at higher temperature showed a predominance of the baking time.

The results for the IH90EU alloy show some inconsistencies: at 130°C baking, for both temperatures, the indentation depth was higher than at 120°C. The diameter, instead, was higher just for the blanks that were baked at 130°C for 10 minutes. These discrepancies took place after a 2% pre-strain: it would have been useful to repeat these tests, if more sheets had been available, to check if it was due to an error in the baking phase, in the dent testing phase with the mechanical pendulum or in the subsequent measurements of the dents. Without further information, the latter case seems to be the most likely because, as already mentioned, the measurement instruments (digimatic indicator and circle template) had accuracies of respectively 0.01 mm and 1 mm, which are not particularly high.

To summarize, indentation depth and diameter showed very similar trends for each alloy and pre-strain condition, in that both factors describe well the superficial mechanical resistance of the alloys. A general outcome is the fact that increasing the baking duration was more effective than raising the baking temperature.

5.4 Comparison between the alloys under examination

After discussing the results for each alloy, it is also helpful to compare their responses to be able to draw conclusions about which alloy, given all the recorded mechanical characteristics, can be the most suitable for automotive industrial applications.

For what concerns the tensile results, it is important to distinguish between strength gain, which is a measure of the bake response of the material, and final yield strength, which represent the overall mechanical strength. Obviously, an alloy with a better strength gain will not necessarily have the greatest final yield stress, since it also depends on the initial yield stress of the "as received" material.

Looking at *Figure 49*, the BR100US alloy exhibits the greatest strength gain for unstrained specimens, with a 42.4% strengthening after baking at 180°C for 20 minutes, which is much more than any other alloy. The second greatest strength gain is reached by the IH90US at 31.8%, a value that is even lower than the gain reached by the BR100US after baking at 170°C for 20 minutes. The least effective alloy without pre-strain is the IH90EU, both at low baking temperatures and at 180°C. On the contrary, the HF90 exhibits an interesting gain of 30.7% when baking at 180°C for 20 minutes. Considering the response of these alloys after a 2% pre-strain (*Figure 50*), the HF90, turns out to be the alloy that exhibits the greatest mechanical response after baking at 180°C for 20 minutes. The IH90EU alloy shows a good bake response at lower temperatures, but does not improve as much as the other alloys when the baking temperature is increased. In any case, the pre-strained specimens showed much more similar results from one alloy to another compared to that of unstrained specimens.

Overall, the IH90US alloy exhibited the best bake response, with maximum gains of 42.4% and 73% for 0% and 2% pre-strain conditions, respectively. The beneficial effect of pre-straining on material strengthening is particularly evident at lower baking temperatures, as shown in *Table 29*.

For what concerns the final tensile strength, the IH90US alloy showed the greatest yield stress after baking for any temperature-time condition, as shown in *Figure 51* and *Figure 52*: it reached 203.6 MPa after baking at 180°C for 20 minutes. Both the European and North American versions of the BR100 alloy showed good strength, with the BR100EU being slightly more resistant. In contrast, the HF90 has the lowest yield strength overall.

The IH90US alloy, other than having the best tensile strength properties, is also the alloy that gives the best results in terms of resistance to indentation, as it exhibits the lowest values of indentation depth and diameter. As expected, the HF90, being the alloy with the lowest yield strength, is also the one that shows the biggest indentations. However, it exhibits better ductility: its tensile elongation reached almost 30% after low temperature baking compared to about 26% or 27% for the other materials. Being an alloy designed for high formability purposes, these outcomes are consistent with what would be expected.

5.5 Correlation with chemical contents

Another interesting aspect to analyze is how the chemical content of one alloy can affect its mechanical properties. Thus, the aim is to try to correlate the results just discussed with the percentage of the alloying elements in each one of the 6xxx series aluminum alloys. For the sake of facilitating the analysis, *Table 2* is reported again here.

	Si	**Fe**	**Cu**	**Mn**	**Mg**	**Cr**	**Zn**	**Ti**
IH90US	0.77	0.21	0.24	0.14	0.61	0.02	-	0.01
IH90EU	0.5 to 1.5	0.35 max	0.25 max	0.20 max	0.25 to 0.9	0.15 max	0.10 max	0.15 max
BR100US	0.79	0.24	0.12	0.084	0.64	0.026	0.008	0.027
BR100EU	0.6 to 1.5	0.35 max	0.25 max	0.35 max	0.2 to 0.8	0.10 max	0.20 max	0.15 max

According to Lloyd [17], the bake hardening response depends in a small measure on the concentration of silicon atoms, and mainly on the presence of free Mg atoms that can form metastable clusters with Si atoms. The aging kinetics, instead, are improved by the copper content of the alloy. Considering the HF90 alloy, whose exact composition is hidden because of industrial sensitive information, it has a low magnesium content with respect to silicon: therefore, the low Mg content probably limits the formation of metastable precipitates, which could explain the relatively poor bake response of the HF90 alloy, especially at low temperatures where the aging kinetics are slower. The IH90EU alloy seems to present a different situation: it has the greatest Mg content, but at the same time the lowest concentration of Si atoms, so that once again, the conditions for cluster formation are probably not ideal.

The IH90US alloy, which previously exhibited the best mechanical properties, both in tensile and dent tests, has the greatest Cu content among all the alloys investigated. This could mean that the good bake response of the IH90US alloy is mainly due to fast aging kinetics, so that the same level of bake-hardening saturation is reached in less time. Therefore, this alloy can probably reach values which are closer to saturation with the same baking time compared to the other alloys. A study on the bake-hardening levels of all the alloys could confirm this hypothesis.

The improved bake response of BR100 alloys, however, does not find a particular motivation at a chemical level, since the Cu content are the lowest and the Si-Mg contents are not as high as for other alloys. However, the concentration ratio between Mg and Si could be such that it is balanced to optimize the formation of Mg-Si metastable clusters. In addition, the baking effectiveness could have been enhanced by treatment prior to shipment, such as pre-aging, as explained by Li et al. [14] and Zhong et al. [15].

6 Conclusions

6.1 Summary and conclusions

In this Thesis, the bake hardening behaviour of five aluminum alloys used for automotive outer panel applications has been experimentally investigated through tensile and dent tests. Among all the alloys, the IH90US stands out as having the best mechanical response, having the greatest final tensile stress after baking and the greatest resistance to indentation. The BR100 alloys, despite a lower initial tensile strength, also exhibit a good bake response; in particular, the BR100US has the greatest strength gain overall and seems to be more suitable for inner parts than the BR100EU, because its initial yield strength is lower, which means it has better formability, but it also has a greater mechanical resistance after baking. In the event that even greater formability is required, the HF90 alloy is the most formable of the five alloys.

Moreover, the effect of pre-strain on the material strength after baking is particularly evident: from 0% to 2% pre-strain, the strength gain can be doubled at high baking temperatures, and it can become even ten times larger at low baking temperatures.

Another important outcome is that mechanical resistance for these alloys is generally enhanced more effectively by increasing baking time by 10 minutes at the same temperature rather than increasing the baking temperature by 10°C and decreasing the time. Furthermore, it was noted that baking temperatures of 120°C and 130°C do not give high bake-hardening values as a result, as they are even matched by the strengthening due to natural aging. However, at 2% pre-strain, the final yield strength and the dent resistance are not extremely different: for example, the IH90 exhibits a final yield strength of around 195 MPa at lower temperatures, and about 235 MPa at higher temperatures. For what concerns indentation depth, it is always below 0.2 mm no matter the temperature, which is an acceptable result. Thus, we can conclude that lower temperature baking (120°C-130°C-150°C) has the potential to still guarantee mechanical resistance requirements like in the case just mentioned; in general, its effectiveness and applicability will obviously depend on the particular requirements that are needed for each part.

Last, the natural aging phenomenon was detected in every alloy and was found not to increase linearly with time, as it gave a similar strengthening amount to each material (around 5 MPa at 2% strain).

6.2 Limitations and further work

As far as the baking phase is concerned, it is important to point out that it partially depends on the oven characteristics. Measuring the baking time based on when the specimen reaches the required temperature allows for an accurate and consistent time count. However, the oven ramp up capability, which will affect how fast the specimen will heat up prior to reaching the target temperature, depends on the available experimental equipment.

As previously mentioned, a sixth aluminum alloy, the HS170, was supposed to be tested. Unfortunately, this was not possible because of technical issues at the laboratories. This high-strength type of alloy could provide very interesting results due to its peculiar characteristics, such as its very high Cu and Mg content, which would be useful to integrate the analysis of the correlation between tensile and dent test results and chemical composition. A good bake response would be expected, both in terms of fast kinetics and bake-hardening saturation level. For these reasons, it would be interesting to carry out the same series of tests on this sixth alloy in the future, as well as adding some steel sheets to the study, especially BH210 alloys from North America and Europe that are of industrial interest.

A more extensive and detailed analysis of the natural aging phenomenon, especially its variation with time, is also required to have a more complete understanding of the bake hardening response of these alloys. Actual aging times could be evaluated by also considering the time delay between solution heat treatment of the alloys and their testing, which was unknown in this project. Moreover, it could be useful to obtain the bake-hardening saturation level for each alloy, in order to compare every test result with the actual saturation level and make interesting evaluations about the hardening kinetics.

In this project, only the no pre-strain and the 2% pre-strain conditions were considered, with the 2% value taken as a representative value for car body panel forming. In the future, a more in-depth study of the effect of the magnitude of the pre-strain on the bake-hardening response could be undertaken by considering a wider range of pre-strain values that can be developed in various regions of a car body panel.

Since all the tests were static, it can be interesting to do fatigue testing with these same alloys in the future. This may not be particularly useful for alloys that are designed for external body applications, but it can turn out to be interesting for alloys that are intended for internal and structural parts, such as the BR100 and the HS170 alloys.

Further effort should be devoted to developing a predictive model of the bake-hardening behaviour of these 6xxx alloys. This might be done using the Harper model equations, but seeking to overcome the main limitations that were encountered during the preliminary optimization that was performed in this study. First, it is necessary to ensure that the optimized parameters do not give a constant bake-hardening value for any temperature and time condition. Then, the radius of the precipitates should be considered a function of time, thus reconsidering the two-layer optimization structure. To do this, the equation expressing the relation between R and time should be revised to make sure that it is not constant, and the MATLAB function "fzero" can find a local minimum which is the R parameter corresponding to each time value. Great attention must be put on the choice of the initial values of the parameters k, which means carefully estimating, or measuring, the material parameters that are required for the Harper model. Succeeding in the development of such an analytical model would be very useful to the OEM as it would allow the prediction of the bake-hardening response of these alloys for a range of baking times and temperatures.

6.3 Research contributions

The research presented in this Thesis is thought to be helpful and relevant to day-to-day engineering needs. Indeed, the experimental results that have been compiled constitute a reliable database of mechanical characterization of some of the aluminum alloys that the OEM uses to form automotive body parts and outer panels. It is expected that this database will be used during the design phase of new vehicles and provide information that would help select the most suitable sheet material for automotive body panels. Moreover, process optimization can be done by consulting the actual data that was gathered in terms of optimum time and temperature to consider during painting. It is not a matter of achieving the best improvements in mechanical properties as an absolute value: the key is, instead, to find the minimum baking temperature and time condition that can still meet the materials mechanical requirements while minimizing the energy consumption of the baking phase.

Finally, the methodology and the proposed simplifications to the Harper model gave an initial overview of what the next step of this research topic is, i.e. using the gathered data as an input for the creation of a predictive model of the bake-hardening behaviour of 6xxx aluminum alloys. Validation of the model, such as that which was attempted in this Thesis would allow it to be implemented into Computer Aided Engineering software that could be used to further enhance the OEM's lightweighting strategies for automotive body design.

References

[1] Gokhale, Amol A., N. Eswara Prasad, and Biswajit Basu. *Light Weighting for Defense, Aerospace, and Transportation*. Springer, 2019, p 39-52, p 89-102.

[2] https://www.ford.ca/trucks/f150/features/tough/

[3] Regulation (EU) 2019/631 of the European Parliament and of the Council, *Setting CO_2 emission performance standards for new passenger cars and for new light commercial vehicles, and repealing Regulations*, 17 April 2019.

[4] BS EN 10325:2006. *Steel - Determination of yield strength increase by the effect of heat treatment [Bake-Hardening-Index]*.

[5] Vasilyev, Alexander A., Hu-Chul Lee, and Nikolay L. Kuzmin. "Nature of strain aging stages in bake hardening steel for automotive application." *Materials Science and Engineering: A* 485.1-2 (2008): 282-289.

[6] Krauss, George. *Steels: processing, structure, and performance*. Asm International, 2015, p 245-246

[7] Ballarin, V., et al. "Mechanisms and modeling of bake-hardening steels: Part I. Uniaxial tension." *Metallurgical and Materials Transactions A* 40.6 (2009): 1367-1374.

[8] J.F. Butler: *J. Mech. Phys*. Solids, 1962, vol. 10, pp. 313–34.

[9] Ballarin, V., et al. "Mechanisms and modeling of bake-hardening steels: Part II. Complex loading paths." *Metallurgical and Materials Transactions A* 40.6 (2009): 1375-1382.

[10] Thuillier, et al. "Modeling bake hardening effects in steel sheets—Application to dent resistance." *Metals* 8.8 (2018): 594.

[11] Kilic, S.; Ozturk, F.; Sigirtmac, T.; Tekin, G. Effects of Pre-strain and Temperature on Bake Hardening of TWIP900cr Steel. Int. J. Iron Steel Res. **2015**, 22, 361–365.

[12] Hill, R. *The Mathematical Theory of Plasticity*, Clarendon Press

[13] Juijerm, Patiphan, Adisorn Kodwichian, and I. Altenberger. "Effects of pre ageing on paint-bake-hardening response of aluminium alloy AA6110."

[14] Li, Hui, Zhaohui Yan, and Lingyong Cao. "Bake hardening behavior and precipitation kinetic of a novel Al-Mg-Si-Cu aluminum alloy for lightweight automotive body." *Materials Science and Engineering: A* 728 (2018): 88-94.

[15] Zhong, Hao, Paul Rometsch, and Yuri Estrin. "Effect of alloy composition and heat treatment on mechanical performance of 6xxx aluminum alloys." *Transactions of Nonferrous Metals Society of China* 24.7 (2014): 2174-2178.

[16] Hirth, S. M., et al. "Effects of Si on the aging behaviour and formability of aluminium alloys based on AA6016." *Materials Science and Engineering: A* 319 (2001): 452-456.

[17] Lloyd, D. J. "Some aspects of the metallurgy of automotive al alloys." *Materials Forum*. Vol. 28. No. 1. 2004.

[18] Wüebbels, T., D. K. Matlock, and J. G. Speer. *The effects of room temperature aging on subsequent bake-hardening of automotive sheet steels*. No. 2002-01-0041. SAE Technical Paper, 2002.

[19] Shi, Ming F., et al. *Static and dynamic dent resistance performance of automotive steel body panels*. No. 970158. SAE technical paper, 1997.

[20] Heat Treating, Vol 4, ASM Handbook, ASM International, 1991, p 841_879.

[21] Spedding, Trevor A., and Z. Q. Wang. "Study on modeling of wire EDM process." *Journal of Materials Processing Technology* 69.1-3 (1997): 18-28.

[22] Quincy Lab bench ovens brochure.

[23] Artmann, Nikolai, R. Vonbank, and Rasmus Lund Jensen. "Temperature measurements using type K thermocouples and the Fluke Helios Plus 2287A Datalogger." (2008).

[24] Thermo Scientific convection ovens brochure.

[25] G. K. Williamson & R. E. Smallman (1956) III. Dislocation densities in some annealed and cold-worked metals from measurements on the X-ray debye-scherrer spectrum, The Philosophical Magazine: A Journal of Theoretical Experimental and Applied Physics, 1:1, 34-46.

[26] Zhao, J.Z., De, A.K. & De Cooman, B.C. Formation of the cottrell atmosphere during strain aging of bake-hardenable steels. *Metall Mater Trans A* **32,** 417–423 (2001).

[27] David Kleiven, Jaakko Akola, Precipitate formation in aluminium alloys: Multi-scale modelling approach, Acta Materialia, Volume 195, 2020, Pages 123-131.

[28] Krasnikov, V.S.; Mayer, A.E.; Pogorelko, V.V.; Gazizov, M.R. Influence of θ 0 Phase Cutting on Precipitate Hardening of Al–Cu Alloy during Prolonged Plastic Deformation: Molecular Dynamics and Continuum Modeling. Appl. Sci. 2021, 11, 4906.

Appendices

Appendix A: Data Fitting and Harper Model

An important aspect to consider is the correlation between theoretical predictions and experimental results, which means finding a model that can describe the experimental phenomena.

The Harper model presented in Chapter 2 was originally developed to predict the bake hardening effect of steel sheets. But since bake-hardening micro-mechanisms are quite comparable for different materials, and since the model contains many material parameters, this model will be used to predict the experimental results obtained for the aluminum alloys used in this study. The general equation of the Harper model is again reported:

$$BH = \delta_{BH} \cdot \Delta\sigma_{max}^{BH} + \delta_{prec} \cdot \Delta\sigma_{max}^{prec}$$

The first contribution, which is given by the saturation level of solute atoms into dislocations over time, can be computed as

$$\delta_{BH} = \frac{N(t)}{N_0} = \frac{1 - \exp\left[3 \cdot (\rho_{f_x} - n_0 a)(\frac{\pi}{2})^{1/3} \left(\frac{ADt}{kT}\right)^{2/3}\right]}{1 - \frac{N_0}{n_0} \cdot \exp\left[3 \cdot (\rho_{f_x} - n_0 a)(\frac{\pi}{2})^{1/3} \left(\frac{ADt}{kT}\right)^{2/3}\right]}$$

The second term in the Harper model considers the subsequent densification of Cottrell atmospheres which causes a certain concentration of precipitates into the dislocations:

$$\delta_{prec} = \frac{R^2}{R_{max}^2}$$

The radius of the precipitates, R, is expressed as a function of time:

$$\frac{dR}{dt} = D \cdot \frac{C_0^{at} \cdot \frac{I\Delta}{\rho_{f_x}} - 0.5 \cdot \left(\frac{R}{\Delta}\right)^3}{0.5 \cdot R} \qquad (16)$$

where D is the diffusion coefficient of solute atoms, Δ is the inter-precipitate distance, C_0^{at} is the amount of solute segregated at the end of the first bake-hardening step, I is the nucleation site density and ρ_{f_x} the dislocation density after x percent pre-strain.

The whole model is very extensive and accounts for the most significant micro-mechanisms that affect the bake hardening response. However, many of the material parameters in the Harper model are not easily determined or estimated for the aluminum alloys studied in this project. In an attempt to simplify the previous equations, the variable parameters can be considered constants, and a reverse approach can be adopted in which the constants can be estimated from the experimental data, as an optimization problem.

Assuming the Harper model can be simplified by using constant material parameters, it would take the following form:

$$BH = k_3 \frac{1 - e^{k_1 \left(\frac{t}{T}\right)^{2/3}}}{1 - k_2 e^{k_1 \left(\frac{t}{T}\right)^{2/3}}} + k_4 R^2 \qquad (17)$$

where R is not an independent variable: from the previous equation, its dependence on time is remarked. It is a separable differential equation, which can be solved by integration:

$$\int \frac{R}{k_5 - R^3} dR = \int k_6 dt \qquad (18)$$

By solving this integral, the dependence of the radius of the precipitates over time is obtained implicitly:

$$t = \frac{ln\left(\left|R\left(R + \sqrt[3]{k_5}\right) + k_5^{2/3}\right|\right) - 2\left(\ln\left(\left|R - \sqrt[3]{k_5}\right|\right) + \sqrt{3} \cdot arctan\left(\frac{2k_5^{2/3} R + k_5}{\sqrt{3} k_5}\right)\right)}{6\sqrt[3]{k_5} \cdot k_6} \qquad (19)$$

The optimal values for the parameters k_1, k_2, k_3, k_4, k_5, k_6 can be numerically computed by means of a least squares' optimization method in MATLAB.

A certain set of optimal parameters will refer to a condition with same pre-strain, as the term ρ_{f_x}, embedded in constant k_3, depends on the amount of pre-strain applied. Then, obviously, all the constants would change again for different alloys, as all the parameters describe the structure and physical behavior of a particular material. Therefore, the simplest approach would be to identify two sets of constants for each alloy, one for 0% prestrain and the other for 2% prestrain.

Thus, a data fitting approach was attempted using the equations of the Harper model. Since there are several parameters in this model that are difficult to determine, they were assumed to be constant, when possible, as shown in Equation (17). The objective of the optimization algorithm was to implement a general optimization for Eq. (17) by means of the MATLAB function "fminsearch". However, the radius of precipitates *R* is not a constant but implicitly depends on time, as shown by Equation (19). Therefore, a sub-optimization with the function "fzero" was needed to find *R* for each time value. The data fitting was then reduced to a six-parameter optimization problem, with temperature, time and experimental BH values as inputs, and the BH values given by the model as an output. Basically, the function "fminsearch" was required to minimize a function of the six parameters which is the sum of the squares of the errors between the experimental and the modelled BH. The two MATLAB scripts are reported below. The first one is the general script, while the second one is a custom function that computes the quadratic error function from the experimental data and the initial values of the *k* parameters and is given as an input to the MATLAB function "fminsearch".

```
%% Input of experimental data about time, temperature
and bake hardening for a specific alloy and pre-
strain value

t = [600 600 600 600 1200 1200 1200 1200 1200 1200];
T = [393 403 443 453 383 393 403 423 443 453];
BH = [11.4 12 27.9 48.6 12.6 13.5 14.6 22.7 54.9
54.8];

%% Initialization of parameters k

k0 = [-2.18e+9 0.295 50e0 1.54e+13 1.54e-27 -7e+14];
k = k0.*ones (1,6);
BH_model = ones(1,10);
```

```
R0 = 1.8e-9;

%% Search of a minimum

[k,fal,exitflag,output] =
fminsearch(error_BH(BH,t,T,k), k0)



function y = error_BH (BH_exp, t, T, k)

BH_model = ones(1,10);
R = ones(1,10);
R0 = 1.8e-9;
for i=1:10 %from k5 e k6 I get R for each t
  funR = @(x)(-
log(abs(x*(x+k(5)^(1/3))+k(5)^(2/3)))+2*(log(abs(x-
k(5)^(1/3)))+2*sqrt(3)*atan((2*k(5)^(2/3)*x+k(5))/(sq
rt(3)*k(5)))))/(6*k(5)^(1/3)*k(6)) - t(i);
  x = fzero(funR, R0)
  if isnan(x)
      x;
  end
  R(i)=x;
  BH_model(i) = k(3)*((1-
exp(k(1)*(((log(abs(R(i)*(R(i)+k(5)^(1/3))+k(5)^(2/3)
))-2*(log(abs(R(i)-
k(5)^(1/3)))+sqrt(3)*atan((2*k(5)^(2/3)*R(i)+k(5))/(s
qrt(3)*k(5)))))./(6*k(5)^(1/3)*k(6))./T(i)).^(2/3)))
/(1-
k(2)*exp(k(1)*(((log(abs(R(i)*(R(i)+k(5)^(1/3))+k(5)^
(2/3)))-2*(log(abs(R(i)-
k(5)^(1/3)))+sqrt(3).*atan((2*k(5)^(2/3).*R(i)+k(5))/
(sqrt(3)*k(5)))))/(6*k(5)^(1/3)*k(6))./T(i)).^(2/3))
))+R(i)^2*k(4);
end


y = @(k)sum((BH_exp-BH_model).^2);
end
```

In the custom function, an optimization sublayer allows all the *R* values to be obtained; then, the modelled bake-hardening is computed as a function of the six parameters that need to be optimized by the main optimization cycle with “fminsearch”. In this case, the experimental data for the IH90US alloy at 2% pre-strain have been

used; each set of optimal parameters should be valid for a particular alloy at a certain pre-strain condition.

Therefore, the optimization functions require proper initial values of the parameters in input, which should be as close as possible to the local minimum that the function is going to compute. From Equations (1) and (17), the six parameters can be defined as follows:

$$k_1 = 3\left(\rho_{f_x} - n_0 a\right) \cdot \left(\frac{\pi}{2}\right)^{\frac{1}{3}} \cdot \left(\frac{AD}{k}\right)^{\frac{2}{3}}$$

$$k_2 = \frac{N_0}{n_0}$$

$$k_3 = \Delta\sigma_{max}^{BH}$$

$$k_4 = \frac{\Delta\sigma_{max}^{prec}}{R_{max}^2}$$

$$k_5 = \frac{C_0 \cdot \frac{I\Delta}{\rho_{f_x}} \cdot \Delta^3}{0.5}$$

$$k_6 = -\frac{D}{\Delta^3}$$

In order to obtain reasonable initial values of the *k* factors, the parameters of the Harper model have to be estimated for each alloy. But since many of them are difficult to evaluate without an in-depth study, their definition was attempted by referring to existing literature which mainly focuses on steels.

First, the dislocation density ρ_{f_x} (in this case after a 2% pre-strain) can be approximately equal to 10^{16} 1/m^2, taking the studies of Williamson et al. [25] and Zhao et al. [26] as a reference. The number of solute atoms in solution per unit volume n_0 was taken as $2.54 \cdot 10^{24}$ 1/m^3 [26]. The dislocation slip distance a was estimated to be 0.2 μm based on the work of Shaha et al. [27], divided by a factor that was kept as 15 in the absence of further information [7]. The term A, which is the interaction energy between dislocations, was taken as $3 \cdot 10^{-29}$ N·m^2, while the diffusion coefficient D,

described by the law $D = 2 \cdot 10^{-6} e^{-84.018/RT}$, which gives D = 1.95·10^{-6} m^2/s (it doesn't vary significantly in the temperature range of the tests) [26]. The number of initial dislocation sites N_0 is equal to ρ_{fx}/a, which is 7.5·10^{23} 1/m^3. Reasonable values for $\Delta\sigma_{max}^{BH}$ and $\Delta\sigma_{max}^{prec}$ were chosen to be 50 MPa, while the maximum radius of precipitates R_{max} was taken as 1.8 nm based on the work of Kleiven et al. [27]. The total solute content segregated at the end of the first hardening step, C_0, was kept the same as indicated by Zhao et al. [7], which is 200 ppm (0.02%), divided by a dislocation length that was approximated at 10^{-8} m, which gave 2·10^6 1/m. The nucleation site density I was taken as 10^5 sites/m^2, while the inter-precipitate distance Δ was found to be 14·10^{-9} m [28]. The estimated initial values for the k parameters are presented in *Table 30*.

Table 30. Computed initial values for the k parameters.

$\boldsymbol{k_1}$	-2.18·10^9 (K/s)$^{2/3}$
$\boldsymbol{k_2}$	0.295
$\boldsymbol{k_3}$	50 MPa
$\boldsymbol{k_4}$	1.54·10^{13} N/mm^4
$\boldsymbol{k_5}$	1.54·10^{-27} mm^3
$\boldsymbol{k_6}$	-7·10^{14} 1/(mm·s)

The parameters k_4, k_5 and k_6 are written in mm as the radius of precipitates is convenient to be in mm to obtain a stress value in MPa.

However, when entering these values in MATLAB and running the code, the inner optimization fails as the equation expressing time as a function of the radius of precipitates is found to be always constant and no minimum exists. Therefore, the function needs to be further checked, both in solving the differential equation by integration and in assigning the initial parameters. In the meantime, an additional simplification was made to check how the general code works. The radius of precipitates was considered as a constant, and the problem was reduced to four parameters. A new script that didn't need the separate custom function was written:

```
%% Input of experimental data about time, temperature
and bake hardening for a specific alloy and pre-
strain value
t = [600 600 600 600 1200 1200 1200 1200 1200 1200];
T = [393 403 443 453 383 393 403 423 443 453];
BH = [11.4 12 27.9 48.6 12.6 13.5 14.6 22.7 54.9
54.8];

%% Initialization of k parameters
k0 = [-2.18e+9 0.3 50e0 1.54e+13];
k = k0.*ones (1,4);
BH_model = ones(1,10);
R0 = 1.8e-9;

%% Error function
error1_BH =@(k) sum((BH-(k(3)*((1-
exp(k(1)*(t./T).^(2/3))))./(1-
k(2)*exp(k(1)*(t./T).^(2/3))))+k(4)*R0.^2)).^2);

%% Search of minimum
[k,fal,exitflag,output] = fminsearch(error1_BH, k0)


for i=1:10
BH_model(i) = k(3)*((1-
exp(k(1)*(t(i)/T(i))^(2/3))))/(1-
k(2)*exp(k(1)*(t(i)/T(i))^(2/3))))+k(4)*R0^2;
end
```

This time, no errors were detected, but as a result the modelled values of BH came out as constant at 27.3 MPa, regardless of the time and temperature conditions (*Figure 59*). It seems that, with the given input data, the MATLAB function "fminsearch" finds a constant function as the one that minimizes the sum of quadratic errors. Obviously, this outcome is not satisfactory, as the scope of this research is to show the change in BH response due to a variation in baking time or temperature. Even though the results don't fit the experimental data, this approach was presented as a first attempt that might be used to assist in future model developments that aim to more accurately describe the bake hardening behaviour of these alloys.

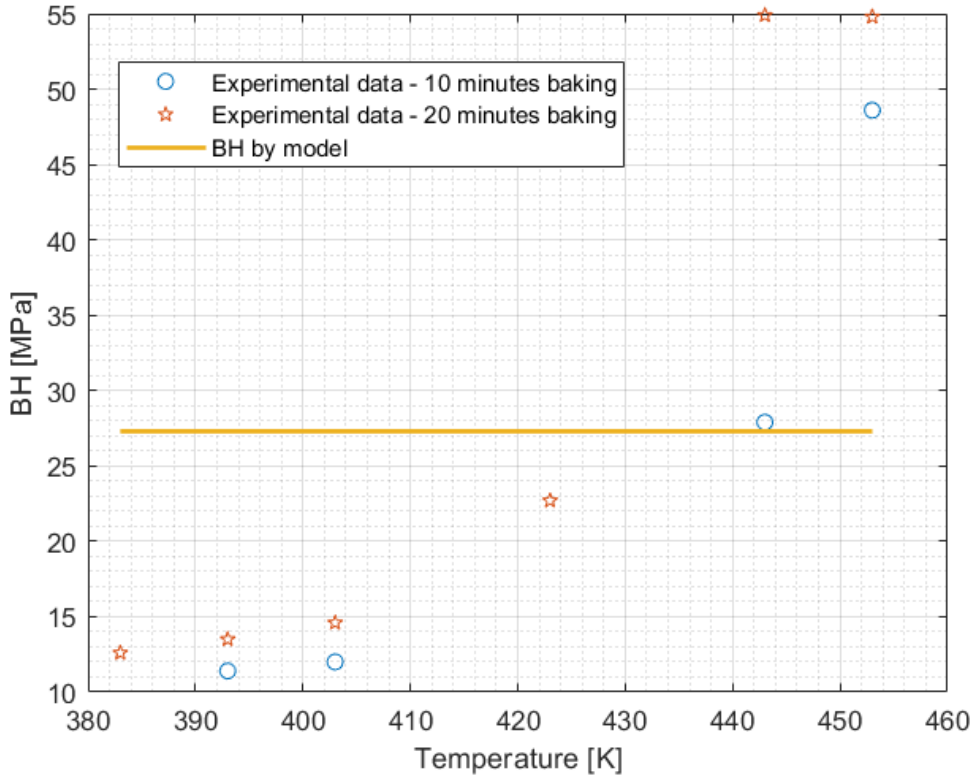

Figure 59. Experimental BH values and BH values predicted by a simplified four-parameter Harper model.

Vita Auctoris

Giorgio Rolle was born in 1998 in Torino, northern Italy, the city of FIAT automotive industry. Since tender age, he developed a strong passion for cars, especially for F1 racing and Michael Schumacher. For this reason, the choice of studying Automotive Engineering at Politecnico di Torino was a natural consequence. In 2020, he got his Bachelor's Degree in Automotive engineering after being part of the Politecnico's excellence program "Percorso per i Giovani Talenti". Right after, he started a Master's degree in Automotive Engineering – Product Development – which led to the past experience at the University of Windsor.